Design, Preparation and Evaluation of Bioactive Nanomaterials Aiming at Control of Physical Properties of Plasma Membrane

脂質二重膜の物理的状態の制御を目的とした、

生物活性ナノ材料の設計・開発並びに評価

2020 年 9 月学位授与予定

延山　知弘

CONTENTS

Preface

The contents of this thesis is based on studies under the direction of Prof. Dr. Tatsuya Murakami at Graduate school of Engineering, Toyama Prefectural University.

The author is deeply indebted to Prof. Dr. Tatsuya Murakami for his significant induction, valuable suggestions, continuous encouragements and other kindness supports.

The author wishes to express his gratitude to Dr.Kasuki Shigyo (Hiroshima University), Dr. Nakatsuji Hirotaka (Osaka University) Dr. Tsutomu Hamada(JAIST) for their advices based on profound insights, especially physical interpretation of his results.

The author is extremely grateful to Dr. Hyungjin Kim (Yamaguchi University) and Mr. Shinnoske honda (Kyoto University) for his kind suggestion, hearty supports and their collaboration of lipid mixing assay and evaluation of lipid translation from nanomaterial to living cells. The author expresses his gratitude to Dr.Kaori Yasuda for their collaboration on quantitative measurement of lipid composition in nanomaterials based her expertise of LC-MS/MS measurements. The author is grateful to Prof. Hiromune Ando (Gifu University) and Dr. Naoko Kawamura (Gifu University) for synthesis and preparation of fluorescent ganglioside probe. The author is grateful to Dr. Masahiro Tsujimoto (Kyoto University) and Mr. Koji Takana (Toyama Industry Technology Center) for transmission electron microscopy measurements.

The author wishes to gratitude to Ms. Misako Sawamura, Ms. Hiromi Hisano, Ms. Misako Sawamura, Ms.Kumiko Shima, Ms. Akiko Soto for their technical supports for protein preparation and purification, and to Ms. Sumiko Sagioka for supports at various kinds of administrative work.

The author wishes to express appreciation to Prof. Dr. Hirohide Sito (Kyoto University), Dr. Hideaki Nakanishi (Kyoto University) and Dr. Kaoru. R. Komatu (Kyoto University) for collaboration for Near Infrared laser irradiation analysis and supports for cell cultures, Prof. Dr. Hiroshi Sugiyama (Kyoto University), Dr.

Ganesh. N. Pandian (Kyoto University) Dr. Masaru Ogasawara (Toyama Prefectural Institute for Pharmaceutical Research), and Mr. Yutaka Murata (Kyoto University) for their expertise suggestion.

The author deeply grateful to financial, administrative and other supports from Kyoto University, Toyama Prefectural University, Toyama Prefecture and Kumano and Yoshida dormitories and their members. The author appreciated JSPS KAKENHI and JSPS DC2 fellowship for their kindness financial supports.

Finally, the author wishes to special thanks to his parents, Yoshiaki Nobeyama and Kyoko Nobeyama. His brother Kazuhiro Nobeyama and all of his friends who the author could not write specify.

Tomohiro Nobeyama
Department of Pharmaceutical Engineering, Faculty of Engineering
Department of Biotechnology, Graduate School of Engineering
Toyama Prefectural University
September 2020

Chapter 1. General Introduction

1-1. A short historical overview of the physical biology of lipid membrane properties

Basis for the physical biology of the lipid membrane

Investigations of the bulk properties of lipids began as early as 1694.[1] The first lipids studied were present in the milk of cows and other female mammals. In the early research, scientists investigated lipid composition, crystal structures, and physical phases.[2] Until the 1960s, through their investigations of milks, researchers discovered the importance of glycolipids.[3, 4] The have an astonishing foresight. Today an in-depth perspective takes into account the studies of lipids' physical behavior and their activities in terms of biology, chemical biology, and physical biology.

In 1858, R. Virchow's book marked the birth of cell biology: "*Omnis cellula e cellula"* ("All cells (come) from cells").[5, 6] His theory and previous announcements by M. J. Schleiden and T. Schwann (that living organisms are composed of cells) and R. Remak and B. Dumortier (the first discoveries of cell division) are now regarded as the foundation of modern cellular biology.[7] The obvious next question became, "*What is the definition of a cell*?" This question initiates the investigation of the molecular and physical biology of lipids.

The first answer, published in 1897, was provided by E. Overton.[8] He was the first to identify the cell as a compartment surrounded by a phospholipid/cholesterol membrane. During his research related to the permeability of sugar and ions into cells, he noticed that cholesterol esters and/or phospholipids might be components of the cell boundary.[9] He also observed that the boundary not only involved a lipid bilayer but also had some mechanism for incorporation of solutes, which today is known as "active transportation." Overton did not use the term "cell membrane," but his discovery led to an acceptable definition of the cell as a structural compartment surrounded by a lipid bilayer. He was also one of the first to point out the possible existence of peculiar structures

at the boundaries of cells and the importance in cell behavior.[10]

As the understanding of cells developed depth, more insights into cell membranes were needed. The outer membrane is where cells accept and react with external information, as Overton suggested. Beginning in the 1890s, there were at least two significant advances in the understanding of lipid bilayers: (1) a proposed model of protein–lipid coexistence and (2) the detailed observation of phase transition in the lipid membrane.

The components of the cell membrane had not yet become clear in the early 1900s. In 1935, J. F. Danielli and H. Davson concluded that the cell membrane was a thin film composed of lipoids (that is lipid-like substances) and proteins.[11] They also reported that the permeability of the film changed depending on the surrounding temperature. E. D. Korn estimated the ratio of the components, including amino acids, cholesterol, and phospholipids, using x-ray diffraction and electron microscopy.[12] Some of the studies that followed focused on the existence of proteins in the fluid membrane of the cell.[13] In 1972, S. J. Singer and G. L. Nicolson proposed a fluid mosaic model for the structure of cell membranes.[14] This model suggests that the cell membrane is a fluid arrangement of lipids in two layers, and membrane proteins are embedded in or protrude into the hydrophobic area of the lipid bilayer. The model explained the data obtained at that point well, so it was accepted. Based on this model, versatile protein working and lipid membrane characteristics, including asymmetric composition and membrane curvature, were revealed, and these aspects continue to be examined.[15, 16]

Second, the behavior of the lipid membrane itself was enthusiastically investigated. J. M. Stain et al. measured the phase transition temperature of the protein-free lipid bilayer and examined the delivery into the living cell lipid membrane using differential scanning calorimetry.[17] They observed that the lipid membrane showed phase transitions whether with proteins or without, and the phase transition temperatures were almost same as those of pure lamellar lipids in water. They concluded that the phases of lipids are not determined by lipid–protein interaction, but rather by hydrocarbon chain interactions between lipid molecules. They also proposed the existence of protein–lipid interactions, based

on their thermodynamics measurements, because they observed perturbation that resulted from protein–lipid interaction.

The effects of other components on lipids, such as cholesterol–lipid interaction or drug–lipid interaction, were also examined.[18] The complexity of the plasma membrane could be seen from various approaches,[12] and various kinds of plasma membranes were also examined.[18] In terms of the complexity shown in physical studies, the lecithin–water system first drew much attention as a model of the cell membrane with its lipid bilayer.[19] A phase diagram of the lipid bilayer was derived using this model, based on the results of x-ray diffraction, nuclear magnetic resonance (NMR), infrared spectroscopy, differential scanning calorimetry (DSC), electron paramagnetic resonance, freeze-fracture electron microscopy, and other technologies.[13, 18]

Before 1980, various measurements had suggested that cholesterol had a peculiar effect in terms of its phase transition. This effect of cholesterol was first measured by Ladbrook et al.[20] Cholesterol prevents lipids in myelin from entering a crystalline phase at body temperature. This team and other researchers demonstrated that cholesterol changes the lipid membrane behavior in terms of sol- and gel-phase lipids.[21, 22] From this research there emerged an assumption that the ordered hydrocarbon chains of lipids were disrupted by insertion of cholesterol, producing a different phase.

Because the sol–gel-phase transition temperature is slightly above room temperature, a mixture of DPPC, which is a phosphatidylcholine, and cholesterol was used for related research.[23] In 1987, based on this research, Ipsen et al. investigated the heat-induced phase transition of this system and proposed that cholesterol-rich lipid bilayer membranes have three representative physical phases: a highly ordered (crystalline) phase, called the solid ordered (So) phase; a liquid-crystalline phase, called the liquid disordered (Ld) phase; and a liquid ordered (Lo) phase, a unique cholesterol-rich phase.[24, 25] These three terms convey the current principal interpretation of the lipid bilayer state and provide the leading concept in physical biology for the lipid membrane. The Lo phase especially seems related to various kinds of cell behavior, based on a concept of

“lipid raft,” as discussed in the following.

Relationship between the properties of the lipid bilayer and cell behavior

The fluid mosaic model for the lipid membrane can be used to explain the cell membrane structure, made up of mobile proteins within the membrane.[15] This model, however, does not reflect the diversity and complexity of the lipid bilayer.[26] The fluid mosaic model assumes a random distribution of lipid and protein molecules, and it does not apply well to local characteristic properties within the plasma membrane; however, these local properties of lipids, such as composition, phase, and fluidity, also play key roles in cell behavior.[18]

The plasma membrane is not merely a complex of uniformly diffused lipid molecules and embedded membrane proteins. Possible restrictions on distribution of the lipid molecules within the plasma membrane have been reported.[26, 27] The reports hypothesize a domain structure for the plasma membrane, based on broadening of the peak seen in high-sensitivity DSC for the mixture of lipids.[28] Moreover, when a phase diagram was prepared from electron spin resonance (ESR) spectra using the nitroxide radical TEMPO, it indicated lateral phase separation in the lipid bilayer. The distribution of lipid molecules in the plasma membrane is the focus of ongoing investigations in both physics and cellular biology.[29]

As compiled reports linked the local physical structure and cellular activities, researchers began to consider the existence of a phenomenon closer to a solid-phase where the plasma membrane recruits membrane proteins to a small area.[30] High-resolution transmission electron microscopy (TEM) also supported the existence of a phase “cluster” at the lipid bilayer, with coexistence of different phases in the same membranes.[31] In 1979, R. D. Klausner et al. substantiated such a domain structure in the lymphocyte plasma membrane, using a fluorescent probe to examine the physical state of the biomembrane.[32] The fluorescent lifetimes of probes were not the same as those found in pure lipids, which was explained by the coexistence of different phases, as previously indicated, in the model lipid bilayer membrane.[28, 33] Since 1980, various kinds of

small molecular probes formed from fluorescent lipid analogs have been developed to provide phase-selective labeling of the lipid bilayer.[34] Such fluorescent probes now make up the most widely utilized method for analysis of domain structure in modeled and actual cell membranes.[35]

From a biological point of view dealing with living cells, sophisticated membrane properties began to be investigated through the perspectives of the immune system and cellular aging. In 1978, I. Zs. Nagy proposed a model of cellular aging that explained the advancing rigidness found in membranes. The report suggested that the old and rigid membrane loses lateral mobility, with a decrease in potassium permeability and a change in the intracellular ion balance, which in turn negatively affects the regulation of chromatin condensation.[36] In 1983, B. Rivnay et al. reported that membrane fluidity influenced the aging of lymphocytes.[37] Lymphocytes from old mice showed increased proliferation when the ratio of cholesterol to phospholipids was reduced through artificial exposure of the cells to lipids. The data indicated that artificial restoration of this membrane property can lead to recovery of cell functions if other significant functions have not already been seriously harmed. Other research in the 1980s with natural killer cells showed that cell-behavior regulation could take place via artificial adjustment of lipid composition at the membrane.[38] The importance of membrane fluidity was confirmed through studies of the relationship between the immune system and membrane composition shifts involving reduction of membrane fluidity, such as in regulation of synthesized fatty acids or peroxidation of fatty acids at the plasma membrane.[39]

Further investigation of the plasma membrane uncovered a central role for gangliosides as cell behavior regulators. Gangliosides are sphingolipids, and have an oligosaccharide containing sialic acid as a head group and a ceramide as a hydrophobic tail group. They generally include an unsaturated hydrocarbon chain, so their phase transition temperature is high. In 1973, T. L. Steck et al. reported, from a study of red blood cell membranes, that gangliosides were embedded into the plasma membrane and that the sugar group poked out from the membrane to the outside of the cell.[40]

The importance of gangliosides in cell behavior was observed in a study of cholera toxin, a protein made up six subunits produced by *Vibrio cholerae*, causing the disease of cholera. One kind of ganglioside, GM1, works as a receptor of for cholera toxin B in the small intestine.[41] In 1975, T. Revesz et al. found that GM1 clustered on the cell membrane of lymphocytes after treatment with cholera toxin, and purified GM1 artificially inserted in the cell membrane exhibited the same clustering.[42] This observation indicated that gangliosides play a key role in domain formation on the cell membrane, the way cholesterol does. TEM images of GM1-containing membrane clearly showed that gangliosides formed circular domains on the lipid bilayer.[43] In the 1980s, the biological importance of gangliosides as an interface between cells and their surroundings was discovered through various phenomena, including membrane fusion between a virus and the lipid bilayer,[44] association with a hormone receptor,[45] binding affinity for tetanus toxin,[46] cell–cell recognition, and others.[47] However, the relationship of sophisticated membrane properties and the biological role of gangliosides remained unclear until 1997.

In 1973 the co-localization of sphingolipids and some proteins was suggested by J. Yu et al.[48] They treated red blood cells with a neutral detergent, Triton-X-100, and the membranes were separated into soluble and insoluble fractions. One fraction was defined as the detergent-resistant membranes (DRMs). DRMs were isolated from various kinds of cells and are now regarded as an acceptance gateway for information on the plasma membrane, involving signal transaction, or as the starting point for endocytosis.

The behavior of the Lo phase membrane and the DRM appeared similar. In a reconstituted system, sphingolipids and cholesterol-rich liposomes are not solubilized by Triton-X-100, and glycosylphosphatidylinositol (GPI)-anchored proteins in the liposome become insoluble, unlike isolated ones. Without cholesterol, the resistance to Triton-X was dramatically decreased, especially with sphingolipids. Unsaturated fatty acids were retracted by Triton-X-100, which did not take place with saturated ones.[49, 50]

In 1997, K. Simon proposed the concept of the “lipid raft,” a cholesterol- and

sphingolipid-rich region on the plasma membrane that recruits membrane protein and then freely drifts on the membrane, like a raft on the sea.[49] This concept of a lipid raft was accepted smoothly, and since 1997, various phenomena of signal transaction, viral infection, immune system function, hormone secretion, cell–cell recognition, and other cell behaviors have been explained using the concept. Evidence demonstrates that the lipid raft is dramatically disrupted and generated on living cells.

On the other hand, some doubts have been expressed about the lipid raft hypothesis. The strongest criticism concerns the difficulty of real-time observation of lipid rafts, even though the lipid raft model, with the domain of the Lo phase, is easily and stably reconstituted on a model lipid bilayer. In 1998, D. A. D. Angelis et al. reported fluorescent observation of raft induction with green fluorescent protein (GFP)-tagged GPI-anchored proteins and an antibody-crosslinking method that selects GFP.[51] Obtaining images for the natural lipid raft is still challenging. K. G. N Suzuki and N. Komura et al. attempted real-time imaging of the lipid raft on cells. They developed a method of single-molecule imaging for lipid-raft-selective proteins with Lo-phase preference fluorescent ganglioside probes and reported the dynamics of lipid raft formation and deformation.[52, 53] From their reports and ongoing research, the current concept of the lipid raft has been adjusted to a small and temporary complex of sphingolipids and membrane proteins recruited within a cholesterol-rich area.

Finally, non-raft nanostructures, such as lipidic clusters, can also relate to cell behavior, as described in the following.

Development of analytical tools for phase separation of the cell-like lipid bilayer

The significance of lipid bilayer property in the functions of the plasma membrane emerged from physical or theoretical fields, as well as from biological scientists. To support these investigations, methods to analyze the properties of lipids are continuously proposed and designed. Among them are preparation of the cell-like lipid bilayer and domain formation, fluorescent probe use for analysis

of domain phases, and real-time imaging methods and equipment for tracking the changes in membrane properties. To generate data about more sophisticated membrane properties, such as the dynamics of lipid rafts, required methods that had higher resolving power than the traditional ones already described.

To analyze the domain structure under cell-like conditions, preparation methods for cell-sized liposomes called giant unilamellar vesicles (GUVs) were developed. In 1969, J. P. Reeves et al. reported their preparation method for GUVs, which they called the hydration method.[54] They made thin lipid films by spreading out lipids dissolved in organic solvents and then evaporating the solvents. An aqueous solution was added onto the film, and the lipids were allowed to swell into large micrometer-scale vesicles. Reeves et al. reported formation of a thin, approximately single-layer lipid membrane with a spherical shape, which was confirmed experimentally in 1983 by P. Mueller et al.[55] In 1982, R. Biischl et al. reported an efficient method of GUV preparation that used electric field-induced fusion of liposomes.[56] In 1986, M. I. Angelova et al. investigated the GUVs method by adding an external electric field.[57] Based on previously compiled discussions, in 1992, M. I. Angelova et al. proposed an efficient and rapid method to form GUVs by applying external AC electric fields, which is called electroformation in today's soft matter physics and biophysics fields.[58] Modified electroformation methods for each research purpose are most widely utilized today for phase-separated GUVs, which embrace at least two different phase domains on a single GUV.[59, 60]

Another artificial cell membrane developed takes the form of giant plasma membrane vesicles (GPMVs). GPMVs are cell-sized lipid vesicles formed by blebbing and/or swelling and isolation of lipidic membrane vesicles that originate from living cells.[61] The artificial blebbing technology was reported by E. S. Ruth in 1911 (utilizing pure water), and a brief summary of the procedures, including other developments, was provided in 1919 by M. J. Hogue.[62] In 1976, R. E. Scott offered a study of the first useful method to prepare vesicles from the plasma membrane.[63] In 1983, D. Holowka et al. developed the methodology of isolating GPMVs from cells.[64] In 2007, phase-separated GPMVs were also prepared by T.

Baumgart, who validated this using fluorescent lipid probes.[65] GPVMs are now widely utilized as a cell-like membrane model, although the composition of the membrane is not artificially determined, so that physical analysis of lipid membrane properties and of characteristics of the lipid molecules or lipid domains on GMPVs requires sophisticated technology. In the research I report here, I utilized GUVs as a cell model, to take advantage of the benefit of definite determination of lipid compositions and of reconstitution of the domain. However, physiological studies, especially those related to asymmetric bilayers, sometimes require GPMVs instead.[66]

Analytical tools for visualizing the phase separation of lipid bilayers also improved from the 1990s to the 2000s. At first, phase conditions of lipid bilayers were studied using spectroscopic analysis, such as nuclear magnetic resonance (NMR), ESR, infrared spectroscopy (IR), isothermal titration calorimetry, circular polarization probes such as diphenylhexatriene (DPH), and others, as I have described in previous sections. These methods, however, are not suitable for observing the phase separation on a single GUV or GPMV.

Instead, to observe the phase condition and phase-separated domain structures, methods that examine lipid membrane fluidity use fluorescent probes, such as laurdan (6-dodecanoyl-2-dimethylaminonaphthalene), and fluorescent lipids and hydrophobic fluorescent molecules that localize on specific phases.

The first fluorescence visualization of phase-separated domains on GUVs was achieved in 1999 by J. Korlach et. al.[67] They prepared ternary GUVs composed of DLPC/DPPC/cholesterol and visualized the GUVs with two fluorescent probes, 1,1′-dieicosanyl-3,3,3′,3′-tetramethylindocarbocyanine perchlorate (DiI-C20) for Ld and 2-(4,4-difluoro-5,7-dimethyl-4-bora-3a,4a-diaza-s-indacene-3-pentanoyl)-1-hexadecanoyl-*sn*-glycero-3-phosphocholine (Bodipy-PC). Previous reports, such as one in 1987 regarding visualization of Ca^{2+}-induced domains in GUVs, could not monitor a nascent domain in GUV.[68] Ions in solution induce a pseudo-domain formation[69] and GUV aggregation,[70] so that native observation of the domain is necessary in order to further the progress of domain analysis.

Fluorescent probes for detecting phase separation on GUVs were systematically

tested in 2007 by T. Baumgart et al.[35] I have focused on fluorescent lipid derivatives. Their localization on the lipid bilayer can be determined when examining both the hydrophilic head group, including a fluorescent group, and the hydrophobic carbon group. It should be noted that a single characteristic will not determine the phase selectivity of these molecules, and the localizations show variation for each probe. For example, both Rho-DPPE (1,2-dipalmitoyl-*sn*-glycero-3-phosphoethanolamine-*N*-(lissamine rhodamine B sulfonyl)) and NBD-DPPE (1,2-dipalmitoyl-*sn*-glycero-3-phosphoethanolamine-*N*-(7-nitro-2-1,3-benzoxadiazol-4-yl)) locate preferentially in the Ld phase, even though the acyl structures present are unsaturated hydrocarbons. As another example from the cholesterol derivatives, NBD cholesterol is preferentially located at the Ld phase, but cholestatrienol, a derivative of cholesterol, partitions into the Lo phase.[35]

Insight into each of the phases has a different history. For Ld, due to both its historical background[71] and low photobleaching,[60] Rho-DPPE has been a top choice among commercial probes for pursuing the details of phase separation, transition, or other related domain modifications.[72, 73] Observation of the Lo phase, however, is relatively difficult. Even though some probes can theoretically monitor the Lo phase region, they disappear or diffuse from the Lo domain through phase transition or domain metamorphosis. Moreover, some of the glycolipid-based probes, such as the commercially available BodipyFL-GM1 or a large portion of the fluorescently labeled sphingomyelin, did not partition into the Lo phase region.[53, 74] Previous studies stained the head group of GM1 with small molecules such as cholera toxin B subunit (CTB) or wheat germ antigen, but the processes themselves induced the formation of new artifact domains.[75, 76] In the 2000s, H. Ando, A. Imamura, K. Fujikawa, and other collaborators devoted sequential efforts to the total synthesis of glycolipid analogs in effective ways.[77-79] Based on these facets from organic chemistry, in 2016, N. Komura and K. G. N. Suzuki developed fluorescent ganglioside probes selective for the Lo phase and revised the definition of the lipid raft on plasma membranes.[53] In 2017, several additional phase-selective sphingolipid analogs were reported from the same group, which used these to elucidate a role for sphingolipids in lipid raft dynamics.[80]

These probes are very effective tools for analysis of domain structures and can be applied to tracking single molecules in living cells, but they are difficult to apply in terms of grasping sequential changes of a membrane property, such as fluidity. One solution is to perform a fluorescence recovery after photobleaching assay to measure the lateral diffusion of lipid molecule, but this requires time-lapse measurement, so real-time imaging of the membrane property is difficult.[81, 82] Another traditional solution is the use of environmentally sensitive probes.

In 1979, G. Weber et al. synthesized a probe sensitive to environmental polarity, Prodan (2-propionyl-6-dimethylaminonaphthalene), which has a large excited-state dipole moment.[83] The fluorescence emission spectrum for Prodan exhibits a wide shift toward red in accordance with the increase of a solvent's polarity.[84] This type of probe is superior to the preceding probes because the researcher can define membrane fluidity as a continuous function of spectrum shift. The normalized value reflecting the shift of spectrum, now called the GP value, has become widely utilized in comparing the local environments around probes.[85] This measurement depends less on the number of probes in an observed area or on the distribution of probe molecules, so that the GP values can define the local condition easily without disturbing it, generating an improvement compared with anilinonaphthalene sulfonate or tetramethylsilane (TMS), probes that reflect the environmental conditions as a function of fluorescent intensity.[86]

Laurdan, a derivative of Prodan for lipid membranes, was applied to analysis of the phospholipid bilayer in 1986 by T. Parasassi et al.[87] Laurdan has a hydrophobic acyl chain that inserts automatically into the lipid membrane. In 1991, T. Parasassi et al. quantified the lipid phase of phospholipid vesicles as a function of GP value.[88] They also observed a radical peak shift for the laurdan emission spectrum near the sol–gel-phase transition temperature. In 1997, T. Parasassi et al. applied two-photon imaging to the excitation of laurdan and prevented photobleaching from affecting the GP value.[89] In 2000, L. A. Bagatolli et al. captured microscopic images of the domains of GUVs, using spectra imaging.[90]

Laurdan has been applied to various kinds of analysis for model membranes, both of GPMV and GUVs and for real plasma membranes.[91] In 1993, R. Fiorini

attempted to use laurdan in the analysis of nanostructures on the plasma membrane of leukocytes. In 2002, K. Gaus et al. achieved two-photon imaging of cell membranes (ref). Other concepts of probes were also investigated, such as probes that contain a carboxyl group to fix molecules near the hydrophilic group (C-laurdan)[92] or that become excited under the relatively long wavelength of a popular light source (di-4-ANEPPDHQ).[93]

These probes were also utilized in the work described in the present thesis, but it should be notified that such probes tend to reflect bulk properties relatively more, and at the time of writing, their resonance is not sufficient for tracking the dynamics of nanoscale domains on plasma membranes. Moreover, a probe molecule can unintentionally transfer from the target membrane to surrounding structures, such as the lipidic nanostructure on the membrane. Thus, this study observed that Laurdan only reflected the attached membrane structure and did not provide information on the target membrane domain structure. Application of each method must be carefully considered in the experiments.

1-2. The relationships between lipid raft and other membrane property with cell behavior

A cell is surrounded by a lipid bilayer membrane and the membrane property is related to various kinds of cell behavior related to reactions to the outer world. Including neurotransmission[94, 95], immune system [96], hormone secretion [97], metamorphose of cell shape [98-100], cell differentiation[101, 102]and development.[103] The property provides the reaction field for a response to stimulations, gathering proteins, functional lipids, and other materials. It should be noted I used the word, membrane property, as not only for the pure physical phase of lipids but for all other characteristics, including domains, complexes with proteins and others, phase-separated domains, clusters, and others exist in/on the model and real plasma membrane in this thesis.

The most well-known property is cholesterol-rich nanodomain. The domain gathers membrane proteins glycolipids such as sphingolipids and gangliosides and dynamically forms the nanoscale lipid-protein complex called lipid raft on the cell membrane. Lipid raft is a typical example of the membrane property which can connect soft matter physics and cellar biology.

For instance, the GPI anchored proteins gathered on cholesterol and sphingolipid rich area and formed lipid-tethered nanostructures on membrane [52, 104]. GPI anchored protein is a group of membrane proteins connected on the plasma membrane by glycosylphosphatidylinositols (GPI) conjugated by amide bond at the C-terminal of proteins. GPI anchored proteins are related to various kinds of cell behavior. A typical example is CD 59 protein on T-cell surface [105]. CD59 is a small GPI-anchor protein and trigger signals for activation of T-cell followed by clustering of CD59 proteins on lipid raft when CD 59 is associated with Antigen-presenting cells. GPI anchor protein is associated with various kinds of cell behavior and it means the significance of lipid raft.

Animal perception of temperature is also related to membrane property.[106, 107] The transition receptor potential (TRP) receptor is a family of receptors that works as a sensor of pain and temperature. One of the TRP channels, TRPV8 activity were reduced by cholesterol depletion from cell membrane [108]. The activity of

TRPV1 channels suppressed by lipid raft disruption by the decrease of the amount of cholesterol, sphingomyelin, or ganglioside by the depletion or inhibition of these molecules. [109, 110]

Lipid-raft is a widely associated immune system[111] and other neural signal transactions[94] and these phenomena have been discussed continuously in scientist community[112]. To light the I would like to focus on new insight of membrane property from the viewpoint of the relation of dynamic membrane re-organization of a process such as elongation and development in animal cells and plant cells. For metamorphosis, the elongation of nerve cells required lipid raft. Glycoprotein M6a(GPM6a) co-localized with D4, a cholesterol-binding protein, and a molecular imaging marker for lipid rafts, filipin. [113] GMP6a activates the downstream signal transaction on lipid rafts and regulates the elongation of nerve cells [114]. GMP6a perhaps works as an inducer of lipid raft clustering on the tops axis. In the developmental process, mouse embryo is enriched in cholesterol, and glycolipids and depletion of cholesterol from the plasma membrane of oocyte inhibit the cell-division in the early stage of development.[115] The same phenomenon is observed in the embryo of amphibian.[116]

The behavior of plant cells is also determined by membrane property. [117] The most famous example is the temperature sensing of a plant cell from the change of fluidity. The change of membrane fluidity regulated genes related to the desaturation of lipids to protect cells from collapse [118]. The exist of lipid raft on plant cell is confirmed by DRM study and other methods [119-121], but, since the less availability of plant lipids in both of commercial way and the difficulty of synthesis of plant peculiar glycolipids, the investigation of plant lipid raft is less advanced in plant cell than in animal cells. [122]

It should be noted that continuous researches have been performed for the non-raft study of the relationship between the plant plasma membrane and cell behavior. For example, the effects of the addition of fatty acid are not explained by lipid raft. In the plant plasma membrane, the amount of DGDG was regulated by the concentration of phosphor ions in the surrounding environment. [123] On other plant cells, GIPC accumulated together and trigger the uptake of calcium

ion [124]. To analyze or manipulate such properties, a direct supplement of lipids is required. The regulation of the content of the lipid membrane is a key factor for both raft- and non-raft- property of cells and determine cell behavior.

As shown in this section, lipid membrane property, lipid raft, and others is a fundamental part of the cell-behavior determination. The methodology of manipulator development would lead new cell engineering tools for understanding cell-behavior and regulation of cells toward industrial application.

1-3. References

1. Brunner, J.R. Physical equilibria in milk:The lipid phase, in *Fundamentals of Dairy Chemistry, 2nd ed*. (eds. B.H. Webb, A.H. Johnson & J.A. Alford) (AVI Publishing Company, Westport.Conn; 1974).
2. Keenan, T.W., Mather, L.H. & D.P.Dylewski Physical Equilibria: Lipid Phase, in *Fundamentals of Dairy Chemistry*. (eds. N.P.Wong, R.Jenness, M.Keeney & E.H.Marth) 511-582 (Springer, Boston; 1988).
3. W.Keenan, T. Milk Lipid Globules and Their Surrounding Membrane: A Brief History and Perspectives for Future Research. *J. Mammary Gland Biol. Neoplasia* **6**, pages365–371 (2001).
4. D.S.Galanos & V.M.Kapoulas Fractionation and identification of milk polar lipids: Triester glycophospholipids. *Biochim. Biophys. Acta* **98**, 293-312 (1965).
5. Bagot, C.N. & Arya, R. Virchow and his triad: a question of attribution. *Br. J. Haematol.* **143**, 180-190 (2008).
6. R.Wirchow *Die Cellularpathologie in ihrer Begründung auf physiologische und pathologische Gewebelehre*. (Verlag von August Hirschwald, Berlin; 1859).
7. B.Amos Lessons from the history of light microscopy. *Nat. Cell Biol.* **2**, E151-E152 (2000).
8. A.Kleinzeller Ernest Overton's Contribution to the Cell Membrane Concept: A Centennial Appreciation. *Physiology* **12**, 49-53 (1997).
9. E.Overton Ueber die osmotischen Eigenschaften der Zelle in ihrer Bedentung für die Toxicologie und Pharmakologie. *Z. Phys. Chem. (N. F.)* **22**, 189-209 (1897).
10. Kleinzeller, A. Chapter 1 Charles Ernest Overton's Concept of a Cell Membrane. **48**, 1-22 (1999).
11. J.F.Danielli & Davson, H. A contribution to the theory of permeability of thin films. *J. Cell. Comp. Physiol.* **5**, 495-508 (1935).
12. E.D.Korn Structure of Biological Membranes. *Science* **153**, 1491-1498 (1966).
13. B.D.Ladbrooke & D.Chapman Thermal analysis of lipids, proteins and biological membranes a review and summary of some recent studies. *Chem. Phys. Lipids* **3**, 304-356 (1969).
14. Singer, S.J. & Nicolson, G.L. The fluid mosaic model of the structure of cell membranes. *Science* **175**, 729-731 (1972).

15. Singer, S.J. Some early history of membrane molecular biology. *Annu. Rev. Physiol.* **66**, 1-27 (2004).
16. Nicolson, G.L. The Fluid-Mosaic Model of Membrane Structure: still relevant to understanding the structure, function and dynamics of biological membranes after more than 40 years. *Biochim. Biophys. Acta* **1838**, 1451-1466 (2014).
17. Steim, J.M., Tourtellotte, M.E., Reinert, J.C., McElhaney, R.N. & Rader, R.L. Calorimetric evidence for the liquid-crystalline state of lipids in a biomembrane. *Proceedings of the National Academy of Sciences* **63**, 104-109 (1969).
18. D.Chapman Phase transitions and fluidity characteristics of lipids and cell membranes. *Q. Rev. Biophys.* **8**, 185-235 (1975).
19. D. Chapman & J.Urbina Biomembrane phase transitions. Studies of lipid-water systems using differential scanning calorimetry. *J. Biol. Chem.* **249**, 2512-2551 (1974).
20. B.D.Ladbrooke, T.J.Jenkinson, V.B.Kamat & D.Chapman Physical studies of myelin I. Thermal analysis. *Biochim. Biophys. Acta* **164**, 101-109 (1968).
21. Kruyff, B.D., R.A.Demel, A.J.Slotboom, Deenen, L.L.M.V. & A.F.Rosenthal The effect of the polar headgroup on the lipid-cholesterol interaction: A monolayer and differential scanning calorimetry study. *Biochim. Biophys. Acta* **307**, 1-19 (1973).
22. G.Lindblom, L.B.A.Johansson & G.Arvidson Effect of cholesterol in membranes. Pulsed nuclear magnetic resonance measurements of lipid lateral diffusion. *Biochemistry* **20**, 2204-2207 (1981).
23. D.J.Recktenwald & H.M.McConnell Phase equilibria in binary mixtures of phosphatidylcholine and cholesterol. *Biochemistry* **20**, 4505-4510 (1981).
24. Ipsen, J.H., G.Karlström, O.G.Mourtisen, H.Wennerström & M.J.Zuckermannc Phase equilibria in the phosphatidylcholine-cholesterol system. *Biochim. Biophys. Acta* **905**, 162-172 (1987).
25. J.H.Ipsen, O.G.Mouritsen & M.Bloom Relationships between lipid membrane area, hydrophobic thickness, and acyl-chain orientational order. The effects of cholesterol. *Biophys. J.* **57**, 405-412 (1990).
26. Jain, M.K. & White, H.B., 3rd Long-range order in biomembranes. *Adv. Lipid Res.* **15**, 1-60 (1977).
27. Pagano, R.E., Cherry, R.J. & Chapman1, D. Phase Transitions and

Heterogeneity in Lipid Bilayers. *Science* **181**, 557-559 (1973).
28. S.Mabrey & Sturtevant, J.M. High-Sensitivity Differential Scanning Calorimetry in the Study of Biomembranes and Related Model Systems, in *Methods in Membrane Biology*. (ed. E.D.Korn) 237-274 (Springer, Boston; 1978).
29. M.J.Karnovsky, A.M.Kleinfeld, R.L.Hoover & R.D.Klausner The Concept of Lipid Domains in Membranes. *J. Cell Biol.* **94**, 1-6 (1982).
30. H.Borochov & .hinitzky, M. Vertical displacement of membrane proteins mediated by changes in microviscosity. *Proceedings of the National Academy of Sciences* **73**, 4526-4530 (1976).
31. B.R.Copeland & H.M.McConnel The rippled structure in bilayer membranes of phosphatidylcholine and binary mixtures of phosphatidylcholine and cholesterol. *Biochim. Biophys. Acta* **599**, 95-109 (1980).
32. R.D.Klausner, A.M.Kleinfeld, R.L.Hoover & M.J.Karnovsky Lipid Domains in Biological Membranes: their Structural and Functional Perturbation by Free Fatty Acids and the Regulation of Receptor Mobility. *J. Biol. Chem.* **255**, 1286-1295 (1979).
33. Sklar, L.A., Hudson, B.S., M.Petersen & J.Diamond Conjugated polyene fatty acids on fluorescent probes: spectroscopic characterization. *Biochemistry* **16**, 813-819 (1977).
34. R.D.Klausner & D.E.Wolf Selectivity of fluorescent lipid analogues for lipid domains. *Biochemistry* **19**, 6119-6203 (1980).
35. Baumgart, T., Hunt, G., Farkas, E.R., Webb, W.W. & Feigenson, G.W. Fluorescence probe partitioning between Lo/Ld phases in lipid membranes. *Biochim. Biophys. Acta* **1768**, 2182-2194 (2007).
36. I.Zs.-Nagy A membrane hypothesis of aging. *J. Theor. Biol.* **75**, 189-195 (1978).
37. B.Rivnay, T.Orbital-Harel, M.Shinitzky & A.Globersonb Enhancement of the reponse of ageing mouse lymphocytes by In vitro treatment with lecithin. *Mech. Ageing Dev.* **12**, 329-336 (1983).
38. M.Provinciali, N.Fabris & C.Pierib Improvement of natural killer cell activity by in vitro active lipids (AL 721) administration in old mice. *Mech. Ageing Dev.* **52**, 245-254 (1990).
39. D.Hwang Essential fatty acids and immune response. *The FASEB Journal* **3**, 2052-2061 (1989).
40. Steck, T.L. & G.Dawson Topographical Distribution of Complex Carbohydrates in the Erythrocyte Membrane. *J. Biol. Chem.* **249**, 2135-2142

(1974).
41. J.Holmgren, I.Lönnroth, J.Månsson & L.Svennerholm Interaction of cholera toxin and membrane GM1 ganglioside of small intestine. *Proceedings of the National Academy of Sciences* **72**, 2520-2524 (1975).
42. T.Révész & M.Greaves Ligand-induced redistribution of lymphocyte membrane ganglioside GM1. *Nature (London)* **257**, 103-106 (1975).
43. T.W.Tillack, M.Wong, M.Allietta & T.E.Thompsonb Organization of the glycosphingolipid asialo-GM1 in phosphatidylcholine bilayers. *Biochim. Biophys. Acta* **691**, 261-273 (1982).
44. A.M.Haywood & B.P.Boyer Fusion and Disassembly of Sendai Virus Membranes with Liposomes. *Biophys. J.* **37**, 128-130 (1982).
45. F.Omodeo-Sale, R.O.Brady & P.H.Fishman Effect of thyroid phospholipids on the interaction of thyrotropin with thyroid membranes. *Proceedings of the National Academy of Sciences* **75**, 5301-5305 (1978).
46. Critchley, D.R., Habig, W.H. & Fishman, P.H. Reevaluation of the Role of Gangliosides as Receptors for Tetanus Toxin. *J. Neurochem.* **47**, 213-222 (1986).
47. S.Hakomori Glycosphingolipids in Cellular Interaction, Differentiation, and Oncogenesis. *Annu. Rev. Biochem* **50**, 733-764 (1981).
48. J.Yu, Fischman, D.A. & Steck, T.L. Selective solubilization of proteins and phospholipids from red blood cell membranes by nonionic detergents. *J. Supramol. Struct.* **1**, 233-248 (1973).
49. Simons, K. & Ikonen, E. Functional rafts in cell membranes. *Nature* **387**, 569–572 (1997).
50. Simons, K. & Ikonen, E. How Cells Handle Cholesterol. *Science* **290**, 1721-1726 (2000).
51. D.A.D.Angelis, G.Miesenböck, B.V.Z. & Rothman, J. PRIM: Proximity imaging of green fluorescent protein-tagged polypeptides. *PRIM: Proximity imaging of green fluorescent protein-tagged polypeptides* **95**, 12312-12316 (1998).
52. Suzuki, K.G. *et al.* Transient GPI-anchored protein homodimers are units for raft organization and function. *Nat. Chem. Biol.* **8**, 774-783 (2012).
53. Komura, N. *et al.* Raft-based interactions of gangliosides with a GPI-anchored receptor. *Nat. Chem. Biol.* **12**, 402-410 (2016).
54. Reeves, J.P. & Dowben, R.M. Formation and properties of thin-walled phospholipid vesicles. *Jornal of cellular physiology* **73**, 49-60 (1969).
55. P.Mueller, T.F.Chien & B.Rudy Formation and properties of cell-size lipid

bilayer vesicles. *Biophys. J.* **44**, 375-381 (1983).
56. R.Büschl, H.Ringsdorf & U.Zimmermann Electric field-induced fusion of large liposomes from natural and polymerizable lipids. *FEBS Lett.* **150**, 38-42 (1982).
57. Angelova, M.I. & Dimitrov, D.S. Liposome electroformation. *Faraday Discuss. Chem. Soc.* **81**, 303-311 (1986).
58. Angelova, M.I., Soléau, S., Méléard, P., Faucon, F. & Bothorel, P. Preparation of giant vesicles by external AC electric fields. Kinetics and applications, in *Trends in Colloid and Interface Science VI. Progress in Colloid & Polymer Science*. (eds. C.Helm, M. Lösche & H. Möhwald) (Steinkopff, 1992).
59. Wesołowska, O., Michalak, K., Maniewska, J. & Hendrich, A.B. Giant unilamellar vesicles — a perfect tool to visualize phase separation and lipid rafts in model systems *Acta Biochim. Pol.* **56**, 33-39 (2009).
60. Morales-Penningston, N.F. *et al.* GUV preparation and imaging: minimizing artifacts. *Biochim. Biophys. Acta* **1798**, 1324-1332 (2010).
61. Sezgin, E. *et al.* Elucidating membrane structure and protein behavior using giant plasma membrane vesicles. *Nat. Protoc.* **7**, 1042-1051 (2012).
62. M.J.Hogue THE EFFECT OF HYPOTONIC AND HYPERTONIC SOLUTIONS ON FIBROBLASTS OF THE EMBRYONIC CHICK HEART IN VITRO. *Journal of Expermental Medicine* **30**, 617-648 (1919).
63. R.E.Scott Plasma membrane vesiculation: a new technique for isolation of plasma membranes. *Science* **194**, 743-745 (1976).
64. Holowka, D. & Baird, B. Structural studies on the membrane-bound immunoglobulin E-receptor complex. 1. Characterization of large plasma membrane vesicles from rat basophilic leukemia cells and insertion of amphipathic fluorescent probes. *Biochemistry* **22**, 3466-3474 (1983).
65. Baumgart, T. *et al.* Large-scale fluid/fluid phase separation of proteins and lipids in giant plasma membrane vesicles. *Proc. Natl. Acad. Sci. U. S. A.* **104**, 3165-3170 (2007).
66. Jorgensen, I.L., Kemmer, G.C. & Pomorski, T.G. Membrane protein reconstitution into giant unilamellar vesicles: A review on current techniques. *Eur. Biophys. J.* **46**, 103-119 (2017).
67. J.Korlach, P.Schwille, Webb, W.W. & Feigenson, G.W. Characterization of lipid bilayer phases by confocal microscopy and fluorescence correlation spectroscopy. *proceedings of the National Academy of Sciences* **96**, 8461-8466 (1999).

68. D.M.Haverstick & M.Glaser Visualization of Ca2l-induced phospholipid domains. *proceedings of the National Academy of Sciences* **84**, 4475-4479 (1987).
69. Shimokawa, N., Hishida, M., Seto, H. & Yoshikawa, K. Phase separation of a mixture of charged and neutral lipids on a giant vesicle induced by small cations. *Chem. Phys. Lett.* **496**, 59-63 (2010).
70. Tsumoto, K., Matsuo, H., Tomita, M. & Yoshimura, T. Efficient formation of giant liposomes through the gentle hydration of phosphatidylcholine films doped with sugar. *Colloids Surf. B. Biointerfaces* **68**, 98-105 (2009).
71. R.A.Parente & B.R.Lentz Fusion and phase separation monitored by lifetime changes of a fluorescent phospholipid probe. *Biochemisty* **25**, 1021-1026 (1986).
72. Hamada, T., Kishimoto, Y., Nagasaki, T. & Takagi, M. Lateral phase separation in tense membranes. *Soft Matter* **7**, 9061 (2011).
73. Hamada, T. *et al.* Size-dependent partitioning of nano/microparticles mediated by membrane lateral heterogeneity. *J. Am. Chem. Soc.* **134**, 13990-13996 (2012).
74. Klymchenko, A.S. & Kreder, R. Fluorescent probes for lipid rafts: from model membranes to living cells. *Chem. Biol.* **21**, 97-113 (2014).
75. Kaiser, H.J. *et al.* Order of lipid phases in model and plasma membranes. *Proc. Natl. Acad. Sci. U. S. A.* **106**, 16645-16650 (2009).
76. Hammond, A.T. *et al.* Crosslinking a lipid raft component triggers liquid ordered-liquid disordered phase separation in model plasma membranes. *Proc. Natl. Acad. Sci. U. S. A.* **102**, 6320-6325 (2005).
77. Ando, H., Koike, Y., Koizumi, S., Ishida, H. & Kiso, M. 1,5-Lactamized Sialyl Acceptors for Various Disialoside Syntheses: Novel Method for the Synthesis of Glycan Portions of Hp-s6 and HLG-2 Gangliosides. *Angew. Chem.* **117**, 6917-6921 (2005).
78. K.Fujikawa *et al.* The First Total Synthesis of Ganglioside GalNAc - GD1a, a Target Molecule for Autoantibodies in Guillain–Barré Syndrome. *Chemistry—A European Journal* **17**, 5451-5651 (2011).
79. A.Imamura, H.Ando, H.Ishida & M.Kiso Ganglioside GQ1b: Efficient Total Synthesis and the Expansion to
Synthetic Derivatives To Elucidate Its Biological Roles. *The Journal of Organic Chemistry* **74**, 3009-3023 (2008).
80. Kinoshita, M. *et al.* Raft-based sphingomyelin interactions revealed by

new fluorescent sphingomyelin analogs. *J. Cell Biol.* **216**, 1183-1204 (2017).
81. Wu, E.S., Jacobson, K. & Papahadjopoulos, D. Lateral diffusion in phospholipid multibilayers measured by fluorescence recovery after photobleaching. *Biochemistry* **16**, 3936-3941 (1977).
82. Maekawa, T. *et al.* Molecular diffusion and nano-mechanical properties of multi-phase supported lipid bilayers. *Phys. Chem. Chem. Phys.* **21**, 16686-16693 (2019).
83. G.Weber & Farris, F.J. Synthesis and Spectral Properties of a Hydrophobic Fluorescent Probe: 6-Propionyl-2-(dimethylamino)naphthalene. *Biochemistry* **18**, 3075-3078 (1979).
84. Bunker, C.E., Bowen, T.L. & Sun, Y. A PHOTOPHYSICAL STUDY OF SOLVATOCHROMIC PROBE 6-PROPIONYL-Z(N,N-DIMETHYLAMINO)NAPHTHALENE (PRODAN) IN SOLUTION. *Photochem. Photobiol.* **58**, 499-505 (1993).
85. Owen, D.M., Rentero, C., Magenau, A., Abu-Siniyeh, A. & Gaus, K. Quantitative imaging of membrane lipid order in cells and organisms. *Nat. Protoc.* **7**, 24-35 (2011).
86. L.Brand & J.R.Gohlke Fluorescence Probes for Structure. *Annu. Rev. Biochem* **41**, 843-868 (1972).
87. T.Parasassi, F.Conti & E.Gratton Time-resolved fluorescence emission spectra of Laurdan in phospholipid vesicles by multifrequency phase and modulation fluorometry. *Cell. Mol. Biol. (Noisy-le-grand)* **32**, 103-108 (1986).
88. T.Parasassi, G.D.Stasio, G.Ravagnan, R.M.Rusch & E.Gratton Quantitation of lipid phases in phospholipid vesicles by the generalized polarization of Laurdan fluorescence. *Biophys. J.* **60**, 179-189 (1991).
89. T.Parasassi, E.Gratton, W.M.Yu, P.Wilson & M.Levi Two-photon fluorescence microscopy of laurdan generalized polarization domains in model and natural membranes. *Biophys. J.* **72**, 2413-2429 (1997).
90. Bagatolli, L.A. & E.Gratton A Correlation between Lipid Domain Shape and Binary Phospholipid Mixture Composition in Free Standing Bilayers: A Two-Photon Fluorescence Microscopy Study. *Biophys. J.* **79**, 434-447 (2000).
91. Gaus, K., Zech, T. & Harder, T. Visualizing membrane microdomains by Laurdan 2-photon microscopy. *Mol. Membr. Biol.* **23**, 41-48 (2006).
92. Kim, H.M. *et al.* A two-photon fluorescent probe for lipid raft imaging: C-laurdan. *ChemBioChem* **8**, 553-559 (2007).
93. Dinic, J., Biverstahl, H., Maler, L. & Parmryd, I. Laurdan and di-4-

ANEPPDHQ do not respond to membrane-inserted peptides and are good probes for lipid packing. *Biochim. Biophys. Acta* **1808**, 298-306 (2011).
94. Allen, J.A., Halverson-Tamboli, R.A. & Rasenick, M.M. Lipid raft microdomains and neurotransmitter signalling. *Nat. Rev. Neurosci.* **8**, 128-140 (2007).
95. Olsen, A.S.B. & Faergeman, N.J. Sphingolipids: membrane microdomains in brain development, function and neurological diseases. *Open Biol* **7** (2017).
96. Luo, C., Wang, K., Liu, D., Li, Y. & Zhao, Q. The functional roles of lipid rafts in T cell activation, immune diseases and HIV infection and prevention. *Cell. Mol. Immunol.* **5**, 1-7 (2008).
97. Dirkx, R., Jr. & Solimena, M. Cholesterol-enriched membrane rafts and insulin secretion. *J Diabetes Investig* **3**, 339-346 (2012).
98. Belletti, B. *et al.* p27kip1 controls cell morphology and motility by regulating microtubule-dependent lipid raft recycling. *Mol. Cell. Biol.* **30**, 2229-2240 (2010).
99. Kirkham, M. & Parton, R.G. Clathrin-independent endocytosis: new insights into caveolae and non-caveolar lipid raft carriers. *Biochim. Biophys. Acta* **1745**, 273-286 (2005).
100. W.Baron, L.Decker, H.Colognato & C.K.Ffrench-Constant Regulation of Integrin Growth Factor Interactions in Oligodendrocytes by Lipid Raft Microdomains. *Curr. Biol.* **13**, 151-135 (2003).
101. Lee, M.Y., Ryu, J.M., Lee, S.H., Park, J.H. & Han, H.J. Lipid rafts play an important role for maintenance of embryonic stem cell self-renewal. *J. Lipid Res.* **51**, 2082-2089 (2010).
102. Bieberich, E. It's a lipid's world: bioactive lipid metabolism and signaling in neural stem cell differentiation. *Neurochem. Res.* **37**, 1208-1229 (2012).
103. Bonaventura, G. *et al.* Laurdan monitors different lipids content in eukaryotic membrane during embryonic neural development. *Cell Biochem. Biophys.* **70**, 785-794 (2014).
104. Mayor, S. & Riezman, H. Sorting GPI-anchored proteins. *Nat. Rev. Mol. Cell Biol.* **5**, 110-120 (2004).
105. Kimberley, F.C., Sivasankar, B. & Paul Morgan, B. Alternative roles for CD59. *Mol. Immunol.* **44**, 73-81 (2007).
106. Taberner, F.J., Fernandez-Ballester, G., Fernandez-Carvajal, A. & Ferrer-Montiel, A. TRP channels interaction with lipids and its implications in disease.

Biochim. Biophys. Acta **1848**, 1818-1827 (2015).
107. Ciardo, M.G. & Ferrer-Montiel, A. Lipids as central modulators of sensory TRP channels. *Biochim Biophys Acta Biomembr* **1859**, 1615-1628 (2017).
108. Morenilla-Palao, C., Pertusa, M., Meseguer, V., Cabedo, H. & Viana, F. Lipid raft segregation modulates TRPM8 channel activity. *J. Biol. Chem.* **284**, 9215-9224 (2009).
109. Szoke, E. *et al.* Effect of lipid raft disruption on TRPV1 receptor activation of trigeminal sensory neurons and transfected cell line. *Eur. J. Pharmacol.* **628**, 67-74 (2010).
110. Sághy, É. *et al.* Evidence for the role of lipid rafts and sphingomyelin in Ca2+-gating of Transient Receptor Potential channels in trigeminal sensory neurons and peripheral nerve terminals. *Pharmacol. Res.* **100**, 101-116 (2015).
111. Varshney, P., Yadav, V. & Saini, N. Lipid rafts in immune signalling: current progress and future perspective. *Immunology* **149**, 13-24 (2016).
112. Meer, G.V., Voelker, D.R. & Feigenson, G.W. Membrane lipids: Where they are and how they behave. *Nat. Rev. Mol. Cell Biol.* **9**, 112-124 (2008).
113. Ishitsuka, R., Saito, T., Osada, H., Ohno-Iwashita, Y. & Kobayashi, T. Fluorescence image screening for chemical compounds modifying cholesterol metabolism and distribution. *J. Lipid Res.* **52**, 2084-2094 (2011).
114. Honda, A. *et al.* Extracellular signals induce glycoprotein m6a clustering of lipid rafts and associated signaling molecules. *J. Neurosci.* **37**, 4046-4064 (2017).
115. Buschiazzo, J. *et al.* Cholesterol depletion disorganizes oocyte membrane rafts altering mouse fertilization. *PLoS One* **8**, e62919 (2013).
116. Buschiazzo, J., Alonso, T.S., Biscoglio, M., Antollini, S.S. & Bonini, I.C. Nongenomic steroid- and ceramide-induced maturation in amphibian oocytes involves functional caveolae-like microdomains associated with a cytoskeletal environment. *Biol. Reprod.* **85**, 808-822 (2011).
117. Mamode Cassim, A. *et al.* Plant lipids: Key players of plasma membrane organization and function. *Prog. Lipid Res.* **73**, 1-27 (2019).
118. N.Murata & D.A.Los Membrane Fluidity and Temperature Perception. *Plant Physiol.* **115**, 875-879 (1997).
119. Mongrand, S. *et al.* Lipid rafts in higher plant cells: Purification and characterization of triton x-100-insoluble microdomains from tobacco plasma membrane. *J. Biol. Chem.* **279**, 36277-36286 (2004).
120. Borner, G.H. *et al.* Analysis of detergent-resistant membranes in

Arabidopsis. Evidence for plasma membrane lipid rafts. *Plant Physiol.* **137**, 104-116 (2005).
121. Furt, F., Simon-Plas, F. & Mongrand, S. Lipids of the Plant Plasma Membrane. **19**, 3-30 (2011).
122. Furt, F., Simon-Plas, F. & Mongrand, S. Lipids of the plant plasma membrane. *Plant Cell Monographs* **19**, 3-30 (2011).
123. Tjellstrom, H., Hellgren, L.I., Wieslander, A. & Sandelius, A.S. Lipid asymmetry in plant plasma membranes: Phosphate deficiency-induced phospholipid replacement is restricted to the cytosolic leaflet. *FASEB J.* **24**, 1128-1138 (2010).
124. Jiang, Z. *et al.* Plant cell-surface GIPC sphingolipids sense salt to trigger ca^{2+} influx. *Nature* **572**, 341-346 (2019).

Chapter 2. Colloidal Stability of Lipid/Protein - Coated Nanomaterials in Salt and Sucrose Solutions

2-1. Introduction

As I discuss in chapter one, development of manipulator for nanostructure on plasma membrane will be a promised novel cell-engineering technology. The design of manipulator, however, have intrinsic difficulties. Almost all biocompatible and/or plasma-membrane oriented nanomaterials are optimized for physiological conditions, including about 300 mM cations and/or anions. To observe the nanomaterial-membrane interaction requires no-salt condition because of the vulnerability of GUVs and reconstituted structures on GUVs against salts. For example, only 0.1 mM of calcium ion or 10 mM of sodium ion destabilized reconstituted model lipid raft (Lo domain) on GUVs and make a pseudo domain [1] [2] so that it is hard to estimate the nanomaterial-raft interaction. Collection precious data of lipid-bilayer and nanomaterial interaction is fundamentally important to proper design of develop and evaluation of bioactive nanomaterial toward control of physical property of plasma membrane but, the fundamental difficulty for *in vitro* analysis prevented researchers from data collection or perspective establishment[3]. It should also be noted that GUV aggregation under high salt condition is not be ignored even prepared by modern method .[3]

In this chapter, I introduced the first detail investigation of salting-in and salting-out effect on biocompatible nanomaterial dispersion. I also reveal that sucrose also show the same effect on a kind of such nanomaterials and cationic dipole-sugar interaction and protein-sugar interaction is essential to let sugar exhibit the salting-in like effects. The investigation proposed the co-stabilization dispersion condition for both of biocompatible nanomaterial and GUVs and will become a new perspective to analyze nanomaterial-cell interaction in detail.

Research on Nanomaterial - cell interfaces is of attracting inter as this serves in understanding the behavior, fate, and functions of cells and control them by using nanomaterials.[4-6] The colloidal stabilization of plasmonic nanomaterial under

physiologically relevant environment is essential part of this study because the tendency of colloidal stability tuning or sometimes completely off the plasmonic nature of nanomaterials[6-8]. For instance, the near-infrared (NIR) absorption peaks of gold nanorods (AuNRs) disappears upon their aggregation. [9]

AuNR is a candidate of a bioactive nanomaterial because of the stability derived from one of gold, local photothermal properties and photodynamic properties originated from the plasmonic absorbance of NIR laser .[10] The surface of AUNR not only have plasmonic characteristic but can intact with bioactive macromolecules and other covering materials including protein and DNA. [10-13] Consequently, processing the surface chemistry of plasmonic nanomaterials is extensively studied owing to the potential biomedical applications.[14-16]

In previous study, high-density lipoprotein (HDL) mutant, a reconstituted discoidal lipid/protein nanomaterial composed of lipid bilayer disk and surrounding Apo-A1 protein[17] bearing with cell penetrating peptide (CPP) was chosen as a good covering material of AuNRs[18]. The HDL mutant efficiently shrouded AuNRs and bound to the plasma membrane without cytotoxicity. AuNRs covered with HDL mutant which is embraced cationic lipids, called plasma membrane-targeted gold nanorods (pm-AuNRs) enables safe photoactivation without membrane disruption on neuronal cells.[19]

Giant unilamellar vesicles (GUVs) are cell-sized liposomes of dozens of μm in diameter, which have been widely recognized as a good model of the plasma membrane to gain mechanistic insight due to their similarity in the size and curvature as living cells and affordability in various kinds of phases, lipid compositions and domain formations. [20, 21]

These features of GUVs represented physical aspects including the mobility of lipid bilayer or the extent of the curve of the plasma membrane profitably. GUVs have already been utilized for analysis of lipid diffusion, reconstitution and investigation of model lipid rafts and for the soft matter aspects of nanomaterial-membrane interactions.[22-25] Additionally, GUVs enable experiments in diversified biophysical conditions, e.g., pH, temperature, etc.[1, 26] However, GUVs are generally aggregated in the presence of salt, e.g., in phosphate-

buffered saline (PBS), while there exist a few methods for GUV preparation under the presence of salt, and sucrose solution is used to stabilize them in salt-free and osmotic aqueous media[26]. To harness the data obtained in GUV systems to nano-science studies toward living cell smoothly, nanomaterials of interest need to be colloidally stabilized and exercise their ability in both salt and sucrose aqueous solutions. Herein, the above-mentioned AuNRs and their derivatives are systematically prepared in surface condition and I investigate their colloidal stability in the two solutions to propose a general strategy to stabilize physiological condition-oriented nanomaterial in GUV-favorable condition.

2-2. Results

As a starting nanomaterial, the above mentioned AuNRs (plasma membrane - targeted AuNRs, pm-AuNR) were chosen (Fig.1) The schematic images of HDL and pm-AuNRs are described in Fig.1A AuNRs were synthesized in Seed-mediated method in CTAB solution and surface CTA+ are replace with sodium oleate proceeded with HDL-covering process. The surface derived from HDL did not effect on plasmonic absorbance of AuNR essentially as shown in Fig.1C. The surface charge of ingredient AuNRs, covered with either CTA+ or oleate, were measured in advance like shown in Fig.1D. Oleate-coated AuNR shows very negative zeta-potential without HDL.

pm-AuNR were prepared from oleate coated AuNRs and HDL including 30% of DOTAP, 1,2-dioleoyl-3-trimethylammonium-propane, a cationic lipid, in a lipid molar ratio. The presence of the protein on the surface of pm-AuNR was confirmed by SDS-PAGE analysis shown in Fig.2 The calculated protein concentration was 38 ug/mL in dispersants containing ca.1mg/mL of AuNR, as same value as previous HDL-coated AuNR dispersants.

pm-AuNRs (ca. 1 mg Au) were centrifuged and re-dispersed in MillQ (deionized and filtrated water), 200 mM sucrose solution, or aqueous PBS buffer (pH 7.4). The dispersed pm-AuNRs were observed by light and electron microscopy (TEM) (Fig.3A, Fig.4). In both conditions, pm-AuNRs were gathered in MilliQ, non-salt condition and well-dispersed in PBS buffer, a physiological condition. Surprisingly, pm-AuNRs also exhibit colloidal stability in 200 mM sucrose solution without salts. Both of bright-field and TEM images said that there was no large aggregation in both of 200 mM sucrose and PBS buffer but, in MilliQ solution, huge aggregates

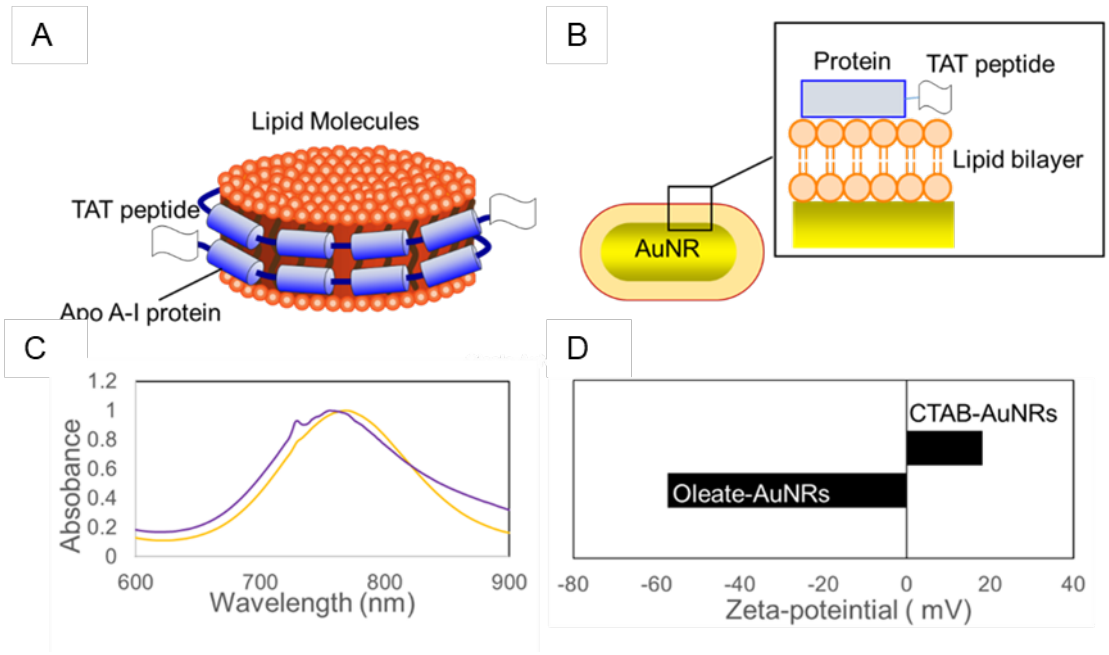

Figure 1. Schematic image of an HDL mutant (A) and pm-AuNR (B) The HDL mutant is assumed to be composed of a discoidal phospholipid bilayer and two copies of a TAT peptide-fused apoA-I protein (Apo-TAT protein. Previous study (T. Murakami et al. ACS Nano 2014, 8, 7370–7376) suggests that the HDL mutant components form a coating on the AuNR surface as shown in the inset. Normalized NIR spectra (C) and Zeta-potentials (D) of as-synthesized (CTAB-coated) and oleate-coated AuNRs are also shown. In C), the spectrum of CTAB-coated AuNRs (orange) was measured in 0.1 M CTAB and that of oleate-AuNRs (purple) measured in deionized water. Zeta-potential measurement was performed after dilution of them by 40-fold with 20 mM Tris-HCl buffer, pH 7.4.

of pm-AuNRs existed. The maximum size shown in Fig. 3A was above 50 μm. Even though the shapes of single AuNRs were essentially same in the three dispersions (Fig3A, lower, and Fig. 5), their NIR absorption spectra of pm-AuNRs in MilliQ were diminished. In contrast, pm-AuNRs in PBS and 200 mM solution exhibited shape NIR absorbance peaks around 760 nm, which are the same as ingredient AuNRs shown in Fig3B.

Dynamic light scattering (DLS) data supported that pm-AuNRs aggregated in deionized H2O and dispersed well in the other two solutions (Fig.6A). DLS

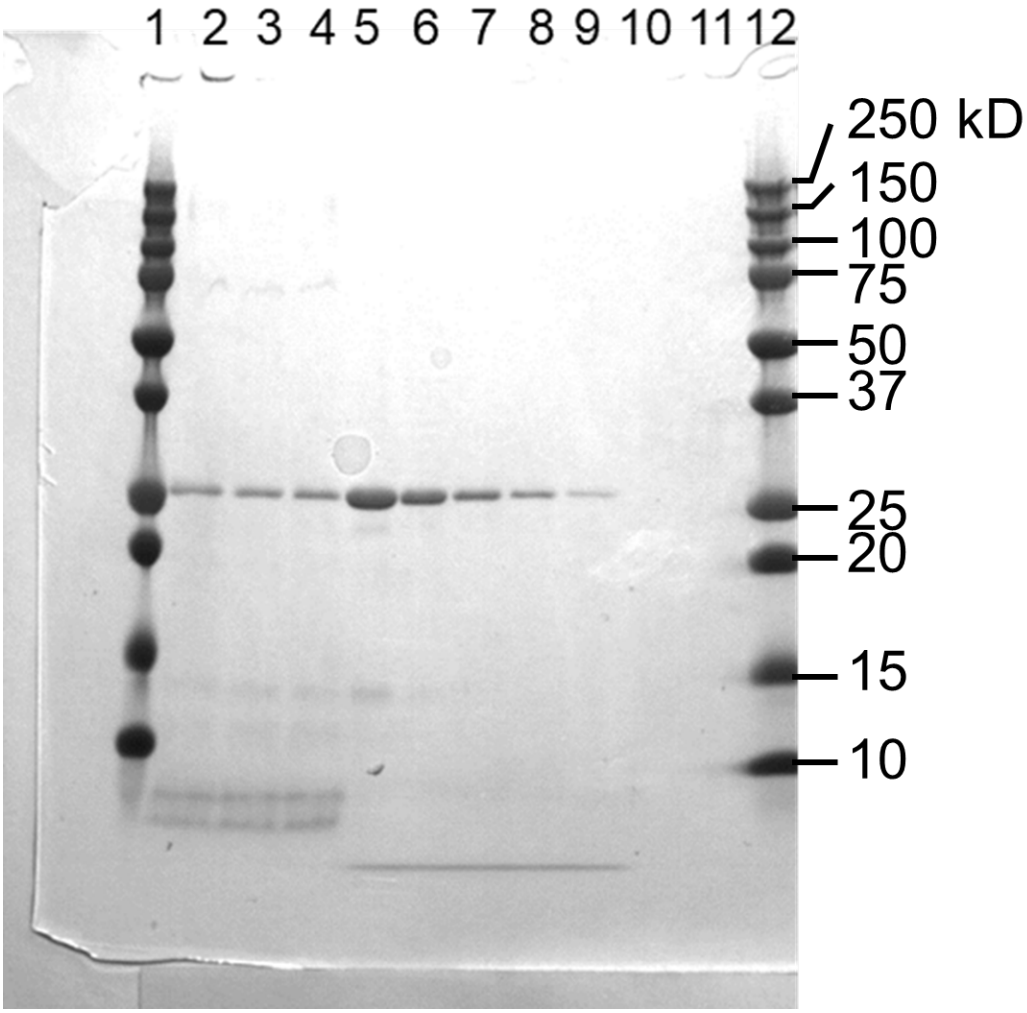

Figure 2. SDS-PAGE Analysis of Apo-TAT protein on AuNR surface. Protein concentration was 38 ug/mL in pm-AuNR dispersion (AuNR concentration was ca. 1 mg/mL). This w/w ratio of protein to AuNR analyzed by SDS-PAGE corresponded with our previous study. (T. Murakami et al. ACS Nano 2014, 8, 7370–7376). Lane 1 and 12: molecular weight marker. Lane 2–4:pm-AuNRs in ca. 1 mg/mL. Lane 5–10: free Apo-TAT protein from 187.5 μg/ml to 5.86 μg/mL.

analysis is known to be applicable to anisotropic nanomaterials such as AuNRs under specific conditions and the relative comparison of hydrodynamic diameter data have been utilized to judge their aggregation[13]. The large material is observed in MilliQ dispersant and not observed in PBS buffer or 200 mM sucrose solution. These results clearly demonstrated that pm-AuNRs can maintain high colloidal stability as in 200 mM sucrose as in PBS[27]. On the other hand, simply

cationized AuNRs with a well-known dispersant, hexadecyltrimethylammonium bromide (CTAB) did not show such dual stability (Fig.5B, Fig.6). The DLS data indicated that CTAB-AuNR is dispersed well in MilliQ after removal of free CTAB by centrifuge and in 200 mM sucrose solution, the colloidal behavior of AuNR were changed. NIR peak wavelength was almost same but the shape of peak broadened in 200 mM sucrose solution compared with MilliQ. And PBS buffer completely destabilized CTAB-AuNRs like in MilliQ condition for pm-AuNRs.

The behavior of CTAB-AuNRs is not surprising because salting-out effect of ions for nanomaterials is wildly acceptable phenomenon. In contrast, the behavior of pm-AnNRs looks like not to obey the role of colloidal chemistry. However, The

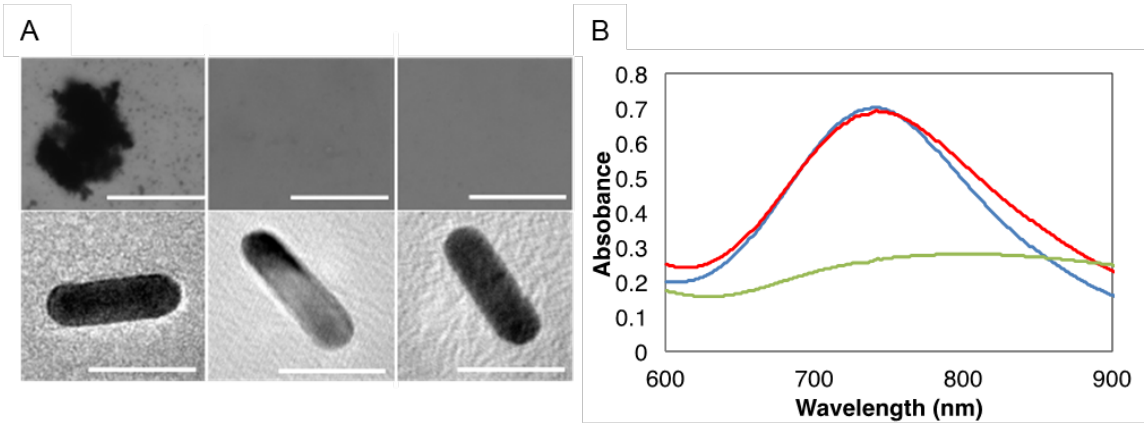

Figure 3. Structures of pm-AuNRs under various conditions. (A) Upper column: Bright field picture of pm-AuNRs dispersion in MilliQ (left), phosphate-buffered saline (PBS, pH 7.4) (middle), and 200 mM sucrose (right). Scale bar, 50 μm. Lower column: Electron microscopic (TEM) image of pm-AuNRs previously dispersed in MillIQ (left), phosphate-buffered saline (PBS, pH 7.4) (middle), and 200 mM sucrose (right). Scale bar, 20 nm. (B) NIR absorption spectra of pm-AuNRs in PBS (blue), 200 mM sucrose solution (red), and MilliQ (green).

better dispersion of pm-AuNRs in PBS than in deionized water would be

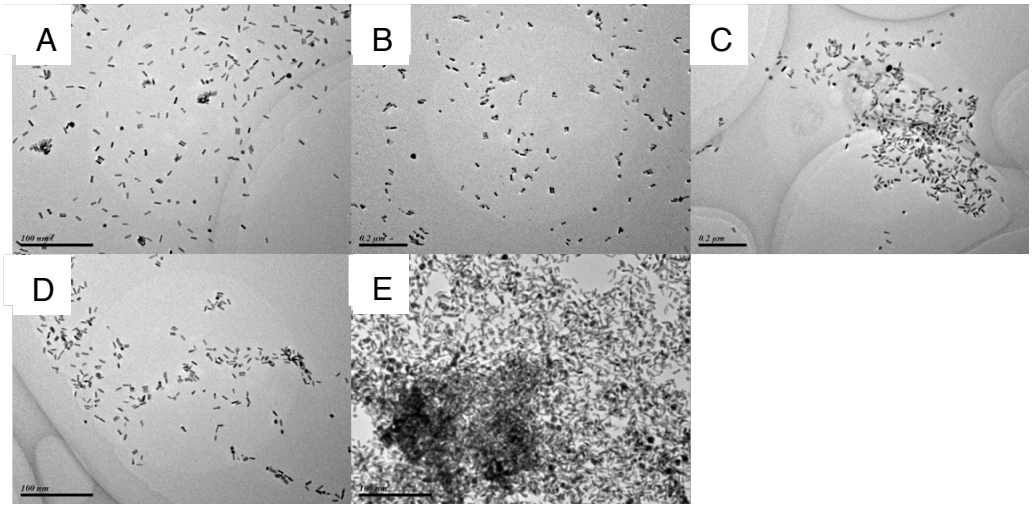

Figure 4. Typical TEM images of gold nanorods. (A) CTAB-coated AuNRs, (B) oleate-coated AuNRs, (C) pm-AuNRs in PBS buffer, (D) pm-AuNRs dispersed in 200 mM sucrose, and (E) pm-AuNRs in MilliQ.

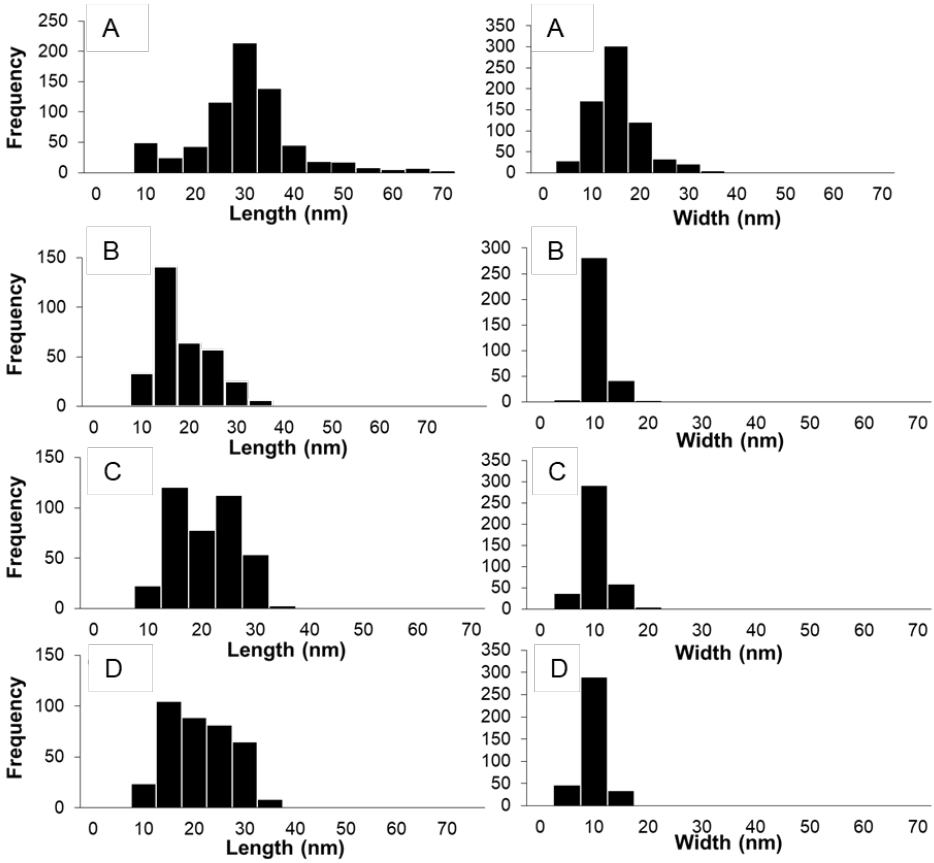

Figure 5. Histogram of the length (left column) and width (right column) of AuNRs in the TEM images of Figure 4. (A) CTAB-AuNRs, (B) oleate-coated AuNRs, (C) pm-AuNRs dispersed in PBS buffer, (D) pm-AuNRs dispersed in 200 mM sucrose. Left column shows the longer length and right column shows the width.

explained by salting-in effects, utilized wildly to explain the well dispersion of macromolecules or proteins in low salt condition[27].

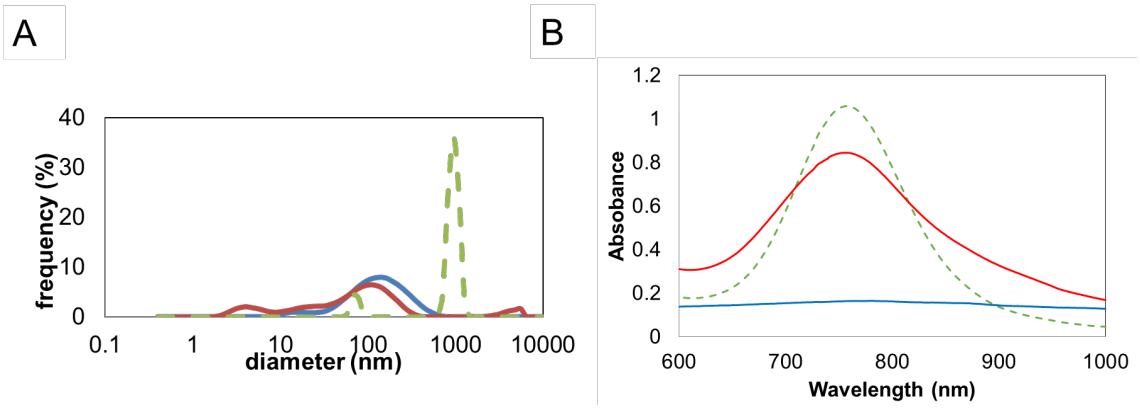

Figure 6. Dispersion of CTAB-AuNRs. (A)Volume size distribution determined by DLS analysis for pm-AuNRs in PBS (blue), 200 mM sucrose (red) and MillIQ (green). (B) NIR absorption spectra of CTAB-coated AuNRs in PBS (blue), 200 mM sucrose (red) and MillIQ (green).

Salting-in effect of pm-AuNRs dispersion is monitored by varying the concentration of PBS buffer. In fact, the NIR absorption peak of pm-AuNRs became the most obvious at 0.05× PBS condition and the intensity was gradually decreased over 0.5× PBS (Fig. 7A, B). The latter results in high-salt concentrations suggested aggregation of pm-AuNRs, which is a typical phenomenon explained by salting-out effects.[28] Figure 8A shows the hydrodynamic diameter data of pm-AuNRs in various PBS concentrations from DLS results. The precipitation of pm-AuNRs precluded the analysis in MilliQ, but in the range of 0.05–0.5× PBS, reasonable hydrodynamic diameter data were obtained, which were comparable to the ones in Fig.1 and Fig.6 In accordance with the results in Figure 7B, the diameter value became larger at >0.5× PBS concentrations. These data clearly demonstrated that the presence of relatively low condition of salts is favorable for the colloidal stabilization of pm-AuNRs, which would be interpreted as the results of salting-in effects. This is a first example of carefully explained salting-in effects on the colloidal stability of metal biocompatible nanomaterials.

Interestingly, a similar concentration tendency was observed for the sucrose dispersions of pm−AuNRs (Fig. 7C, 7D and 3B). The NIR peak intensity of pm -

AuNRs showed a bell-shaped profile with a maximum at 400 mM (Fig.7D), and the hydrodynamic diameter was the smallest at the same concentration (Fig.8B). These data suggested that the colloidal stability of pm-AuNRs in sucrose solutions was determined under similar mechanisms to salting-in and salting-out effects in PBS. To gain insight into the mechanisms, the zeta potential of pm-AuNRs was measured at different concentrations of sucrose (Fig.9). As a result, the value was gradually decreased along with the increase of sucrose concentration from 50 to 400 mM and appeared to reach a plateau of 20 mV, although sucrose molecules are neutral. This graph indicate that sucrose molecules somehow shield the positive surface charge of pm-AuNRs and increase their colloidal stability in the range of 50-400 mM. This mechanism is just similar to one of salting-in effects observed at relatively low salt concentrations.[29]

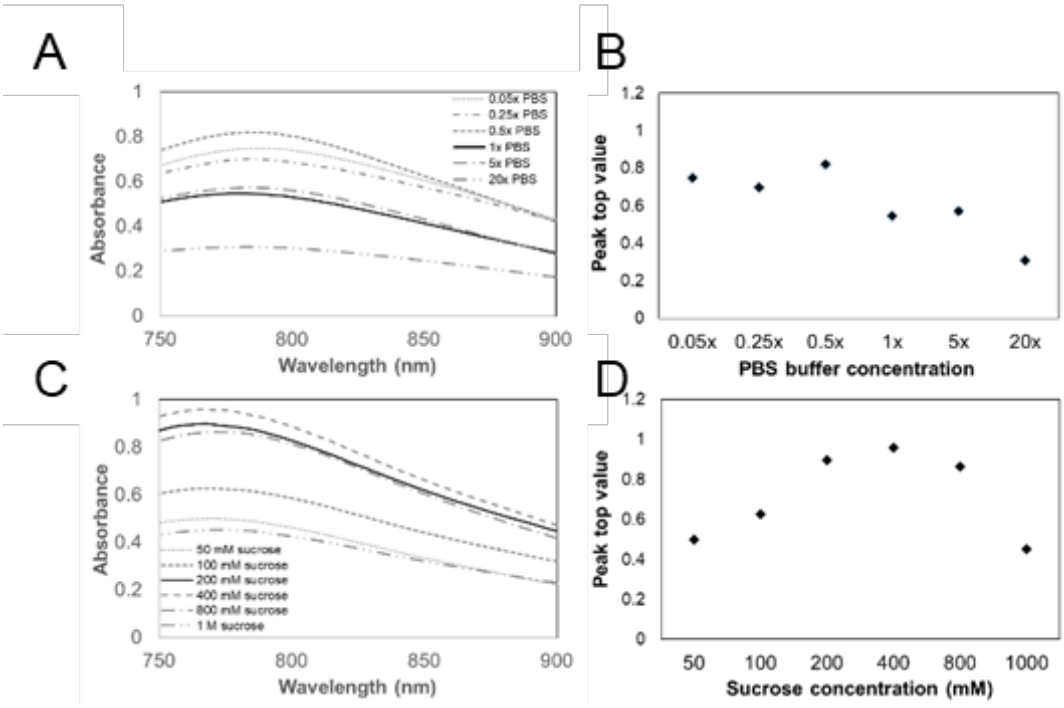

Figure 7. Effects of the concentration of PBS (A, B) and sucrose (C, D) on the colloidal stability of pm- AuNRs.(A) NIR absorption spectra of pm-AuNRs in 0.05x, 0.25x, 0.5x, 1x, 5x or 20x PBS. (B) Peak top absorbance values in (A). (C) NIR absorption spectra of pm-AuNRs in 50 mM, 100 mM, 200 mM, 400 mM, 800 mM or 1000 mM sucrose solution. (D) Peak top absorbance values in (C)

To the best of our knowledge, this is the first obviously demonstration that

hydrophobic colloids like metal nanomaterials were dispersible in both PBS and sucrose solutions and that salting-out effects and salting-in effects governed the colloidal stability of nanomaterials in physiologically relevant media and sugar solution. [30, 31]

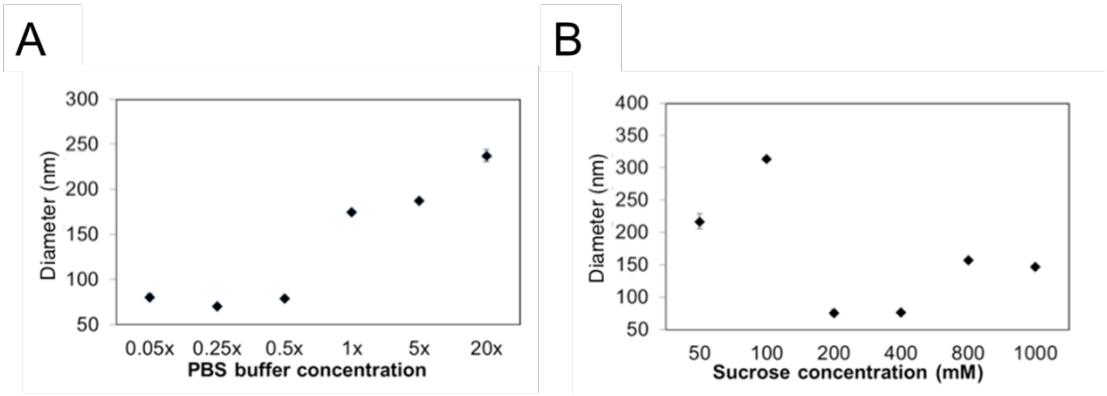

Figure 8. Hydrodynamic diameter based on dynamic light scattering (DLS) data of pm-AuNRs in various concentrations of PBS (a) and sucrose (b).

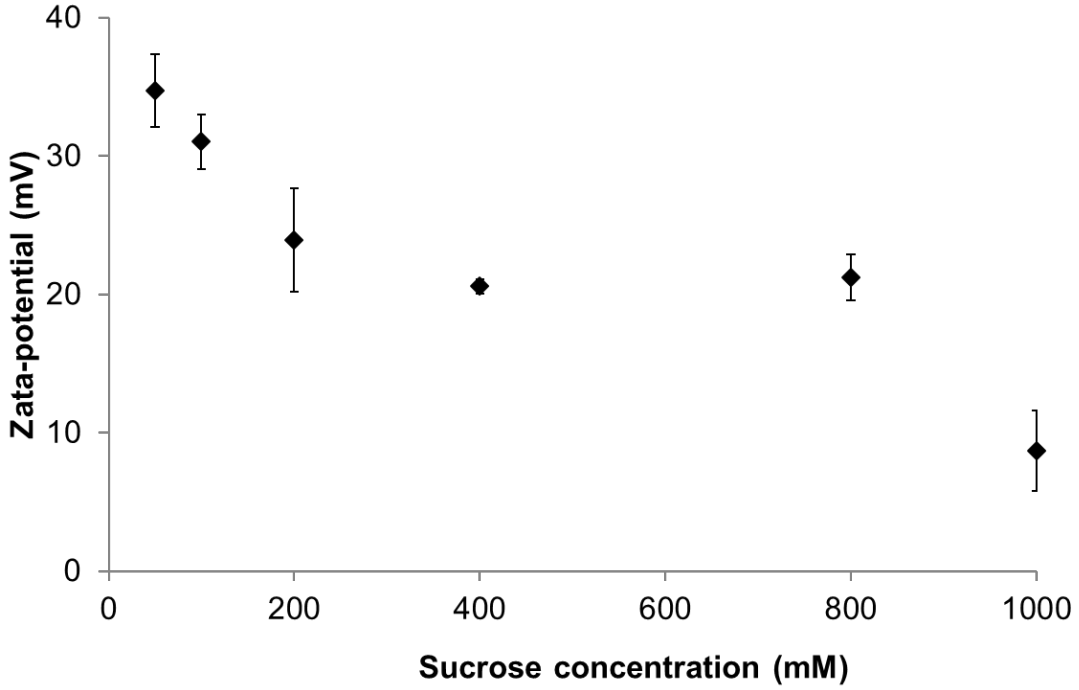

Figure 9. Zeta-potentials of pm-AuNRs in various concentration of sucrose concentration Zeta potential analysis in the absence of sucrose, i.e., in MillIQ, was precluded by aggregation of pm-AuNRs (see Figure 2).

By this sucrose concentration-dependent neutralization of the surface charge

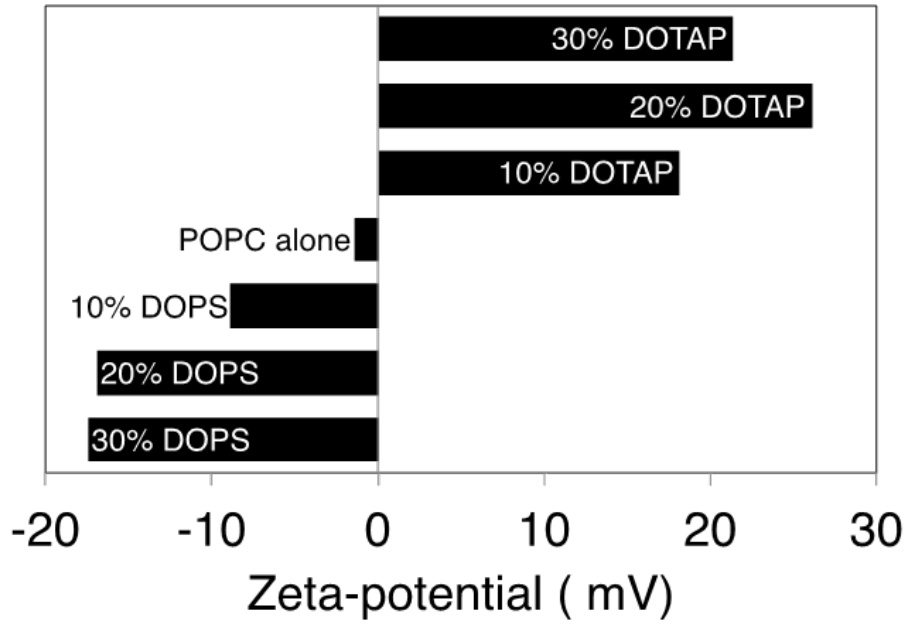

Figure 10. Zeta-potentials of HDL derivatives prepared with various contents of a neutral lipid (POPC) and a positively (DOTAP) or a negatively (DOPS) charged lipid. Lipid contents are shown in the graph. HDL samples were diluted by 40-folds with 20 mM Tris-HCl buffer (pH 7.4) before measurement.

of pm-AuNRs, I suspected some putative involvement of electrostatic interaction between sucrose molecules and the surface material of pm-AuNRs in the increase in colloidal dispersibility. To validate this hypothesis, six types of pm-AuNRs bearing different surface. These pm-AuNRs were prepared from HDL derivatives which included DOTAP or DOPS, 1,2-dioleoyl-sn-glycero-3-phospho-L-serine, a anionic lipids in the bilayer of each HDLs from 0 % to 30 %. As expected, newly prepared six kinds of HDL mutants exhibited different zeta-potential values in accordance with the ratio of charged lipids (Fig. 10). It should be noted that the yield of cationic HDL decreased depending on the ratio of DOTAP and, above 30% DOTAP ratio, it is quite hard to prepare nanomaterials which can be presumed to be HDL (data not shown) so I limited the amount of charged lipid ratio to 30%.

Six types of pm-AuNR derivatives were synthesized with these HDL mutants in a similar manner. As inferred from the absorption spectra (Fig.11), like their original counterparts from HDL bearing 30% DOTAP (original pm-AuNRs), all

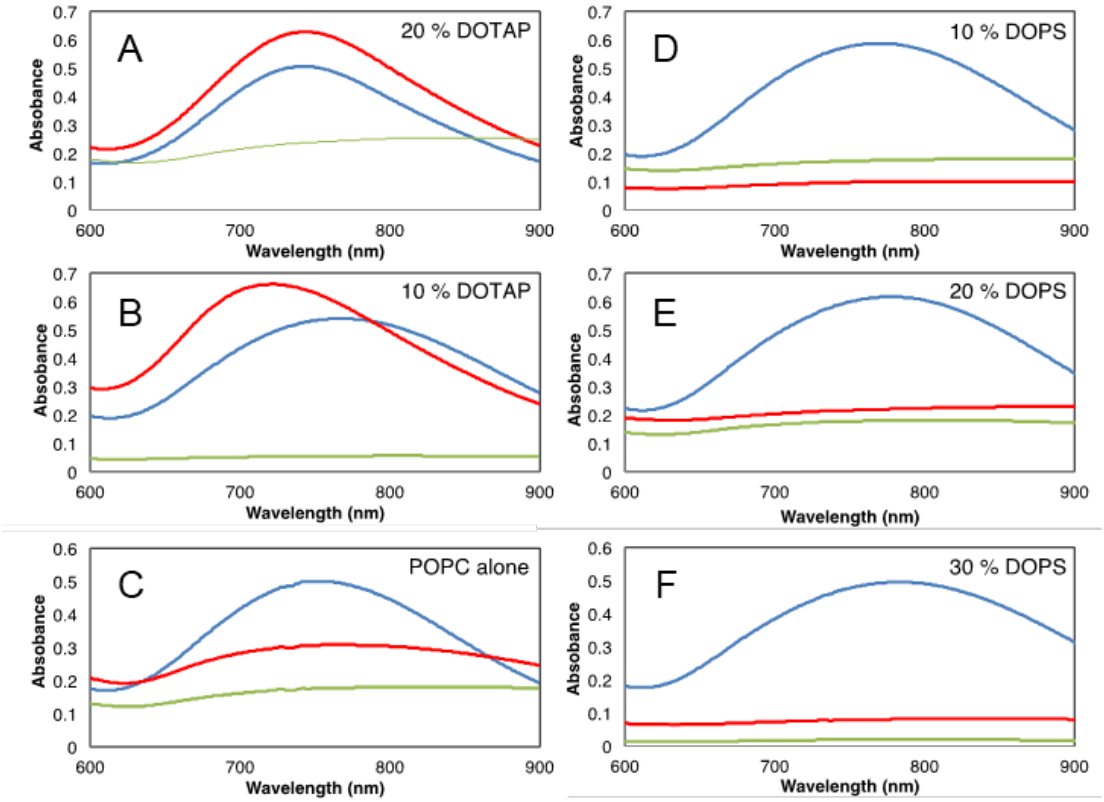

Figure 11. NIR absorbance spectra of AuNRs containing the various amount of a positively (DOTAP) or negatively charged lipid (DOPS) in PBS (blue), 200 mM sucrose solution (red), or MillIQ (green). Lipid contents are shown in the graph.

derivatives were dispersed well in PBS buffer and not in MiliQ. However, in 200 mM sucrose solution, their colloidal stability dwindled as the degree of the cationization of AuNRs was decreased. Under 10 % DOTAP concentration or anionic pm-AuNR did not dispersed well in 200 mM sucrose solution. The size distribution of the derivatives showed the same tendency (Fig.12). Cationic pm-AuNRs show peaks around 100 to 200 nm diameter in both PBS and sucrose solutions. In 10 % DOTAP concentrations, peak in 200 mM sucrose solution shifted to larger area compared with PBS buffer dispersion samples. And in neutral or anionic samples, the peaks of pm-AuNRs were almost same in 200 mM sucrose solution and MilliQ. These data strongly support my hypothesis about the reason why sucrose cause salting-in like effects.

It has been reported that sucrose can stabilize proteins and lipid bilayer vesicles

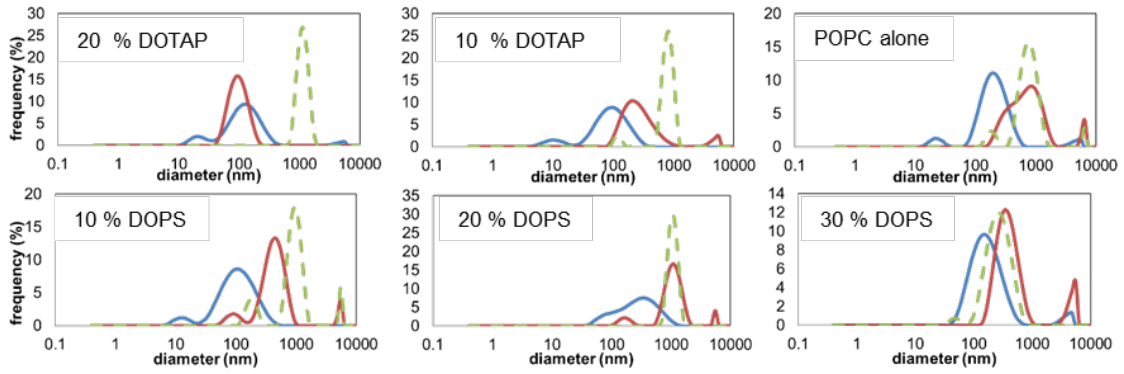

Figure12. Volume size distribution determined by DLS analysis for six types of pm-AuNR derivatives, prepared with different lipid contents, in PBS (blue), 200 mM sucrose (red) and MillQ (green). Lipid contents are shown in the graph.

during lyophilization, possibly via hydrogen bonding,[32-35] but no report is available yet regarding the application of sucrose for stabilization of nanomaterials in solution. To investigate the role of the pm-AuNR components, i.e., DOTAP, apoA–I protein and TAT peptide, in bestowing the stability, pm-AuNRs lacking either of them were prepared. In the absence of TAT peptide (Fig.13, Fig.14A, B, C), pm-AuNRs were dispersed in both PBS and sucrose, to a similar degree, relatively regardless of the charge of lipids. Both of DOTAP 30% and 0 % HDL surface can disperse pm-AuNRs in both of PBS buffer and 200 mM sucrose condition. NIR peaks intensity of anionic pm-AuNRs bearing DOPS in 30% ratio slightly decreased in the 200 mM sucrose solution but not diminished completely.

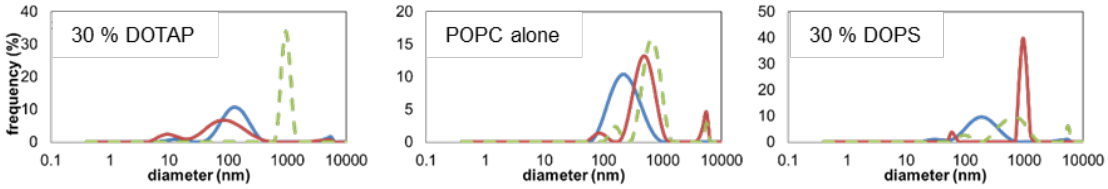

Figure 13. Volume size distribution determined by DLS analysis for of pm-AuNR derivatives lacking TAT peptide, prepared with different lipid contents, in PBS (blue), 200 mM sucrose (red) and MillIQ (green). Lipid contents are shown in the graph.

In the absence of both apoA–I protein and TAT peptide, on the other hand, the colloidal stability of pm-AuNRs in PBS and 200 mM sucrose was significantly decreased (Fig.14D) and completely lost without DOTAP (with POPC alone) (Fig. 14E). These spectra indicated that both DOTAP and apoA–I protein play a

significant role in the colloidal stability of pm-AuNRs in PBS and 200 mM sucrose, respectively. The stabilization by the apoA–I protein in PBS would be attributed to salting-in effects.

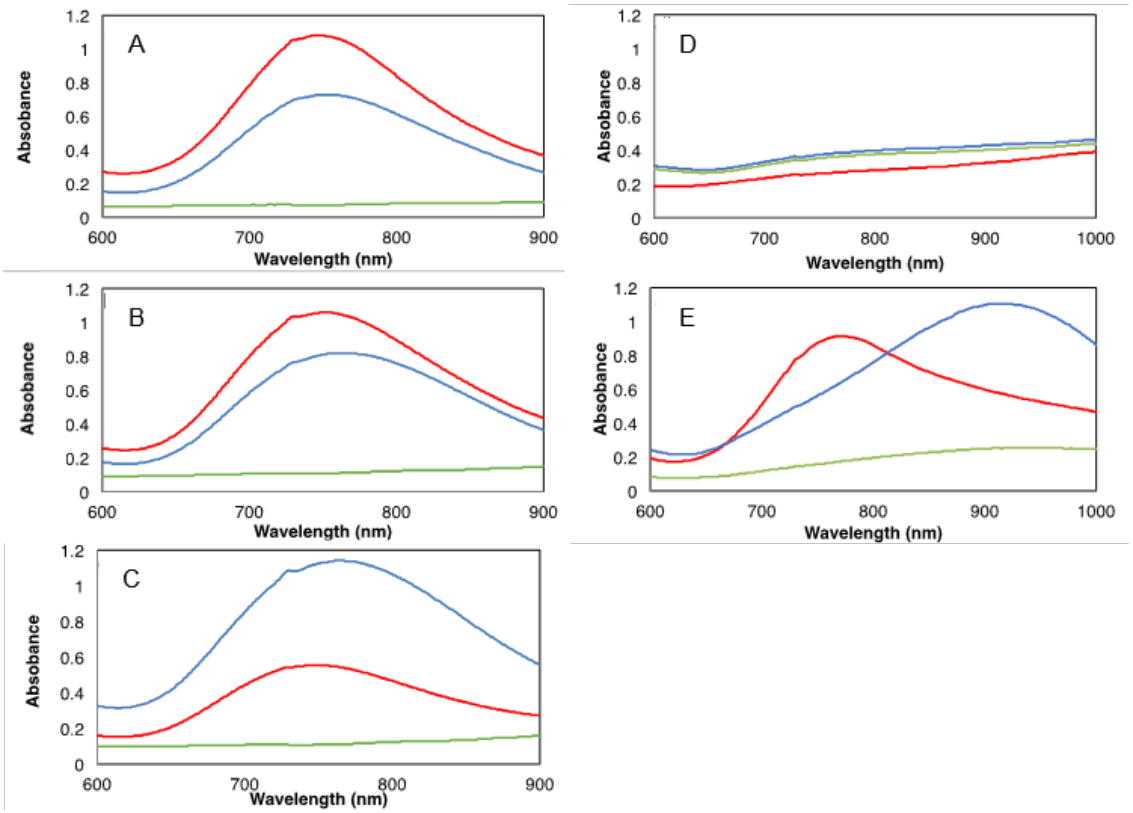

Figure 14. NIR absorbance spectra of various pm-AuNRs, lacking TAT peptide with (A) 30% DOTAP, (B) POPC alone, and (C) 30% DOPS and lacking both apoA-I and TAT peptid with (D) 30% DOTAP and (E) POPC alone, in PBS (blue), 200 mM sucrose solution (red), or MilliQ (green)

At this moment, the precise reason behind the stabilization by DOTAP in sucrose solution is still enigma, but it is reasonable to presume from the data in from Fig.5 to 8 that the ion-dipole interaction between the cation of DOTAP and the dipole of sucrose (hydroxyl groups) plays a role via salting-in like effects.

Finally, a nanomaterial-membrane interaction study was performed in 200 mM sucrose with fluorescently-labeled pm-AuNRs and GUVs with a liquid order (Lo) membrane, which allowed the binding of small particles of ≤200 nm in diameter. As shown in Fig.13, the bright filed image observed by a phase difference microscope showed that a GUV appeared to be spherical even in the presence of pm-AuNRs and pm-AuNRs accumulated on the Lo phase region as soft matter

physics predicted. This data demonstrated that well-dispersed pm-AuNRs in 200 mM sucrose are applicable to nanomaterial-lipid bilayer interaction studies with GUVs.

2-3. Discussion

Our data suggested that sucrose can bind to the surface of pm-AuNRs in certain conditions like serum proteins forming protein coronas of nanomaterials.[36, 37] The UV/Vis/NIR spectra of each pm-AuNR in each surrounding condition support the hypothesis that the interaction between sucrose molecule to the surface of original, DOTAP 30% pm-AuNRs. The salting-in effect like shift of pm-AuNR colloidal stability, observed by plasmonic peak intensity assay and DLS measurement also suggest the surface-sucrose interaction as ion-surface interaction in the previous salting-in effects.

Apo-A1 mutant also plays a key role on the well-dispersion of pm-AuNR in sucrose solution. The existence of TAT peptide caused the law stability in 200 mM sucrose in cationic, anionic, and neutral charged pm-AuNRs. In the previous purification method of apo-A1 mutant with TAT peptide expressed in E. coli, salting-in effect was utilized in the process of ammonium sulfate precipitation.[18] The protein part may be susceptible to the salting-in effect.

This phenomenon let researchers to dream that some interaction between pm-AuNRs and sugar-grope of molecules within the plasma membrane, e.g., gangliosides, inositol phospholipids, etc.[38] These glycolipid works as fundamental part of nanostructure on plasma membrane in various kinds of livings from animal to plant.[39, 40] Recent report says pm-AuNR can activate a kind of ion channel for heating or pain, transient receptor potential vanilloid type I (TRPV1)[19] was affected by the integrity of lipid rafts,[41] in which some gangliosides are localized.[42] Nanomaterial-cell interactions have attracted researchers from a wide range of disciplines, from physics to biology. Surprisingly, there are very few reports of detailed analysis of lipid domains-nanomaterials interactions in terms of fundamental physics viewpoint. I speculate that a major limitation is derived from the small investigation on colloidal stability of biocompatible nanomaterials: despite the establishment of the concept of the salting-in effect by Hofmeister et al. in the 1880s, few biomaterial scientists have attempted to apply this concept to biomaterial plasmonic nanoparticles. [29] In this chapter, I suggest that surface charge shielding is important in considering the dispersed state of biomaterial

nanoparticles, which is fundamental information for the application of physical theory of nanoparticle interactions with other objects.

2-4. Conclusions

I established a method to disperse AuNRs in both PBS and around 200 mM sucrose aqueous solution with HDL mutants-coating as well as its mechanism. Two part of a pm-AuNR, a cationic lipid (DOTAP) and a lipid binding protein (apoA–I), were found to contribute to the colloidal stabilization. Our systematic studies explained that this stabilization was basically brought by salting-in effects by PBS buffer and their allied influences by sucrose molecules. Thus, similar stabilization of other nanomaterials may be achieved by modifying their surface with both proteinous and cationic coating material or, perhaps, designed protein corona[43]. It is significant to note here that PBS is one of the most-widely utilized physiologically relevant media and around 200 mM sucrose solution, which is isotonic to PBS, has been chosen for GUV studies in aqueous media. Consequently, our findings would enable detailed investigation of bioactive nanomaterial-lipid bilayer interaction, especially lipid membrane domain formation or deformation under cell-free conditions and the subsequent live cell studies with the same nanomaterials.

2-5. Experimental section

General information

Materials General reagents including sucrose were purchased from Nacalai Tesque (Kyoto, Japan). 1× PBS buffer contains 137 mM of NaCl, 8.1 mM of NaH_2PO_4, 2.68 mM of KCl and 1.47 mM of KH_2PO_4. The PBS composition is popular and adjusted as neural pH in these compositions These inorganic salts were also obtained from Nacalai Tesque Inc. (Kyoto, Japan). L(+)-ascorbic acid, Silver nitride, and sodium oleate were obtained from Wako (Osaka, Japan). Gold (III) chloride and sodium borohydride were purchased from Sigma-Aldrich (Saint Louis, MO, USA). 1-palmitoyl-2-oleoyl-snglycero-3-phosphocholine (POPC) and 1,2-dioleoyl-sn-glycero-3-phospho-Lserine (sodium salt) (DOPS) 1,2-dipalmitoyl-sn-glycero-3-phosphocholin (DPPC) were obtained from NOF (Tokyo, Japan). N-(7-nitro-21,3-benzoxadiazol-4-yl)-1,2-dipalmitoyl-sn-glycero-3-phosphoethanolamine (NBD-PE), 1,2dioleoyl-3-trimethylammonium-propane (chloride salt) (DOTAP) and cholesterol were purchased from Avanti Polar Lipids, Inc. (Alabaster, AL, USA). Nap 5 column were purchased from GE Healthcare Life Sciences (Little Chalfont, Buckinghamshire, UK).

Synthesis of AuNRs (CTAB-coated)

AuNRs are synthesized in aqueous media in a seed-mediated method. [44]Typically, In all preparation, MilliQ was utilized as a solvent. Seed solution was prepared by rapid reduction of Au^{3+}. CTAB was freshly dissolved in 9.6 mL MilliQ at 30˚C. 50 μL of 50 mM $HAuCl_4$ aq were added while stirring. 600 μL of freshly-prepared and ice-cold 0.1 M $NaBH_4$ aq were added. Final concentration of CTAB was 0.1 M. After 1 h reaction with gentle stirring at 30˚C, seed solution was collected and was kept at room temperature. The color of seed solution was freshly prepared for each AuNR preparation and the color of seed solution was always brownish yellow. To growth AuNR. 600 μL of this seed solution was added to the mixture of 18. 3 mL of 0.1 M CTAB, 400 μL of 50 mM $HAuCl_4$, 800 μL of 0.2 mM $AgNO^3$, 320 μL of 1.6 mM L-ascorbic acid in a 50 mL glass vial tube while stirring vigorously. Just after this mixing process, stirring was stopped immediately and the reaction

solution was incubated at 30°C overnight under dark condition. The AuNRs were collected from dispersion by centrifuge at 20,000 × g for 40 min and the pellet was re-dispersed in 0.1 M CTAB aqueous solution as ca. 1 mg/mL in AuNR weight concentration for purification from residual reactants.

Preparation of pm-AuNRs

pm-AuNRs were synthesized according to our previous report. [45] Briefly, 1 mL of CTAB-coated AuNRs in 0.1 M CTAB (ca. 1 mg/mL) were pelleted by centrifugation and treated with sodium oleate solution. AuNR were collected from 1 mL the dispersant by centrifuge at 20,000 × g for 40 min and washed by MillIQ by removal of 900 μL of supernatant and fresh MilliQ to the reaction tube. After the centrifuge, 750 mL of supernatant was removed again and added freshly prepared 16 mg/mL of sodium oleate solution. It should be notified that the solution were sonicated vigorously to dissolve all of sodium oleates include small clear oleate crystal-like something. After that, the reaction solution was vortexed well and heated at 50 ˚C for 1h to replace surface CTAB to oleate. All residues were removed by Nap5 disposal column purification.

The resulting oleate-coated AuNRs were mixed with HDLs, which were prepared with a cell penetrating peptide (TAT peptide)-fused apoA-I protein, POPC and DOTAP[18, 19, 46]. After 1h reaction at 50 ˚C for coating, the reaction solution was centrifuged at 20,000 × g for 40 min, removed all supernatant. pm-AuNRs were re-dispersed by sonication and vortex in 1 mL of PBS, MilliQ, or 200 mM sucrose solution (ca. 1 mg/mL AuNR), respectably after washing with the corresponding solution (1 mL) once.

Lipid coating of AuNRs

Lipid films were dissolved in PBS containing 30 mg/mL sodium cholate at 13.6 mg/mL. The dispersions and oleated-coated AuNRs (ca.1 mg/mL) were mixed at a lipid/AuNR ratio of 10 and then coating reaction was performed by heating for 1 h at 50˚C. The heated mixture was centrifuged at 20,000 × g for 40 min, removed all supernatant, resuspend with 1ml of PBS, MilliQ, or 200 mM sucrose

solution and centrifuged again at 20,000 × g for 20 min to wash the lipid-coated AuNRs. After centrifuged, these AuNRs were re-dispersed as same as pm-AuNRs with the corresponding solutions (ca. 1mg/mL).

NIR absorption spectroscopy

The UV/VIS/NIR spectra of all AuNRs in this study were measured by a V630 spectrometer (JASCO, Tokyo, Japan). Each sample was diluted 20-fold with corresponding solutions just before applied into a measurement cell.

TEM and Zeta-potential measurement

TEM Images were obtained using JEM-2100 and analyzed with ImageJ.[47] Zeta-potential of HDLs and pm-AuNRs were measured by Zetasizer Nano-Z (Malvern, Worcestershire, UK) and viscosity of solutions, especially of sucrose solution, were calculated in advance and considered in the measurements by the Zetasizer software.

To gain data, samples were diluted 40-fold with 20 mM Tris-HCl buffer (pH 7.4) or appropriate sucrose solutions. In the case of pm-AuNRs, vortex and sonication were performed before measurement.

DLS measurement

pm-AuNRs were briefly sonicated and vortexed to disperse well as long as I can to gain correct data and then diluted 40-folds with the corresponding solution, PBS buffer, 200 mM sucrose or MilliIQ, before measurement with a Zetasizer Nano ZSP (Malvern, Worcestershire, UK).

GUV study

GUVs were prepared by electroformation method [48], a most widely utilized method to prepare GUVs having intended property. [49] 50 mM of DPPC and 50 mM cholesterol in chloroform solution were mixed in a small glass tube. A portion of the lipid mixture (5.7 mmol) was dropped and spread on an surface of ITO glass (8–12 Ω/sq, Sigma-Aldrich, MO). After heating for 5 min on a heater at 50˚C

to make all lipid to gel phase and evaporated organic solvents, the lipid film was further spread to make thin layer by a single drop of hot chloroform and then drying in vacuo for ≥2 h to remove any solvents completely. The sample glass was covered with another clean ITO glass to sandwich a silicon sheet (ca. 1 mm thickness) with a 1.5 mm square hole to prepare a small chamber on the lipid film. The inner space of the chamber was filled with 200 mM sucrose solution. An alternating current voltage (10 Hz, 0.6 mV) was applied to the chamber with an AFG-2005 function generator (TEXIO TECHNOLOGY CO., Japan) at 50˚C for 2 h, and then the sucrose solution containing GUVs was collected from the chamber. Fluorescently-labeled pm-AuNRs were synthesized in a similar manner to above-mentioned pm-AuNRs with the HDL mutant that was containing 6 mol% NBD-DPPE in lipid molar ratio. As-prepared GUVs and fluorescently labeled pm-AuNRs (ca. 1 mg Au/mL) were mixed in a 1:1 volume ratio and then the mixture was analyzed by an ECLIPSE Ti epifluorescence microscope (Nikon, Tokyo, Japan) with a lens for phase contrast imaging an appropriate filter.

2-6. References

1. Shimokawa, N., Hishida, M., Seto, H. & Yoshikawa, K. Phase separation of a mixture of charged and neutral lipids on a giant vesicle induced by small cations. *Chem. Phys. Lett.* **496**, 59-63 (2010).

2. Himeno, H. *et al.* Charge-induced phase separation in lipid membranes. *Soft Matter* **10**, 7959-7967 (2014).

3. Stein, H., Spindler, S., Bonakdar, N., Wang, C. & Sandoghdar, V. Production of Isolated Giant Unilamellar Vesicles under High Salt Concentrations. *Front. Physiol.* **8** (2017).

4. Nel, A.E. *et al.* Understanding biophysicochemical interactions at the nano-bio interface. *Nat Mater* **8**, 543-557 (2009).

5. Behzadi, S. *et al.* Cellular uptake of nanoparticles: journey inside the cell. *Chem. Soc. Rev.* **46**, 4218-4244 (2017).

6. Aggad, D. *et al.* Gemcitabine Delivery and Photodynamic Therapy in Cancer Cells via Porphyrin-Ethylene-Based Periodic Mesoporous Organosilica Nanoparticles. *ChemNanoMat* **4**, 46-51 (2018).

7. Tebbe, M., Kuttner, C., Mannel, M., Fery, A. & Chanana, M. Colloidally stable and surfactant-free protein-coated gold nanorods in biological media. *ACS Appl Mater Interfaces* **7**, 5984-5991 (2015).

8. Chanana, M., Correa-Duarte, M.A. & Liz-Marzan, L.M. Insulin-coated gold nanoparticles: a plasmonic device for studying metal-protein interactions. *Small* **7**, 2650-2660 (2011).

9. Cao, J., Sun, T. & Grattan, K.T.V. Gold nanorod-based localized surface plasmon resonance biosensors: A review. *Sensors Actuators B: Chem.* **195**, 332-351 (2014).

10. Dreaden, E.C., Alkilany, A.M., Huang, X., Murphy, C.J. & El-Sayed, M.A. The golden age: gold nanoparticles for biomedicine. *Chem. Soc. Rev.* **41**, 2740-2779 (2012).

11. Huang, X., Jain, P.K., El-Sayed, I.H. & El-Sayed, M.A. Plasmonic photothermal therapy (PPTT) using gold nanoparticles. *Lasers Med. Sci.* **23**, 217-228 (2008).

12. Matthews, J.R., Payne, C.M. & Hafner, J.H. Analysis of Phospholipid Bilayers on Gold Nanorods by Plasmon Resonance Sensing and Surface-Enhanced Raman Scattering. *Langmuir* **31**, 9893-9900 (2015).

13. Liu, H., Pierre-Pierre, N. & Huo, Q. Dynamic light scattering for gold nanorod size characterization and study of nanorod–protein interactions. *Gold Bulletin* **45**, 187-195 (2012).

14. Hutter, E. & Maysinger, D. Gold nanoparticles and quantum dots for bioimaging. *Microsc. Res. Tech.* **74**, 592-604 (2011).

15. Srinivasan, M., Rajabi, M. & Mousa, S. Multifunctional Nanomaterials and Their Applications in Drug Delivery and Cancer Therapy. *Nanomaterials* **5**, 1690-1703 (2015).

16. Alexandre Albanese, C.D.W., Jonathan B. Olsen, Hongbo Guo, Andrew Emili, and Warren C. W. Chan Secreted Biomolecules Alter theBiological Identity and CellularInteractions of Nanoparticles. *ACS Nano* **8**, 5515-5526 (2014).

17. Denisov, I.G. & Sligar, S.G. Nanodiscs in Membrane Biochemistry and Biophysics. *Chem. Rev.* **117**, 4669-4713 (2017).

18. Murakami, T., Wijagkanalan, W., Hashida, M. & Tsuchida, K. Intracellular drug delivery by genetically engineered high-density lipoprotein nanoparticles. *Nanomedicine (London, U. K.)* **5**, 867-879 (2010).

19. Nakatsuji, H. *et al.* Thermosensitive Ion Channel Activation in Single Neuronal Cells by Using Surface-Engineered Plasmonic Nanoparticles. *Angew. Chem. Int. Ed.* **54**, 11725-11279 (2015).

20. Wesolowska, O., Michalak, K., Maniewska, J. & Hendrich, A.B. Giant unilamellar vesicles - a perfect tool to visualize phase separation and lipid rafts in model systems. *Acta Biochim. Pol.* **56**, 33-39 (2009).

21. Baumgart, T., Hunt, G., Farkas, E.R., Webb, W.W. & Feigenson, G.W. Fluorescence probe partitioning between Lo/Ld phases in lipid membranes. *Biochim. Biophys. Acta* **1768**, 2182-2194 (2007).

22. Fenz, S.F. & Sengupta, K. Giant vesicles as cell models. *Integr. Biol. (Camb.)* **4**, 982-995 (2012).

23. Hammond, A.T. *et al.* Crosslinking a lipid raft component triggers liquid

ordered-liquid disordered phase separation in model plasma membranes. *Proc. Natl. Acad. Sci. U. S. A.* **102**, 6320-6325 (2005).

24. Hamada, T. *et al.* Size-dependent partitioning of nano/microparticles mediated by membrane lateral heterogeneity. *J. Am. Chem. Soc.* **134**, 13990-13996 (2012).

25. Ba, H., Rodriguez-Fernandez, J., Stefani, F.D. & Feldmann, J. Immobilization of gold nanoparticles on living cell membranes upon controlled lipid binding. *Nano Lett.* **10**, 3006-3012 (2010).

26. Tsumoto, K., Matsuo, H., Tomita, M. & Yoshimura, T. Efficient formation of giant liposomes through the gentle hydration of phosphatidylcholine films doped with sugar. *Colloids Surf. B. Biointerfaces* **68**, 98-105 (2009).

27. Kunz, W. Specific ion effects in colloidal and biological systems. *Current Opinion in Colloid & Interface Science* **15**, 34-39 (2010).

28. Sato, K., Hosokawa, K. & Maeda, M. Rapid Aggregation of Gold Nanoparticles Induced by Non-Cross-Linking DNA Hybridization. *J. Am. Chem. Soc.* **125**, 8102-8103 (2003).

29. Baldwin, R.L. How Hofmeister ion interactions affect protein stability. *Biophys. J.* **71**, 2056-2063 (1996).

30. Kulig, W. *et al.* How well does cholesteryl hemisuccinate mimic cholesterol in saturated phospholipid bilayers? *J. Mol. Model.* **20**, 2121 (2014).

31. Sadeghi, R. & Jahani, F. Salting-in and salting-out of water-soluble polymers in aqueous salt solutions. *J. Phys. Chem. B* **116**, 5234-5241 (2012).

32. Lee, J.C. & Timasheff, S.N. The Stabilizationof Proteins by Sucrose. *The Journal of Biological Chemistry* **256**, 7193-7201 (1981).

33. Chen, C., Han, D., Cai, C. & Tang, X. An overview of liposome lyophilization and its future potential. *J. Control. Release* **142**, 299-311 (2010).

34. Mensink, M.A., Frijlink, H.W., van der Voort Maarschalk, K. & Hinrichs, W.L. How sugars protect proteins in the solid state and during drying (review): Mechanisms of stabilization in relation to stress conditions. *Eur. J. Pharm. Biopharm.* **114**, 288-295 (2017).

35. Strauss, G. & Hauser, H. Stabilization of lipid bilayer vesicles by sucrose

during freezing. *Proc. Natl. Acad. Sci. U. S. A.* **83**, 2422-2426 (1986).

36. Lundqvist, M. Nanoparticles: Tracking protein corona over time. *Nat Nanotechnol* **8**, 701-702 (2013).

37. Tenzer, S. *et al.* Rapid formation of plasma protein corona critically affects nanoparticle pathophysiology. *Nat Nanotechnol* **8**, 772-781 (2013).

38. Lingwood, D. & Simons, K. Lipid rafts as a membraneorganizing principle. *Science* **327**, 46-50 (2010).

39. Furt, F., Simon-Plas, F. & Mongrand, S. Lipids of the Plant Plasma Membrane. **19**, 3-30 (2011).

40. Sezgin, E., Levental, I., Mayor, S. & Eggeling, C. The mystery of membrane organization: Composition, regulation and roles of lipid rafts. *Nat. Rev. Mol. Cell Biol.* **18**, 361-374 (2017).

41. Sághy, É. *et al.* Evidence for the role of lipid rafts and sphingomyelin in Ca2+-gating of Transient Receptor Potential channels in trigeminal sensory neurons and peripheral nerve terminals. *Pharmacol. Res.* **100**, 101-116 (2015).

42. Komura, N. *et al.* Raft-based interactions of gangliosides with a GPI-anchored receptor. *Nat. Chem. Biol.* **12**, 402-410 (2016).

43. Pederzoli, F. *et al.* Protein corona and nanoparticles: how can we investigate on? *Wiley Interdiscip Rev Nanomed Nanobiotechnol* **9** (2017).

44. Jana, N.R. Gram-scale synthesis of soluble, near-monodisperse gold nanorods and other anisotropic nanoparticles. *Small* **1**, 875-882 (2005).

45. Tatsuya Murakami *et al.* Mesoscopic Metal Nanoparticles Doubly Functionalized with Natural and Engineered Lipidic Dispersants for Therapeutics. *ACS Nano* **8**, 7370-7376 (2014).

46. Kim, H. *et al.* Membrane fusogenic high-density lipoprotein nanoparticles. *Biochim Biophys Acta Biomembr* **1861**, 183008 (2019).

47. Schneider, C.A., Rasband, W.S. & Eliceiri, K.W. NIH Image to ImageJ: 25 years of image analysis. *Nat. Methods* **9**, 671-675 (2012).

48. Hamada, T. *et al.* Size-dependent partitioning of nano/microparticles mediated by membrane lateral heterogeneity. *J. Am. Chem. Soc.* **134**, 13990-13996 (2012).

49. Wesołowska, O., Michalak, K., Maniewska, J. & Hendrich, A.B. Giant unilamellar vesicles — a perfect tool to visualize phase separation and lipid rafts in model systems *Acta Biochim. Pol.* **56**, 33-39 (2009).

Chapter 3. Control of Lipid Bilayer Phases of Cell-sized Liposomes by Surface-Engineered Plasmonic Nanoparticles

3-1. Introduction

In chapter two, I demonstrated that the sucrose shows the salting-in and salting-out effect on the colloidal stability of biocompatible nanomaterials and It is applicable to establish experimental systems for the analysis of nanomaterial-GUV interaction without salt disturbance. This is very significant results, as Arepeatedly informed in previous chapters, although the on-demand handling of the nanostructures is promised to open the door of new cell-engineering, the stabilities of GUVs themselves and reconstituted domain structure on GUV was sensitive under salt-rich condition so that this is a bottleneck of collecting fundamental insight to design nanomaterial toward the manipulation of nanostructure, such as lipid raft and other clusters. I previously tried ix a biocompatible nanomaterial prepared for salt-rich solutions and GUVs dispersed in sucrose solution, but, in results, both Are aggregated.

In this chapter, I introduce pm-AuNRs as a manipulator of model lipid raft. Pm-AuNRs consist of rod-shaped plasmonic gold nanoparticles and high-density lipoproteins (HDL) mutants on their surfaces, the former having a photothermal effect and the latter a function of Cholesterol transporter. I evaluated the effect of pm-AuNRs on domain formation/deformation in 200 mM sucrose solution without the disturbance of salts. I achieved the control of model lipid raft formation/deformation by cleverly combining these functions and demonstrate the first manipulated of model lipid raft formation/collapse to multiple GUVs at the same time.

Lipid bilayers can have three representative physical phases, which are solid-order (So), liquid-disorder (Ld), and liquid-order (Lo) phases.[1-3] Especially, Lo phase regions are enriched in Cholesterol. In the Cholesterol rich region of the plasma membrane, sphingolipids and membrane proteins assemble to generate clusters called lipid rafts. [4-6] It is Ill known that the dynamic formation/collapse of lipid rafts is associated with clustering and/or activation of membrane proteins

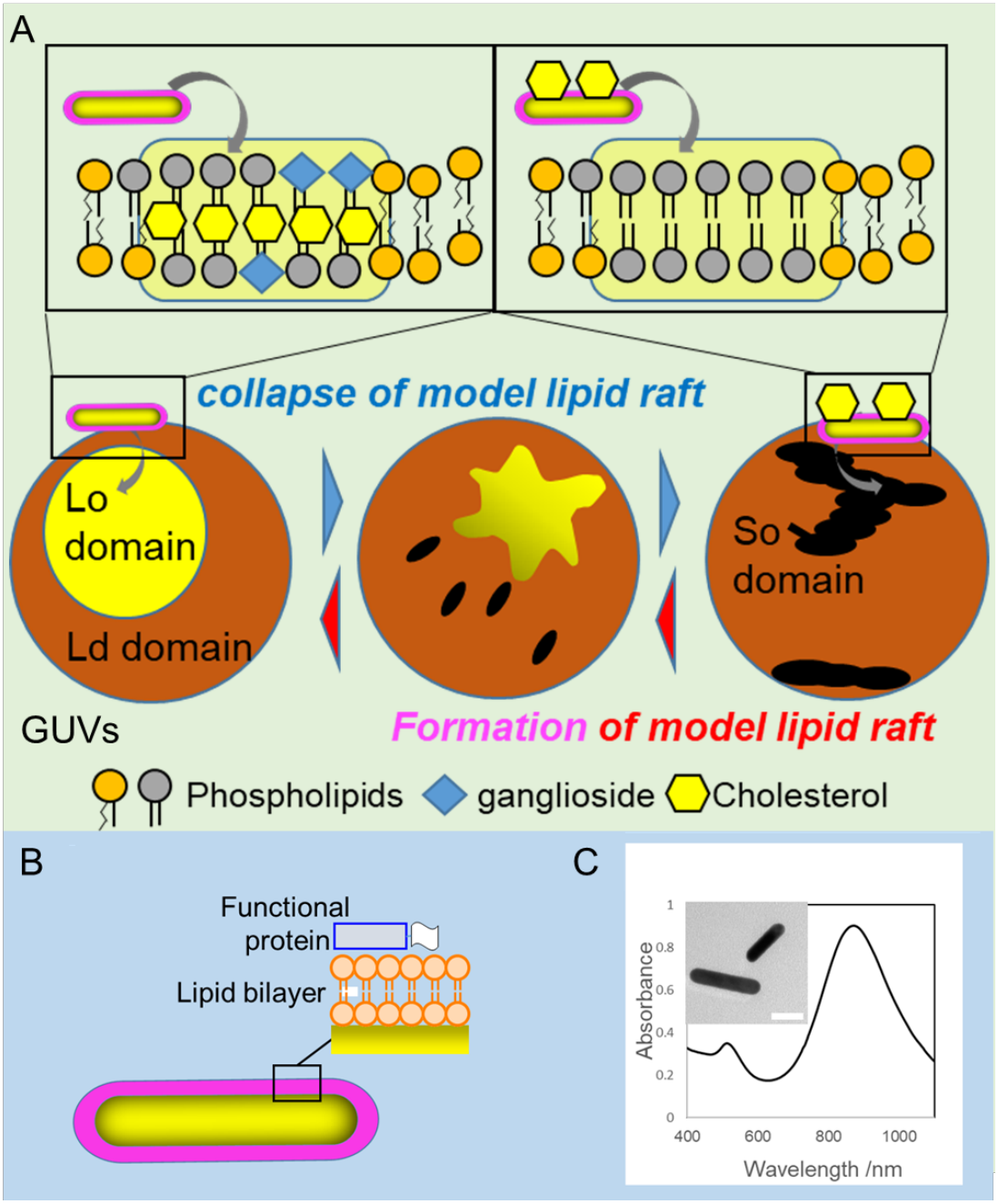

Figure 1. Schematic illustration of the concept of model lipid raft control by using plasmonic gold nanorods (AuNRs) with high-density lipoprotein (HDL) which can absorb cholesterol like a spongy. (A) Spontaneous (forward) and optical (reverse) control of lipid bilayer phases by pm-AuNRs and cholesterol-loaded pm-AuNRs, respectively. (B) Chemical architecture of plasma membrane-targeted AuNRs (pm-AuNRs) used in this study, of which the components of mutant, a cationic lipid bilayer and a cationic peptide-fused apoA-I protein are bound to the surface. (C) UV/Vis/NIR absorption spectrum and Typical TEM image of pm-AuNRs. *Scale bar*, 10 nm.

such as T cell receptors and MHC2 complexes in the mammalian immune system and several TRP channels involved in neurotransmission.[7-11] A specific type of internalization, i.e., caveolae-mediated endocytosis, also occurs through forming vacuole followed by clustering membrane proteins on lipid rafts. Conventional method to control lipid raft formation/collapse has been craved. I demonstrate here that the formation/collapse of Lo phase domains can be controlled by plasmonic nanoparticles with the surface functioning as a membrane glue as well as a Cholesterol sponge (Fig. 1A).

Nano-bio interface is defined as a place where nanomaterial meets the plasma membrane. [11] This is a key concept to under-stand material-plasma membrane interaction. The size, shape and surface chemistry/material of nanomaterials and the mobility of the plasma membrane play a key role on their interaction. From the nanomaterial side, therefore, the development of bioactive surfaces is one of the key strategies to control the nano-bio interface. To do that, I focus on the physiological function of a biomaterial in my body.

High-density lipoprotein (HDL) is a lipid/protein nanocomposite existing mainly in the blood circulation. One of its physiological functions is Cholesterol (Chol) efflux from the plasma membrane.[12] I have previously mentioned that HDL can be a biocompatible surfactant for hydrophobic colloids, such as gold nanorods (AuNRs) and that AuNRs coated with a cationic mutant of HDL (Fig. 1B) show a high affinity to the plasma membrane of living cells with negligible cytotoxicity, compared to those with a few types of cationic synthetic polymers.[13] Upon illumination around the near-infrared absorption maximum (Fig. 1C), the HDL mutant-coated AuNRs, designated as ‘plasma membrane-targeted’ AuNRs (pm-AuNRs), are able to activate a heat-sensitive ion channel via the localized photothermal heating.

Giant unilamellar vesicles (GUVs) have been widely utilized as models of the plasma membrane. [14] [15] GUVs and living mammalian cells are comparable in terms of the size, meaning they potentially have similar membrane curvature. Lo/Ld phase-separated GUVs (Lo/Ld-GUVs) are recognized as a model of the plasma membrane of living mammalian cells.[16] In this context, nanoparticles with

the size of ≤200 nm Are reported to show preferential binding to the Lo phase domains of Lo/Ld-GUVs, which could be accounted for by the free energy cost for small nanoparticle binding-induced bending deformation of Lo phase membrane being insignificant[16]. Thme, pm-AuNRs (~50 nm in longitudinal length) would preferentially bind to the Lo domains. Herein, I show that pm-AuNRs not only absorb Chol of Lo/Ld-GUVs in a Lo domain binding-dependent manner to induce Lo-to-So phase transition but also mediate the reverse phase transition on So/Ld-GUVs upon near-infrared illumination when pre-loaded with Chol (Fig. 1A).

3-2. Results

At first, I confirmed that pm-AuNRs bound to Lo-phase GUVs much more efficiently than Ld-phase GUVs, which was in accordance with the rule as described above (Fig. 2). [17] Almost all Lo phase GUVs were covered by pm-AuNR but almost No Ld phase GUVs interact with pm-AuNRs. This result was consistent with the results of soft matter physics that small nanoparticle preference to attach on Lo phase domain and large nanoparticles accumulated on Ld phase domain. Next, I investigated the effect of pm-AuNR on the membrane phase of Lo/Ld GUVs. The type of the phase is generally identified on the basis of the domain shape, which is circular for Lo domains and non-circular for So domains (Fig.3A).[18, 19] When pm-AuNRs are added to Lo/Ld-GUVs (DOPC:DPPC:Chol=2:2:1), their circular Lo phase domains (Fig. 3B) are immediately diminished and instead non-circular (string-shaped) domains emerged on the surface of GUVs (Fig.3C). The phase transition rale is very high. I show the typical fluorescent images of whole observation are in Fig.3. pm-AuNRs attached almost all Lo domain in one-time simple mixing and induced

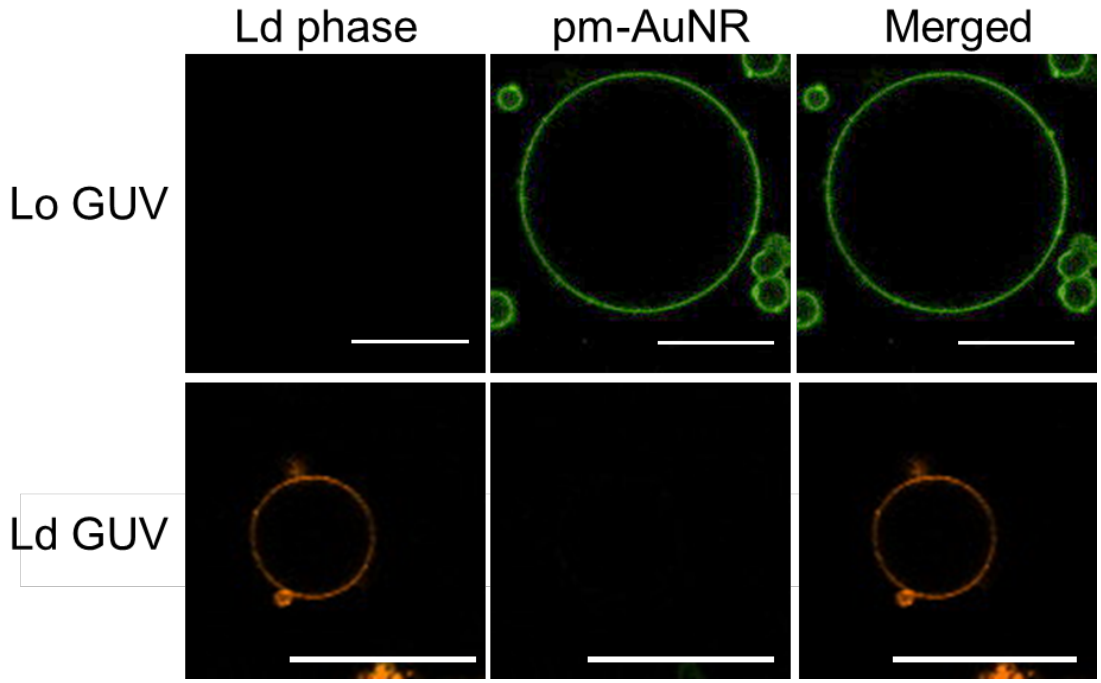

Figure 2. Lo phase selective adhesion of NBD-PE labeled pm-AuNRs adhesion. Lo GUV contained DPPC and cholesterol in 2:1 molar ratio and Ld phase GUVs contained DOPE with 1% Rhodamine-DPPE, a kind of florescent lipid which is located on Ld phase selectively.

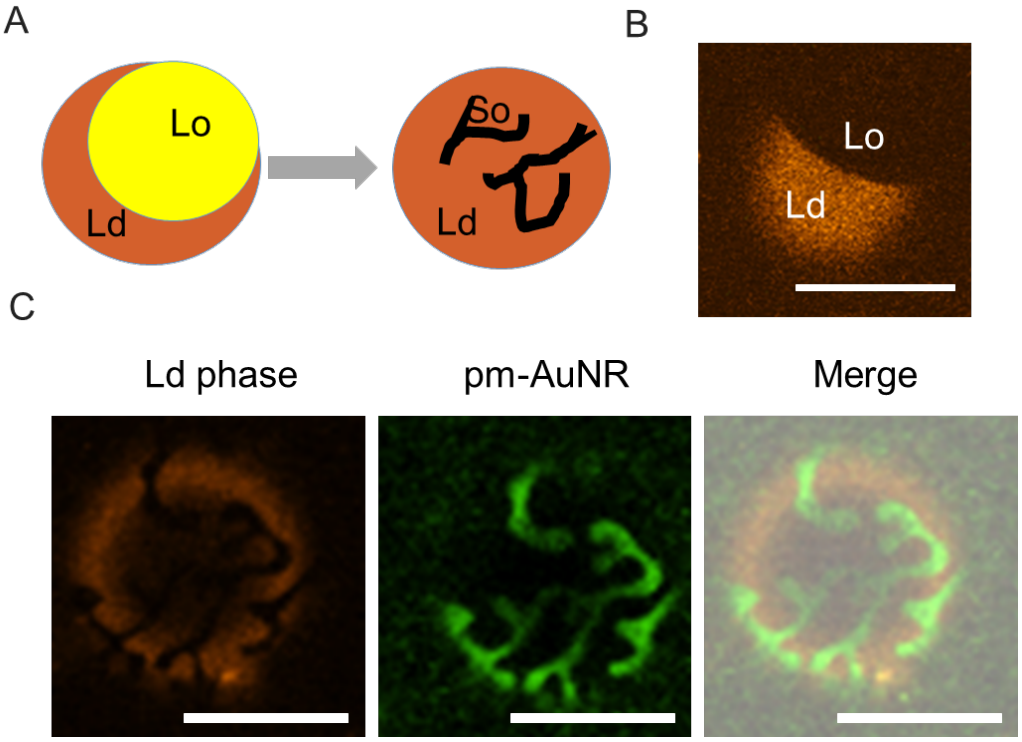

Figure 3. Phase transition in GUVs induced by pm-AuNRs. (A) Schematic image of the phase transition in GUVs. (B) Fluorescence image of typical Lo/Ld GUVs, of which the Ld domains were labeled with Rho-DPPE. Scale bar = 10 μm. (C) Fluorescence image of dispersed model lipid raft and self-assembled pm-AuNR on noncircular shape So phase region. Ld-phased were labeled with Rho-DPPE (left) and pm-AuNRs were labeled with NBD-DPPE (middle). Scale bar = 20 μm. At least 30 independent pictures of GUV were utilized for each condition.

phase transition. The amount of the new domains depended on the concentration of pm-AuNRs added, and the addition of neither the buffer alone (no pm-AuNRs) nor the cationic HDL mutant alone (no AuNRs) induced a similar phase transition (Fig.5A, 6). This data indicated that the probable contamination in the pm-AuNR dispersant did not cause this phase transition. The new domains are stable at 40°C that was over the phase transition temperature for the DPPC Lo phase (Fig 7A). To monitor the temperature of the small amount of reaction dispersant preciously, I made direct observation system of temperature by using a fiber thermometer and heater (Fig. 7B). At this time, pm-AuNRs existed on the new domains. These results suggest that the newly emerged domains are

characteristic of So phase and that the adhesion of pm-AuNRs to the Lo domains of Lo/Ld-GUVs induced this Lo-to-So phase transition. Moreover, considering the higher transition temperature than So phase, pm-AuNR adhesion itself would be stabilized the domains.

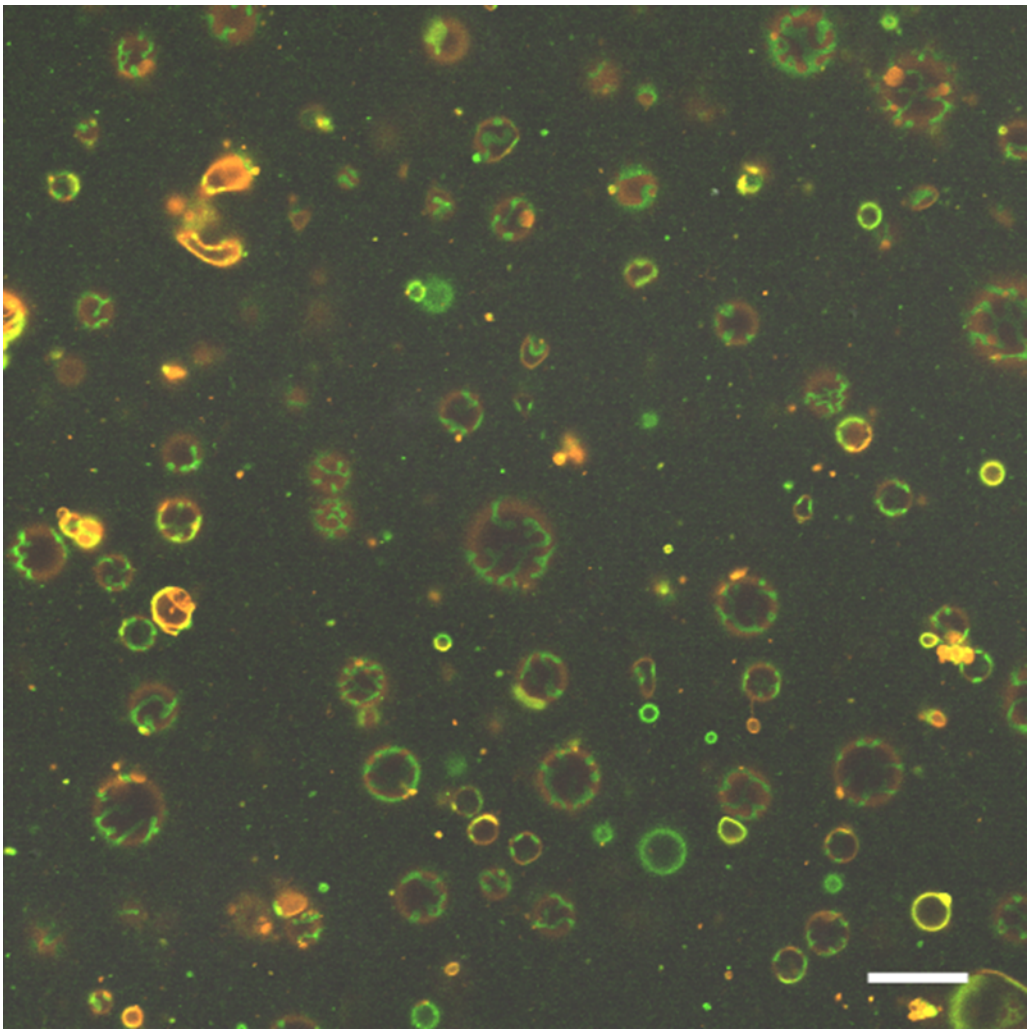

Figure 4. Entire image of GUVs after addition of pm-AuNRs. Ld phase regions were labeled with Rhodamine-PE (dark brown). and pm-AuNRs were labeled with NBD-PE (green). Scale bar = 20μm

Next, localization of a fluorescently labeled monosialodihexosylganglioside (ATTO-GM3) (Fig. 8A), which is a fluorescent ganglioside localizing in lipid rafts in live mammalian cells[20] and in Lo phase domains in GUVs[21], was examined upon the treatment of ATTO-GM3-bearing Lo/Ld GUVs (Fig. 8B) with pm-AuNRs. The red fluorescence signal pattern changed from circle to string and was colocalized with the green fluorescence signal from pm-AuNRs (Fig. 5B

8B, 8C), both of which were consistence with the observation in Fig. 3C. This result suggests that pm-AuNRs can not only transform the membrane phase but also control the location of GM3 in GUVs.

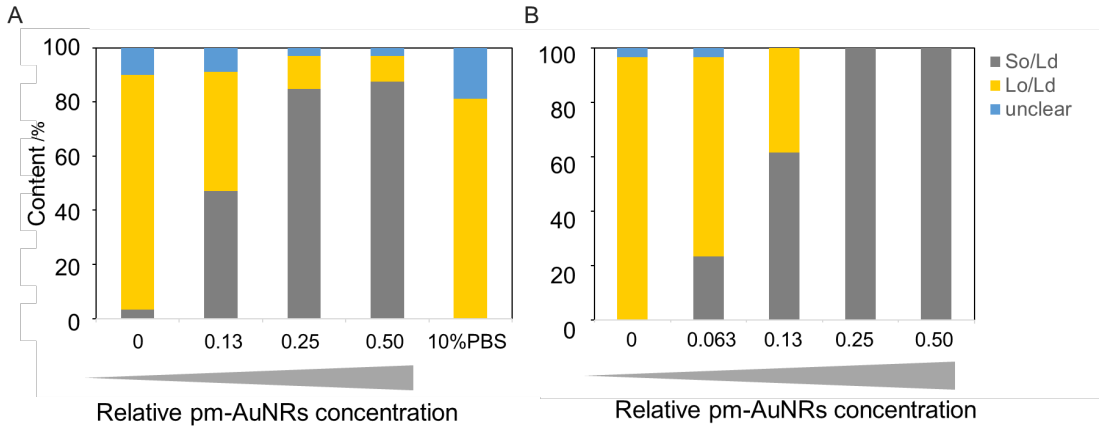

Figure 5. pm-AuNRs concentration dependency of phase transition. Judged by localization of Rhodamine-DPPE (A) or ATTO-GM3 (B). 1 of relative concentration value was equal to ca. 1 mg/mL. On the right of the graph A means GUV contents mixed with not pm-AuNRs but PBS buffer to eliminate the effects of contaminated salt in pm-AuNRs dispersion on phase transition. All content of GUVs was calculated from at least 30 independent GUV images

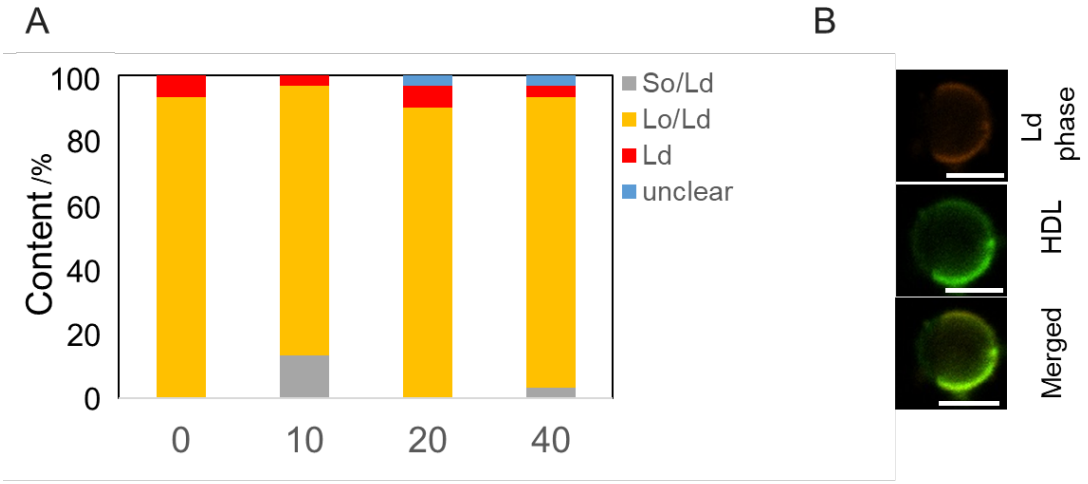

Figure 6. Cationic HDL dependency of Lo-to-So phase transition (A). HDLs were diluted in 200 mM sucrose solutions previously. All ratio of phase separation of GUVs was calculated at least 30 independent GUV images. (B) Representative image of HDL attached Lo/Ld GUV. HDL concentration was 40 μg/mL Scale bar = 5 μm

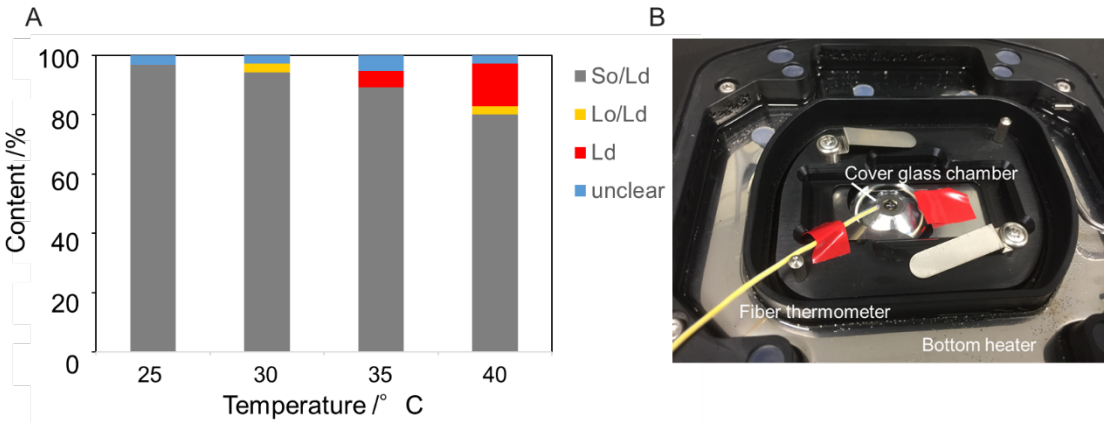

Figure 7. Temperature dependency of phase transition caused by pm-AuNRs adhesion(A). All ratio of phase separation of GUVs was calculated at least 30 independent GUV images. (B) Experimental apparatus for heating GUVs with pm-AuNRs. Cover glass chamber was set on the objective lens of a microscopy after the mixture of GUVs and pm-AuNRs were loaded. Silver bottom heater was set on the stage of the microscopy. Temperature were measured by yellow fiber thermometer. This apparatus was covered with top heater (not shown) during experiments to keep the temperature constant.

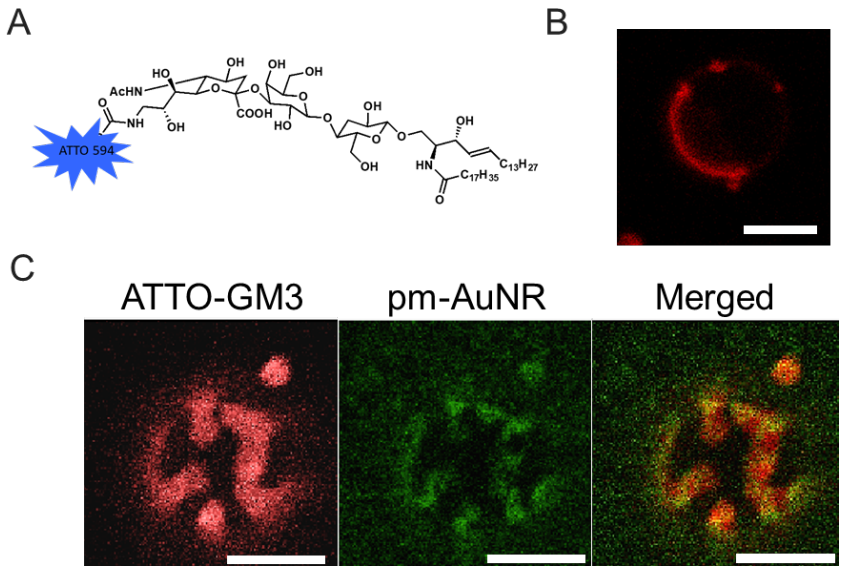

Figure 8. Control of ganglioside localization in GUVs by pm-AuNRs. (A) Chemical structure of a fluorescent ganglioside known to localize in lipid rafts and Lo membranes (ATTO-GM3). (B) Representative image of Lo/Ld GUVs containing ATTO-GM3 (red). (C) ATTO-GM3 labeled Lo/Ld GUVs after the addition of pm-AuNRs (green). Scale bar =5 μm

To gain insight into the mechanism of this Lo-to-So phase transition, I sought to conduct a real-time imaging analysis of this process. Micro chambers, in which the gradual mixing of pm-AuNRs and GUVs were allowed, are developed by sandwiching a 100 μm-thick silicon sheet with a single 6 mm hole with two slide glasses. To achieve such gradual mixing, the two droplets of each of them Are put apart within the hole of the silicon sheet on one slide glass and allowed to be mixed by putting another slide glass on it. Then, the boundary at which the two droplets are mixing was analyzed by fluorescence microscopy (Fig. 9A). In GUV rich region, GUV kept Lo/Ld phase separation. On the boundary, however, pm-AuNRs accumulated on Lo domain selectively. When observed the pm-AuNR rich areas, the boundary of two phase started to destabilized and started to transform to noncircular domain (Figure 9B.C). The time lapse images were took for a GUV on the boundary of the two dispersant (Fig.9D) The image of a single GUV near the boundary suggested that pm-AuNRs predominantly attached on the Lo phase region, which triggered the mixing of the two phase membranes, indicated by the formation of yellow area at 0', 1'3", and 1'41", and finally lead the formation of non-circular domains at 5', which are characteristic of So phase. During this Lo-to-So phase transition, small microdomains with the green fluorescence appeared. These micro-domains appeared to gather each other to form larger non-circular domains.

I also performed to the high-resolution imaging of the process of domain metamorphose by using fluorescent microscopy (Fig. 10). It should be noted that this data is a preliminary one and further investigation is required, but I observed the microdomains were emitted from one phase region to another and form noncircular shape domains through the gathering and/or intrusion of domains from one to another. At 4', 35" the boundary of Lo and Ld domain were stable but slight intrusion of Lo domain with pm-AuNR were observed. Ld domain also started to intrude to Lo phase region at 4', 57". Small Ld domain were already emitted to Lo phase region. The protruded part of Ld domain were left form the parent domain, formed stripe-shaped pattern, and broken into small microdomains. The domain boundary became non-circular at 13', 9".

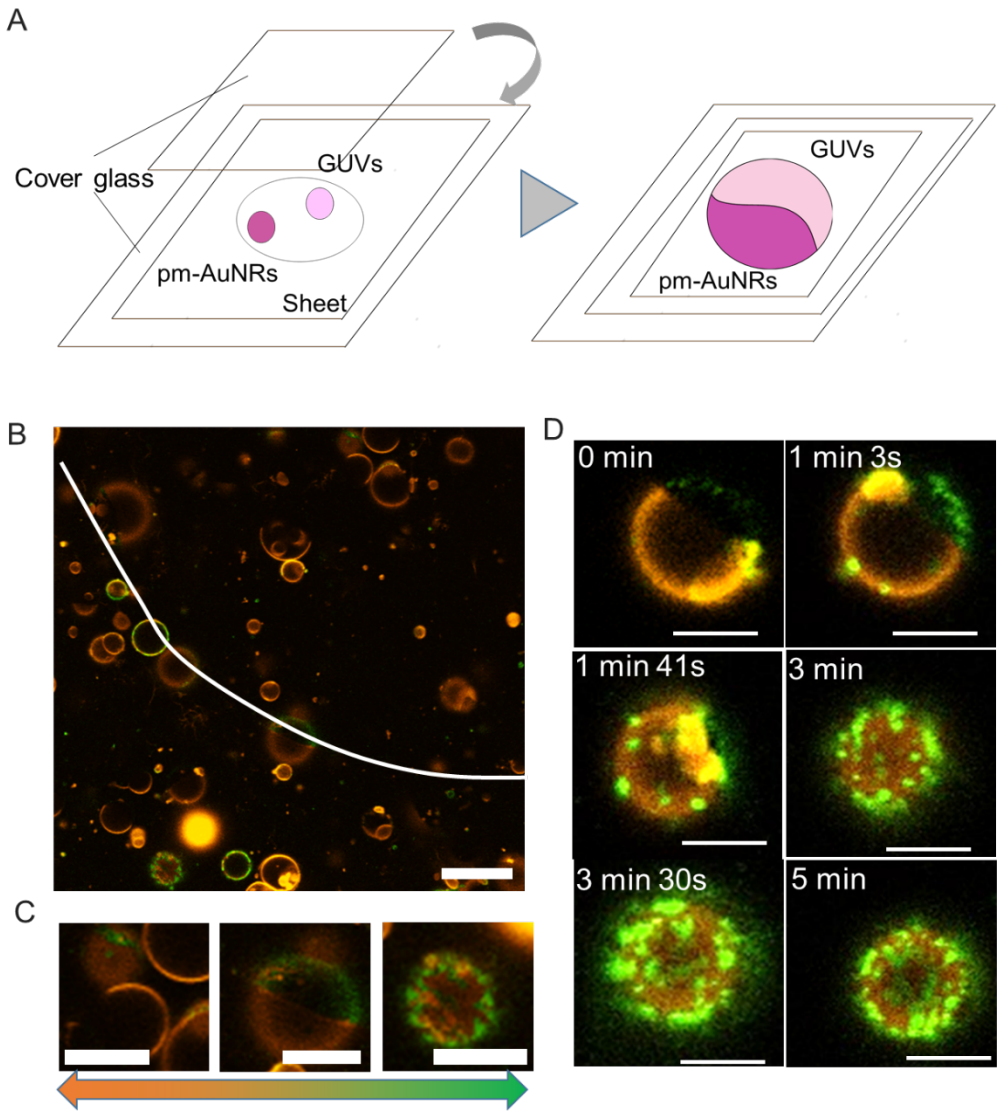

Figure 9. (A): Schematic image of observation of the boundary of pm-AuNRs and GUVs dispersants. A droplet of GUVs dispersants and of pm-AuNRs dispersants were loaded on a cover glass chamber as shown in left. A boundary was formed on the cover glass chamber as shown in right. (B) Fluorescence image near the contact area between pm-AuNRs dispersion and Lo/Ld GUVs dispersion. Wight line means the boundary between pm-AuNRs rich area and Lo/Ld GUVs rich area. (B) Extended GUV images on Figure (C). Scale Bar= 10 μm (D) Time-lapse fluorescent images during the Lo-to-So phase transition in GUVs. Just starting observation (0 min), the green fluorescence of pm-AuNRs was already shown from the Lo domains specifically. Then, the boundary of the Lo and Ld phase came to be unstable and the area of Lo domains decreased, while instead small microdomains increased with time, which finally assemble to form string-shaped domains. Scale bar, 5 μm.

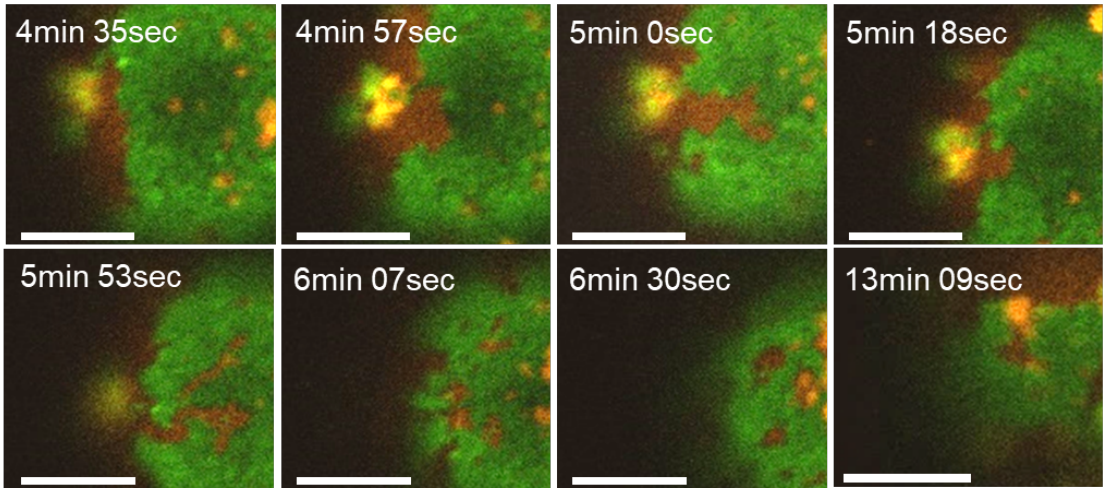

Figure 10. Lo-region-focused high-resolution time-lapse fluorescent images of Lo-to-So phase transition process. Small microdomains were emitted on Lo phase region according to destabilization of the boundary structure of two phase domains. Ld phase domain protrude into Lo phase and diffused as microdomains. Scale bar, 5 μm.

Two mechanisms have been proposed for the nanoparticle binding-induced phase transition of lipid bilayers at a constant temperature. One is arearrangement of multiple lipid molecules by single nanoparticles through electrostatic interaction, resulting in fluid-to-gel transition in 200 nm liposomes. [22] [23] Although such electrostatic interaction would be involved in my phase transition becamee pm-AuNRs had the cationic surface, the occurrence of such electrostatic interaction-induced local rearrangement is intrinsically limited to nanometer-scale areas, and its contribution would be only for the initial binding of pm-AuNRs to Lo/Ld-GUVs.

Another possible mechanism is an alternation of the lipid composition in lipid bilayers derived from HDL, which was involved on the pm-AuNR surface, was capable of withdrawing Chol from Lo/Ld-GUVs.[24] Reduction of the Chol content in the GUVs leads to the disappearance of Lo domains on the basis of the phase diagram of the GUVs. In this previous study, however, no new phase domain was not detected, while the Lo do-mains disappeared. I also confirmed with my HDL mutant chosen for the surface modification that the mutant alone did not induce the phase transition (Fig. 6). In contrast, upon the treatment of my Lo/Ld-GUVs with 10 mM methyl-β-cyclodextrin (MβCD) [25], almost all Lo membranes vanished,

while many non-Ld small domains appeared and the formation of non-circular membranes was rare (Fig. 11). On the basis of these consideration and my observation of the localization of the fluorescence of pm-AuNRs on the non-circular membranes (Fig. 3C,4), I hypothesize that the HDL mutant components of pm-AuNRs can adsorb Chol from the Lo/Ld-GUVs in an en-hanced manner compared with the mutant alone to induce the Lo-to-So phase transition and that the self-assembly of pm-AuNRs on the membrane affects the shape of the So domains.

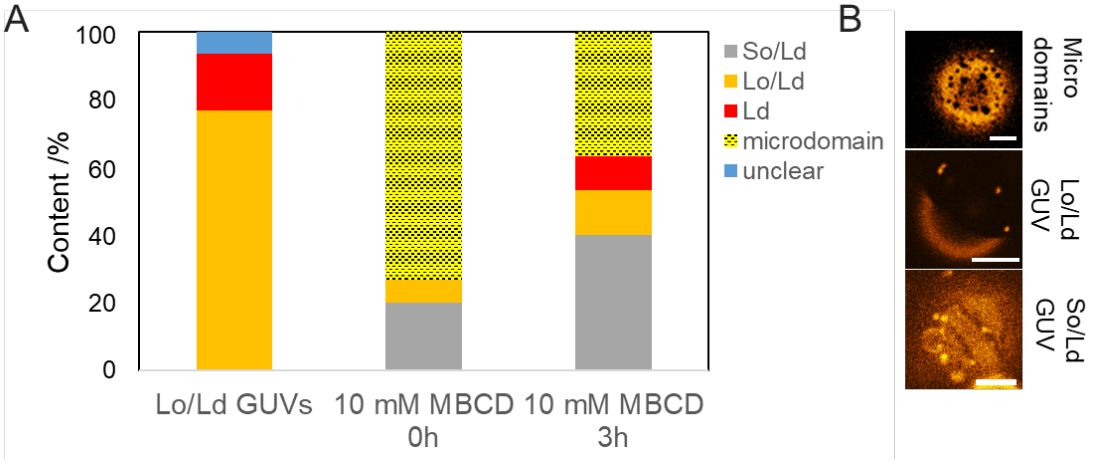

Figure 11. Effects of MβCD for phase transition for Lo-to-So phase transition GUVs were treated with above-mentioned final concentration of MBCD. (A) Ratio of GUV domain pattern. Observations were performed 0 (middle) or 3(left) h after MBCD treatement. All content of GUVs was calculated from at least 30 independent GUV images (B) Representative image of each domain pattern. Scale bar = 5 μm

To verify the former hypothesis, I sought to induce the reverse phase transition from So to Lo by by using Chol-loaded pm-AuNRs (pm-AuNRs-Chol, Fig. S9) and So/Ld phase-mixed GUVs (So/Ld-GUVs). Just mixing them at r.t. did not affect the phase significantly, but upon heating at 50°C for 10 min, followed by cooling to room temperature circular domains appeared (Fig.12), clearly validating my former hypothesis. The circular shape domains often moved on the GUVs. This is a well-known characteristic of relatively small Lo domains Lo/Ld phase separated GUVs so that I convinced that the phase of the circulat domain is Lo. Heat-induced Lo membrane formation motivated me to examine whether its optical control is possible because AuNRs are capable of photothermal heat

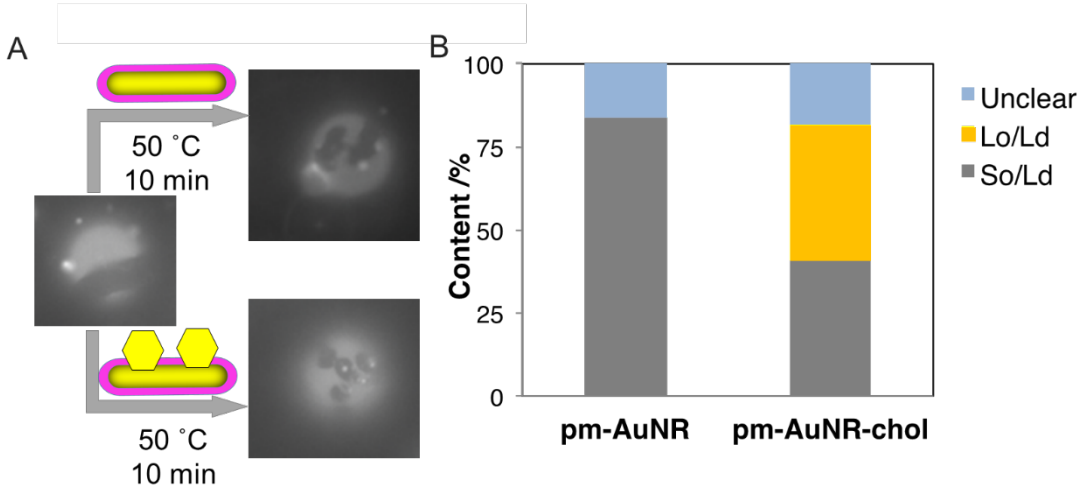

Figure 12. (A) Typical images of So/Ld GUVs. So/Ld GUVs without any nanoparticle addition (left), after heating with pm-AuNRs (right, upper) or with pm-AuNR-chols (right, lower). (B) Ratio of GUVs phase separation pattern after heating with pm-AuNR (light) or pm-AuNR-chols (left).

generation. I constructed the NIR laser experimental system shown in Fig.13. The NIR laser was introduced from light source as blue arrows indicates and sample were irradiated by NIR laser (Fig.13A). To prevent samples from rapid heat diffusion through the contact between samples and metal desk which has high heat conductivity, the samples were set on air by using a single well plates (Fig.13 B.C).

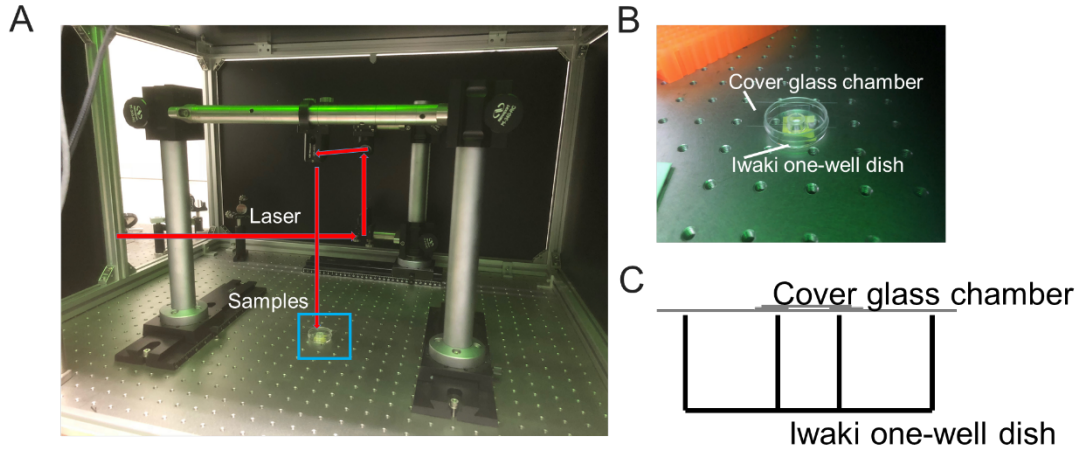

Figure 13. (A) Experimental apparatus for NIR laser irradiation for the mixture of pm-AuNR-chols and So/Ld GUVs. Optical path of NIR laser were shown in red arrows. (B) Enlarged view of blue rectangle in (A). Cover glass chambers were set on Iwaki one-well dish. (C) Schematic image of a side view of figure (B).

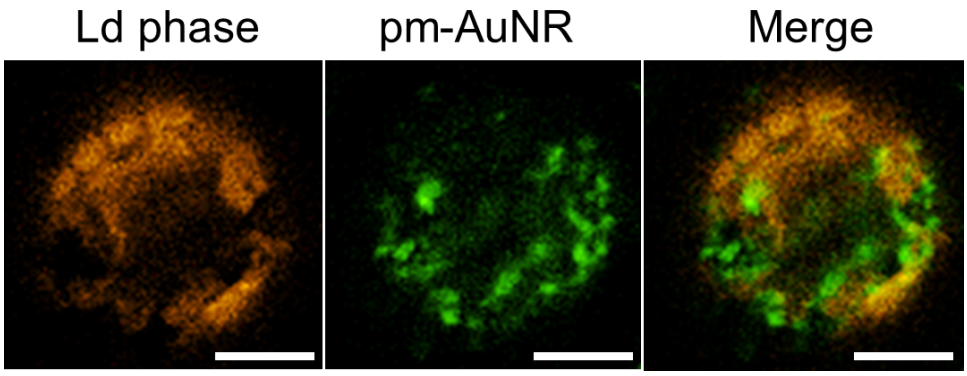

Figure14. Representative image of pm-AuNR-chols on So/Ld GUVs without any heat stimulation. Scale bar, 5 μm.

When the mixture of pm-AuNR-chols and So/Ld-GUVs at room temperature, the fluorescence of the AuNRs was detected from the So domains (Fig. 14). This data is accordance with the results in Fig.12 and it indicated that pm-AuNR retain cholesterol near acceptor lipid bilayer. This would be caused by the high ability of original HDL membrane. Upon illumination at 852 nm for 5 min, small circular Lo membranes are observed after cooling to r.t. (Fig.15A, upper). This formation depended on the presence of Chol (Fig. 5A, IoIr) and the illumination (Fig. 15B, 0 mW). The content of Lo/Ld-GUVs was increased by increasing the laser power intensity (Fig. 15B). Meanwhile, it was reported that high power laser irradiation on GUV cause the formation of pseudo domains via photochemical cross-linking between unsaturated lipids and fluorescent probes[26]. Fig. 15C excluded this possibility became no circular-shaped domain formation was induced by the laser irradiation in the absence of Chol. These results clearly demonstrated the So-to-Lo phase transition was due to photoinduced Chol transfer from pm-AuNRs-Chol to GUV membranes. This result also supports the above-mentioned Chol absorption hypothesis for the Lo-to-So phase transition.

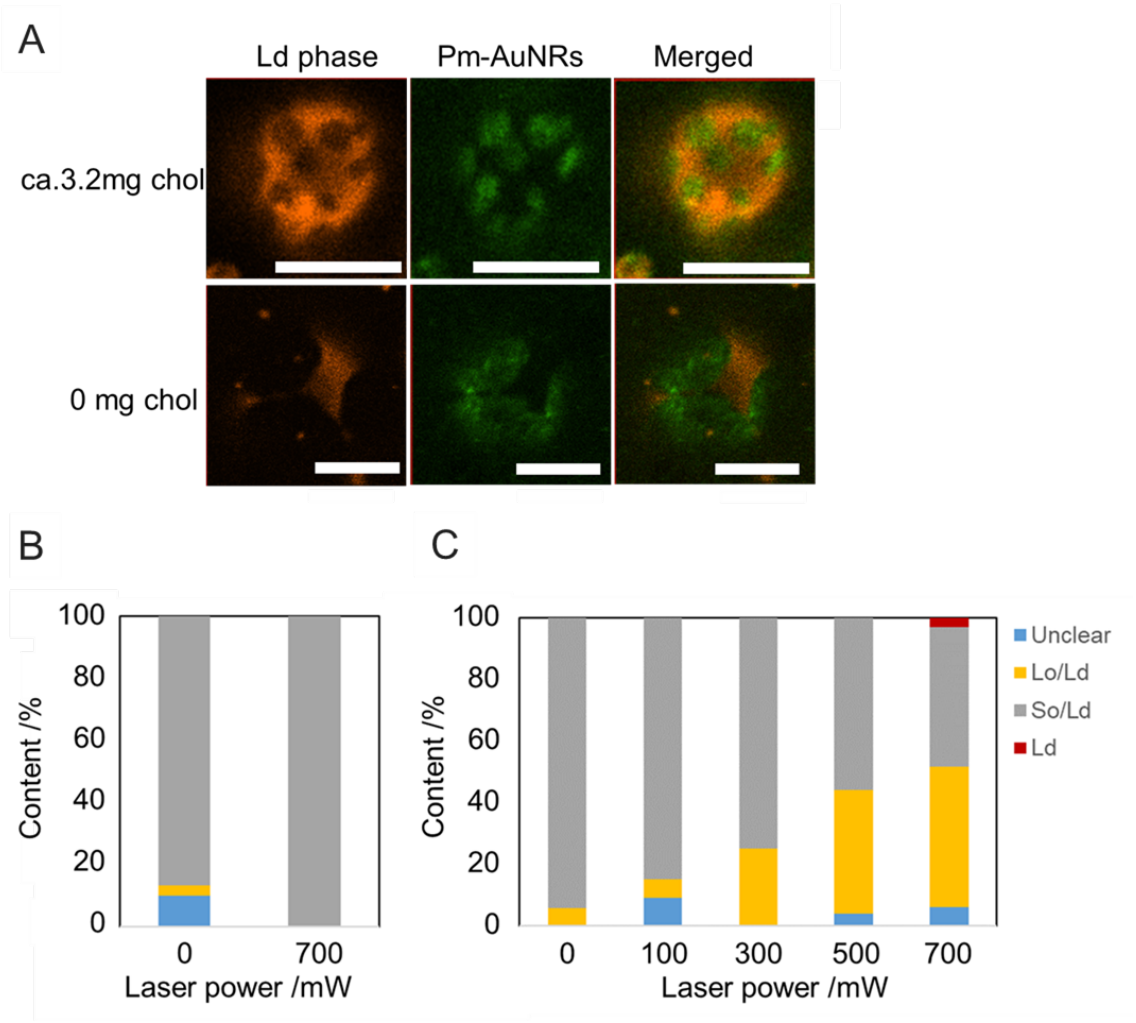

Figure 15. (A) Typical Image of 700 mW laser-irradiated So/Ld GUVs. Upper GUV was treated with pm-AuNR-chols containing ca. 3.2 mg/mL cholesterol (Chol). Lower GUV was treated with pm-AuNR-chols without cholesterol. (B) Laser power dependency of Lo/Ld GUVs emergence when So/Ld GUVs were treated with pm-AuNR-chols without cholesterol. (C) Laser power dependency of Lo/Ld GUVs emergence with So/Ld GUVs treated with pm-AuNR-chols containing ca. 3.2 mg/mL.

3-3. discussion

There were two common reagents for manipulation of cholesterol. One is filipin, a kind of polyene antibiotics. Filipin was widely utilized as a probe of cholesterol localization in fixed cells but it is difficult to apply it on living cell because it causes membrane disruption and leads cell death. Another is MβCD [2728]. MβCD was well-known donor-accepter of cholesterol to study lipid raft related processes in living cells. Cholesterol poor MβCD extract cholesterol from cell membrane and cholesterol enriched MβCD-cholesterol complex donate cholesterol on the membrane. As long as we know, however, there were no MβCD-based materials designs enabling recognition of Lo or So domains. Recent GUVs studies suggested MβCD removed cholesterol rather Ld phase region [25]. Moreover, NIR laser triggered cholesterol enrichment on lipid bilayers have not achieved. The spongy of cholesterol-like character of pm-AuNRs distinguish this material from mere donor-accepter of cholesterol such as MβCD. They removed cholesterol after attachment on lipid bilayer and cholesterol enriched pm-AuNR was able to stop cholesterol penetration into lipid bilayers without stimulation. This character is completely different from MβCD and cholesterol enriched MβCD, which were widely used as a passive transporter of cholesterol from and to lipid bilayers.

I also evaluated the effect of Chol-loaded MβCD (MβCD-Chol) in my experiment system because the insertion and withdrawal of Chol to the plasma mem-brane are known to be possible with methyl-β-cyclodextrin (MβCD). [28-30] MβCD-Chol was utilized to transfer Chol to So/Ld-mixed GUVs for the first time. Under my experimental condition, such a transition was confirmed with So/Ld-GUVs. The number of So domains could also be controlled by changing the amount of MβCD-Chol (Fig. 16). With my pm-AuNR-Chol, on the other hand, the initiation, as lll as the degree of the transition, was controllable by laser illumination. Although the reason why the spontaneous Chol transfer from the AuNRs to GUVs does not occur like the reverse case as shown in Fig. 2C is unclear at present, pm-AuNRs-Chols are unprecedented optical tools to spatiotemporally control membrane phases via photothermal Chol transfer to

membranes.

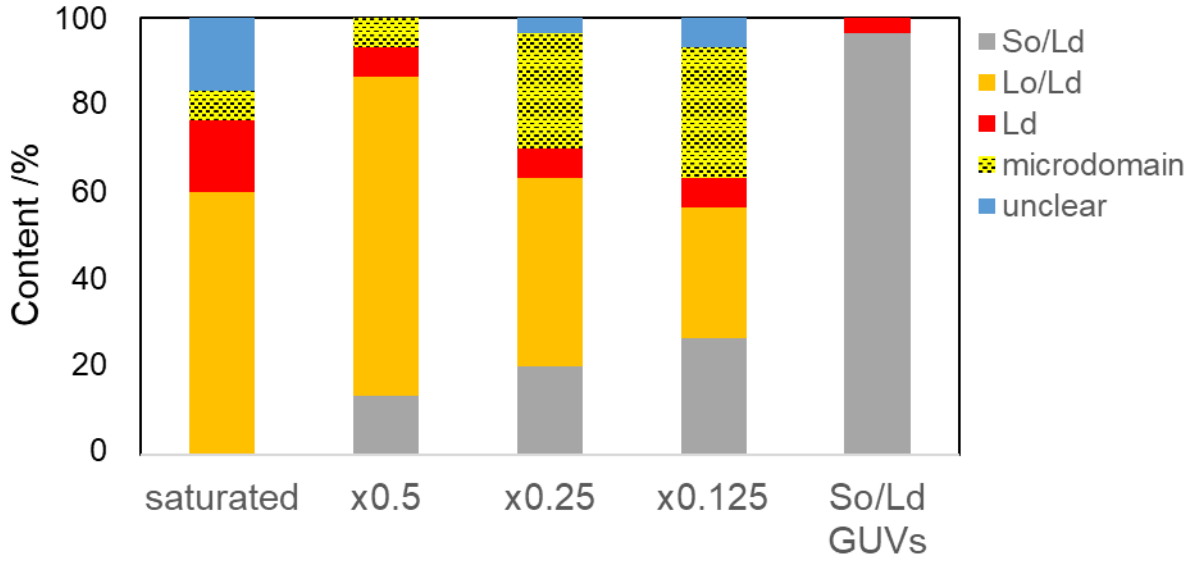

Figure 16. Saturated mBCD-chol induced So-to-Lo phase transition. Saturated mBCD-chol solution included ca.1.3 mM cholesterol. All content of GUVs was calculated from at least 30 independent GUV images.

There are a few reports showing induction of the membrane phase transition in GUVs by NIR laser [31-33]. Their transitions are sol-to-gel and limited in a very small area[31, 32] and their mechanism was through photothermal heating of water[32] or immobilization of single GUVs with optical tlezers.[31-33] Compared with these methods, my pm-AuNRs based system can control much larger area and much larger number of GUVs at the same time. Taken together with the fact that the plasma membrane is the most fragile organelle in living cells, pm-AuNRs-Chol are potentially safer and more practical tools for cell biology studies.

pm-AuNRs utilized in this study are capable of the photo-thermal activation of TRPV1 without a significant membrane disruption, which was impossible with other AuNRs with the cationic surface.[13] It has been reported that Chol depletion by MβCD did not alter the thermo-sensitivity of TRPV1, while the temperature threshold of the activation was increased upon Chol enrichment[34]. Meanwhile, mammalian cells rigidify the plasma membrane by increasing the amount of saturated lipids and/or Chol when exposed to heat. Based on these considerations, how are my results obtained with GUVs interpreted in terms of

the safe TRPV1 activation in living mammalian cells? If a similar Lo-to-So phase transition occurs in TRPV1-expressing mammalian cells upon the treatment of pm-AuNRs, the thermo-sensitivity of TRPV1 may, at least, not be increased and the plasma membrane may become more fragile, both of which apparently contradict to previous reports. These observations are suspected to be due to the limitation of the model system using GUVs or suggest the existence of unknown mechanisms for the So-phase membranes in the plasma membrane.

3-4. Conclusion

In summary, pm-AuNRs bound to the Lo phase membranes selectively in Lo/Ld GUVs, which spontaneously caused a Lo-to-So phase transition. With hand-made microchamber system and fluorescently labeled pm-AuNRs and GUVs, the membrane phase transition process was successfully visualized for the first time. During the transition, microdomains Are emitted from the blebbing edge of the circular Lo domains and then assembled as string-shaped So domains, from which the pm-AuNRs fluorescence signal was detected. The fluorescence signal of a ganglioside (GM3) localizing in lipid rafts and Lo membranes was also detected from the So domains after pm-AuNRs treatment. The reverse transition in So/Ld-GUVs was possible by utilization of Cholesterol-enriched pm-AuNRs, and interestingly, its initiation was strictly controlled by NIR laser illumination. This is the first example of the Lo-to-So and So-to-Lo phase transitions in GUVs with nanomaterials, and its success is most likely derived from the bioactive AuNR surface created by an HDL mutant. This study marks the beginning of the spatiotemporal control of lipid raft formation/collapse with nanomaterials bearing bioactive surface designed in view of biological chemistry, photo-chemistry, and cell biology.

3-5. Experimental section

General Information

General reagents Are purchased from Nakalai Tesque (Kyoto, Japan). Gold(III) chloride and sodium borohydride (NaBH4) Are obtained from Sigma-Aldrich (Saint Louis, MO, MEA). Silver nitrate, L-(+)-ascorbic acid, and sodium oleate Are purchased from Wako (Osaka, Japan). 1-Palmitoyl-2-oleoyl-sn-glycero-3-phosphoCholine (POPC) was obtained from NOF (Tokyo, Japan). 1,2-Dioleoyl-3-trimethylammonium-propane (DOTAP), 1,2-dipalmitoyl-sn-glycero-3-phosphoethanolamine-N-(7-nitro-2-1,3-benzoxadiazol-4-yl) (NBD-PE), and 1,2-dipalmitoyl-sn-glycero-3-phosphoethanolamine-N-(lissamine rhodamine B sulfonyl) (Rhodamine-PE) Are purchased from Avanti Polar Lipids, Inc (Alabaster, AL, MEA). Methyl-beta-cyclodextrin (MβCD) and Cholesterol (Chol) Are obtained from Sigma-Aldrich (Saint Louis, MO, MEA). ITO glasses Are purchased from Sigma, and the fluorescent ganglioside probe (ATTO-GM3) was obtained from Prof. Hiromune Ando [21]. Visible/near-infrared (Vis/NIR) spectra are measured by using the V-630 spectrometer (JASCO Cooperation, Tokyo, Japan). Giant unilamellar vesicles (GUV) images Are obtained by using Zeiss LSM 800 confocal fluorescent microscope or Nikon Ti eclipse fluorescent microscope. The concentration of the cationic high-density lipoprotein mutant (catHDL) on a protein basis was measured with a DC Protein Assay kit (Bio-Rad, CA, MEA). The hydrodynamic diameter of catHDL was measured utilizing Nanotrack UPA-UT151 apparatus (MicrotracBEL, Osaka, Japan).

catHDL preparation

The preparation of catHDL was described previously [13] [17]. Briefly, POPC and DOTAP Are mixed in ethanol in a round-table flask at a molar ratio of 7:3. A 6 mol% solution of NBD-PE in ethanol was added if necessary. The reaction mixture was concentrated and dried under reduced pressure to remove all solvents. The lipid film formed at the bottom of the flask was dispersed by using 30 mg/mL sodium Cholate solution in phosphate-buffered saline (PBS, pH 7.4). Following incubation at 37 °C for at least 2 h, are recombinant apoA-I mutant with

a deleted N terminal 43 amino acid, and a cell-penetrating TAT peptide fused at the C terminal Are mixed at a protein-to-lipid molar ratio of 100 in PBS containing 4 M urea. The reaction mixture was incubated at room temperature (r.t.) overnight. The mixture containing catHDL was dialyzed against 3 L PBS for at least 4 h, changing the dialysate three times to remove urea, sodium Cholate, and unreacted proteins. Subsequently, the sample was centrifuged to remove debris. The hydrodynamic diameter of catHDL was determined at approximately 37 nm by using Nanotrack UPA-UT151 apparatus.

Synthesis of CTAB-coated AuNRs

AuNRs Are synthesized utilizing the seedless method [35]. Typically, 1200 μL of a 4 mM aqueous solution of AgNO3, 400 μL of 50 mM aqueous solution of HAuCl4, and 258 μL of 100 mM solution of aqueous L-ascorbic acid Are added to 40 mL of 0.1 M aqueous solution of hexadecyltrimethylammonium bromide (CTAB). After the color of the reaction mixture turned from yellow to colorless, 48 μL of 35% HCl and 30 μL of a freshly prepared ice-cold aqueous solution of NaBH4 Are added while stirring. AuNRs formed in the mixture Are pelleted by centrifuging at 20,000 × g for 40 min at 25 ˚C, followed by incubation at 30 ˚C overnight. Finally, the AuNRs Are re-dispersed in 0.1 M CTAB at ca. 1 mg/mL.

Preparation of pm-AuNR

pm-AuNRs Are synthesized according to my previous report [13 17]. Briefly, 1 mL of CTAB-coated AuNR (ca. 1 mg/mL) was centrifuged at 20,000 × g for 20 min at 25 ˚C followed by removal of 900 μL of supernatants. The sample was re-dispersed with the resting 100 μL supernatants, diluted with 900 μL of deionized water, then centrifuged at 20,000 × g for 20 min at 25 ˚C. Subsequently, 750 μL of the supernatant was removed and 250 μL of 16 mg/mL sodium oleate solution was added to the samples. This mixture was heated for 1 h at 50 ˚C and the products (oleate-coated AuNRs) Are purified by using the Nap5 gel column (GE Healthcare). Oleate-coated AuNRs Are mixed with catHDL in a 1:0.4 molar ratio and then heated for 1 h at 50 ˚C in a 1.5 mL microtube. The products (pm-AuNRs)

Are centrifuged at 20,000 × g for 20 min at 25 ˚C and all supernatants Are carefully removed. pm-AuNRs are suspended in a 200 mM sucrose solution at ca. 1 mg/mL.

Preparation of GUVs

GUVs Are prepared by using the electro-formation method [36]. 40 mM of DPPC, DOPC, and Cholesterol in chloroform Are mixed in a Durham tube. 1 mg/mL solution of Rhodamine-PE or ATTO594-GM3 in ethanol was added if necessary. A portion of the mixture (5.7 mmol lipids) was dropped and spread on an ITO glass (8–12 Ω/sq, Sigma-Aldrich, MO). The ratios of lipids and Cholesterol for Lo, Ld, Lo/Ld, and So/Ld GUVs Are DPPC:DOPC:Chol = 2:0:1, 0:1:0, 2:2:1 or 1:1:0, respectively. After heating for 5 min at 50 ˚C, the lipid film was further spread by adding a single drop of hot chloroform, then drying in vacuo for ≥2 h. The sample glass was covered with another ITO glass by using a silicon sheet (ca. 1 mm thickness) with a 1.5 cm square-shaped hole to create a small chamber on the lipid film. 0.3×102 μL of 200 mM sucrose solution was added into the chamber and a home-made electric circuit was made of thin foil, the chamber, and an arbitrary function generator AFG-2005 (GW Instek). For So/Ld GUVs, the procedure was slightly modified. The lipid film for So/Ld GUVs was heated at 70 ˚C for 5 min instead of 50 ˚C, and the 200 mM sucrose solution and other apparatus. Are heated at 70 ˚C prior to electrification. Electric power (10 Hz, 1.4 vpp, 0.35 mV) was applied to the chamber with the arbitrary function generators at 50 ˚C in an ICI-1 incubator (AS One) overnight. After cooling the chamber to room temperature, the dispersion of GUVs was recollected from the chamber with a disposable syringe and stored in 1.5 mL tubes at room temperature.

Observation of GUVs

A chamber for GUV observation was prepared by sandwiching a single 0.1 mm thick silicon sheet with a ca. 6 mm hole between two 0.13–0.17 mm thick cover glasses (24 mm × 50 mm and 18 mm × 18 mm, respectively). Typically, after mixing 5 μL of the GUV dispersion and 5 μL of the pm-AuNRs dispersion in a

microtube, 3.5 μL of the mixture was dropped within the hole on one cover glass. After the hole was covered with another cover glass to close the chamber, the phase separation pattern of GUVs was observed under a microscope.

Observation of the temperature dependency of the phase separation.

After the mixtures of GUVs and pm-AuNRs Are loaded into it, the above-mentioned chamber was set in an INUBG2-ONICS stage-top incubator (TOKAI HIT) equipped with an ECLIPSE Ti microscope. The temperature was controlled with the bottom and top heaters of the incubator. The sample temperature was monitored by attaching the tip of an optical microfiber thermometer onto the slide glass near the area of observation.

Observation of the phase transition process

2 μL of pm-AuNRs and 2 μL of Lo/Ld GUVs (DPPC:DOPC:Chol = 2:2:1) Are dropped within the above-mentioned hole on one cover glass. Placing another cover glass on top alloId mixing the two substances. The area near the boundary was then observed by using an LSM 800 microscope.

Cholesterol depletion by using MβCD

MβCD was dissolved in a 200 mM sucrose solution at 20 mM and stored at 4 ˚C. The MβCD solution was warmed at r.t. and mixed with the GUV dispersant. Microscopic observation was performed at r.t.

Preparation of pm-AuNR-Chols

pm-AuNRs dispersion was mixed with 1/10 volume of 32 mg/mL Chol in 2-propanol and centrifuged at 20,000 × g for 20 min at 25 ˚C. All supernatants Are removed carefully and the pellet was re-dispersed in a 200 mM sucrose solution at ca. 1 mg/mL.

Observation of the heating-induced So-to-Lo phase transition

pm-AuNR-Chols and So/Ld GUVs (DPPC:DOPC:Chol = 1:1:0), in which the Ld

phase was labeled with 0.1 mol % Rhodamine-DPPE, Are mixed in a 1:1 volume ratio and heated at 50 ˚C for 10 min in a microtube. The mixture was placed into the chamber and the domain patterns of GUVs Are observed by using the ECLIPSE Ti microscope.

Observation of the NIR laser-induced So-to-Lo phase transition

The chamber containing the above-mentioned mixture was set on a glass-bottom dish (IWAKI) and illuminated at 852 nm with a Chameleon femtosecond-pulsed laser (Coherent). Then, the chamber was cooled to r.t. for at least 10 min prior to the analysis.

Observation of the phase transition induced by saturated Chol-loaded MβCD (MβCD-Chol)

MβCD-Chol preparation was described previously[29]. MβCD and Chol Are dissolved in 200 mM sucrose solution at 5 mM and in a 1:1 chloroform:2-propanol solution at 64.7 mM, respectively. 1 mL of the MβCD solution and 19.3 μL of the Chol solution Are mixed, then rotated at 37 ˚C overnight to obtain a clear solution. The mixture was then filtrated with a 0.45 μm pore size filter (Millipore) and mixed with GUVs in a 1:1 volume ratio.

3-6. References

1. Simons, K. & Sampaio, J.L. Membrane organization and lipid rafts. *Cold Spring Harb. Perspect. Biol.* **3**, a004697 (2011).
2. Meer, G.V., Voelker, D.R. & Feigenson, G.W. Membrane lipids: Where they are and how they behave. *Nat. Rev. Mol. Cell Biol.* **9**, 112-124 (2008).
3. Heberle, F.A. & Feigenson, G.W. Phase separation in lipid membranes. *Cold Spring Harb. Perspect. Biol.* **3**, a004630 (2011).
4. Simons, K. & Ikonen, E. Functional rafts in cell membranes. *Nature* **387**, 569–572 (1997).
5. Simons, K. & Ikonen, E. How Cells Handle Cholesterol. *Science* **290**, 1721-1726 (2000).
6. Suzuki, K.G. *et al.* Transient GPI-anchored protein homodimers are units for raft organization and function. *Nat. Chem. Biol.* **8**, 774-783 (2012).
7. Anderson, H.A. & Roche, P.A. MHC Class II association with lipid rafts on the antigen presenting cell surface. *Biochim. Biophys. Acta* **1853**, 775-780 (2015).
8. David E Clapham, Loren W Runnels & Strübing, C. The TRP ion channel family. *Nat. Rev. Neurosci.* **2**, 387-396 (2001).
9. Liu, M., Huang, W., Wu, D. & Priestley, J.V. TRPV1, but not P2X, requires cholesterol for its function and membrane expression in rat nociceptors. *Eur. J. Neurosci.* **24**, 1-6 (2006).
10. Doherty, G.J. & McMahon, H.T. Mechanisms of endocytosis. *Annu. Rev. Biochem* **78**, 857-902 (2009).
11. Nel, A.E. *et al.* Understanding biophysicochemical interactions at the nano-bio interface. *Nat Mater* **8**, 543-557 (2009).
12. Lewis, G.F. & Rader, D.J. New insights into the regulation of HDL metabolism and reverse cholesterol transport. *Circ. Res.* **96**, 1221-1232 (2005).
13. Nakatsuji, H. *et al.* Thermosensitive Ion Channel Activation in Single Neuronal Cells by Using Surface-Engineered Plasmonic Nanoparticles. *Angew. Chem. Int. Ed.* **54**, 11725-11279 (2015).
14. Wesolowska, O., Michalak, K., Maniewska, J. & Hendrich, A.B. Giant unilamellar vesicles - a perfect tool to visualize phase separation and lipid rafts in model systems. *Acta Biochim. Pol.* **56**, 33-39 (2009).
15. Dietrich, C. *et al.* Lipid rafts reconstituted in model membranes. *Biophys. J.* **80**, 1417-1428 (2001).
16. Hamada, T. *et al.* Size-dependent partitioning of nano/microparticles mediated by membrane lateral heterogeneity. *J. Am. Chem. Soc.* **134**, 13990-

13996 (2012).
17. Nobeyama, T. *et al.* Colloidal Stability of Lipid/Protein-Coated Nanomaterials in Salt and Sucrose Solutions. *ChemistrySelect* **3**, 8325-8331 (2018).
18. Hamada, T., Kishimoto, Y., Nagasaki, T. & Takagi, M. Lateral phase separation in tense membranes. *Soft Matter* **7**, 9061 (2011).
19. Veatch, S.L. & Keller, S.L. Separation of Liquid Phases in Giant Vesicles of Ternary Mixtures of Phospholipids and Cholesterol. *Biophys. J.* **85**, 3074-3083 (2003).
20. Inokuchi, J. GM3 and diabetes. *Glycoconj J* **31**, 193-197 (2014).
21. Komura, N. *et al.* Raft-based interactions of gangliosides with a GPI-anchored receptor. *Nat. Chem. Biol.* **12**, 402-410 (2016).
22. Wang, F., Curry, D.E. & Liu, J. Driving Adsorbed Gold Nanoparticle Assembly by Merging Lipid Gel/Fluid Interfaces. *Langmuir* **31**, 13271-13274 (2015).
23. Wang, B., Zhang, L., Bae, S.C. & Granick, S. Nanoparticle-induced surface reconstruction of phospholipid membranes. *Proc. Natl. Acad. Sci. U. S. A.* **105**, 18171-18175 (2008).
24. Puff, N., Lamaziere, A., Seigneuret, M., Trugnan, G. & Angelova, M.I. HDLs induce raft domain vanishing in heterogeneous giant vesicles. *Chem. Phys. Lipids* **133**, 195-202 (2005).
25. Sanchez, S.A., Gunther, G., Tricerri, M.A. & Gratton, E. Methyl-beta-cyclodextrins preferentially remove cholesterol from the liquid disordered phase in giant unilamellar vesicles. *J. Membr. Biol.* **241**, 1-10 (2011).
26. Morales-Penningston, N.F. *et al.* GUV preparation and imaging: minimizing artifacts. *Biochim. Biophys. Acta* **1798**, 1324-1332 (2010).
27. Aimee E. Christian, M. Page Haynes, Michael C. Phillips & Rothblat, G.H. Use of cyclodextrins for manipulating cellular cholesterol content. *The journal of Lipid Research* **38**, 2264-2272 (1997).
28. Zidovetzki, R. & Levitan, I. Use of cyclodextrins to manipulate plasma membrane cholesterol content: evidence, misconceptions and control strategies. *Biochim Biophys Acta* **1768**, 1311-1324 (2007).
29. Aimee E. Christian, M. Page Haynes, Michael C. Phillips & Rothblat, G.H. Use of cyclodextrins for manipulating cellular cholesterol content. *J. Lipid Res.* **38**, 2264-2272 (1997).
30. Mahammad, S., Dinic, J., Adler, J. & Parmryd, I. Limited cholesterol

depletion causes aggregation of plasma membrane lipid rafts inducing T cell activation. *Biochim. Biophys. Acta* **1801**, 625-634 (2010).

31. Rorvig-Lund, A., Bahadori, A., Semsey, S., Bendix, P.M. & Oddershede, L.B. Vesicle Fusion Triggered by Optically Heated Gold Nanoparticles. *Nano Lett.* **15**, 4183-4188 (2015).

32. Andersen, T., Kyrsting, A. & Bendix, P.M. Local and transient permeation events are associated with local melting of giant liposomes. *Soft Matter* **10**, 4268-4274 (2014).

33. Friddin, M.S., Bolognesi, G., Salehi-Reyhani, A., Ces, O. & Elani, Y. Direct manipulation of liquid ordered lipid membrane domains using optical traps. *Commun Chem* **2**, 6 (2019).

34. Liu, B., Hui, K. & Qin, F. Thermodynamics of Heat Activation of Single Capsaicin Ion Channels VR1. *Biophys. J.* **85**, 2988-3006.

35. Jana, N.R. Gram-scale synthesis of soluble, near-monodisperse gold nanorods and other anisotropic nanoparticles. *Small* **1**, 875-882 (2005).

36. Angelova, M.I. & Dimitrov, D.S. Liposome Electroformation. *Faraday Discuss. Chem. Soc.* **81**, 303-311 (1986).

Chapter 4 Membrane Fusogenic High-density Lipoprotein Nanoparticles

4-1. Introduction

In previous chapters, I focused on the manipulation of domain structure on lipid bilayer with biocompatible nanomaterial. I developed a methodology to estimate nanomaterial-lipid interaction based on newly revealed salting-in and sugar assisted salting-in like effects of biocompatible nanomaterials. And I estimated nanomaterial-membrane domain interaction without any disturbance of cationic and anionic ions to build an orientation for development of model lipid raft and other phase-separation structure on lipid bilayer on both of model and cell membrane.

In this chapter, I Introduced another way of membrane manipulation method, direct supply of lipids based on membrane fusion approach. Lipid supply from fusogenic lipid/protein nanocarrier (HDL) was observed and characterized toward both of model membrane and living cell membrane. This fusogentic HDL achieved a kind of environmental selective lipid supply. At mildly acidic pH, endosomal or tumor-like condition, well-optimized fusogenic HDL mutant exhibited the fusogenic activity higher than known fusogenic liposomes. I proposed the fusogenic HDL-based direct manipulation of lipid composition would also be a novel tool for control property of structure on lipid bilayers.

Lipid bilayer membrane fusion, including that in fertilization[1], development[2], viral infection[3, 4], and membrane trafficking between intra-cellular organellars[5], is a fundamental and universal process in biology. Membrane fusion requires sophisticated fusion machinery and is often executed by membrane-binding proteins via zippering process that generate intertangle contact of molecules between the two membranes and arrange hydrophobic atmosphere within the contact area to be fused[6]. For example, viruses utilize their envelope proteins on the surface such as neuraminidase and hemagglutinin to complete infection process into cytosol under moderate acidic pH in the endosomes of the host cell to introduce their nucleic acid into its cytosol. As I discussed in previous chapters, control of lipid composition of cell membrane would be a key intermediate

millstone to achieve the manipulation of two-dimensional structure on cell membrane. In the pharmaceutical field, artificial membrane fusion is also regarded as a novel and reasonable tactics to potentiate the efficacy of nanocarrier-mediated drug delivery systems. Herein, I sought to apply a human-derived lipoprotein into a virus-like drug nanocarrier via design of membrane-fusogenic surface by genetic and chemical engineering. The smart membrane fusion system not only modified membrane condition but a novel drug delivery carrier in the future.

HDL is a complex of lipid and protein, which have approximately 10 nm in diameter, and a cholesterol (Chol) carrier on reverse cholesterol transport process from peripheral tissues to the liver and steroidogenic tissues in human body. In its nascent form, HDL has a discoidal lipid bilayer circumscribed by lipoproteins and may be artificially reconstituted in vitro with recombinant apolipoprotein A-I (apoA-I) and phospholipid-cholate micelles[7]. Due to its intrinsic biocompatibility, small size, development of in vitro preparation method, and capability to incorporate hydrophobic drugs, HDL has been considered as a amazing drug carrier [8-14]. HDL mutants have a kind of flexibility on design. The horizonal surface of the discoidal structure show different characters as the “head and tail “of lipid molecules and the vertical surfaces, covered with apoA-I could be modified by genetically fused peptide at the terminal of apoA-I mutant. For example, fused-cell penetrating peptide (CPP) at the C-terminal of N-terminal 43 residue-deleted apoA-I enhance the intracellular delivery of drugs on HDL. This mutant, termed as cpHDL, was prepared with Apo-A1 mutant bearing TAT peptide, which sequences is derived from HIV (Human Immunodeficiency Virus) Tat (Trans-activator of transcription) protein and POPC (1-Palmitoyl-2-oleoylphosphatidylcholine), a kind of phospholipid.[15, 16] Electron microscopy (EM) measurement informed that cpHDL really exhibits a discoidal structure like the wild-type HDL and was attached to the plasma membrane in a face-to-face manner [17]. Inspired by these results, I tried to invent a fusogenic HDL nanoparticle in the viewpoint of modification of the Nano-bio interface of HDL and target bilayer by the detail insights about the effects of HDL variants surfaces

4-2. Results

I chose DOPC (phospholipids with dioleoyl groups 1,2-dioleoyl-*sn*-glycero-3-phosphocholine) and DOPE (1,2-dioleoyl-*sn*-glycero-3-phosphoethanolamine)[18]as the staring lipid components of fusogenic cpHDL derivatives, owing to their abilities to form relatively fluidic membranes and the amino grope of DOPE. The phase transition temperature (Tm) of DOPC and DOPE, which are 18:1(Δ9-Cis) lipids, is -22°C and -16°C, respectively so lipid bilayer of these lipids are fluidic phase in our handing condition. Contradictory, 16:0-18:1 pair of phospholipids, POPC and POPE shows white aggregation and condensation of lipid and protein conjugation due to their high phase transition temperature, -3°C and 25°C respectably. I also realized the lipid film preparation process perturb the yield and stability of HDLs derived from 16:0-18:1 pair of phospholipids and it was slightly difficult to handle. The rotation speed of evaporator looks critical to good film but it is troublesome and the best sample is not stable because it transition temperature is over storage temperature so the sample tend to gel and sometimes irreversible even though lipoprotein required low storage temperature. I decided to use 18:1(Δ9-Cis) pair phospholipids

HDL derivatives	Lipid				pH 7.4		pH 5.5	
	DOPC	DOPE	CHEMS	Chol	Diameter (nm)[a]	ζ-potential (mV)[b]	Diameter (nm)[a]	ζ-potential (mV)[b]
1/TAT	100	–	–	–	9.1 ± 0.3	− 13.0 ± 2.7	10.1 ± 0.2	− 0.3 ± 0.3
2/TAT	50	50	–	–	9.5 ± 0.2	− 17.1 ± 0.5	9.1 ± 0.9	− 0.4 ± 0.5
3/TAT	37.5	50	12.5	–	11.0 ± 0.1	− 20.6 ± 6.1	10.6 ± 0.4	− 0.4 ± 0.3
4/TAT	25	50	25	–	11.1 ± 0.1	− 31.3 ± 1.6	10.5 ± 1.0	− 0.2 ± 0.5
5/TAT	75	–	25	–	9.6 ± 0.1	− 22.7 ± 4.3	9.7 ± 0.2	− 1.6 ± 0.3
6/TAT	25	50	20	5	8.3 ± 0.3	− 22.2 ± 0.8	8.8 ± 0.5	− 0.5 ± 0.4
7/TAT	25	50	12.5	12.5	11.0 ± 0.8	− 18.1 ± 2.5	9.7 ± 0.9	− 0.6 ± 0.4
8/TAT	25	50	–	25	9.0 ± 0.9	− 14.0 ± 0.3	9.7 ± 0.9	− 0.2 ± 0.3
1/mock	100	–	–	–	9.0 ± 1.2	− 12.6 ± 1.4	8.2 ± 0.6	− 0.1 ± 0.3
4/mock	25	50	25	–	8.9 ± 0.1	− 35.5 ± 1.4	9.5 ± 0.5	− 8.0 ± 0.8
4/PN					9.7 ± 0.1	− 33.5 ± 0.4	10.5 ± 0.2	− 0.4 ± 0.3
4/R8					12.1 ± 0.1	− 22.1 ± 2.1	12.5 ± 1.0	− 1.9 ± 0.4

Table1. The summarized characteristics of prepared HDL derivatives. Lipid composition in preparation, diameter by using DLS measurement, and ζ-potential of HDL derivatives at different pH conditions are shown.

instead of 16:0-18:1 pair in this section. The Amino group generally protonated at weak acidic condition and make hydrogen bonding between the protonated amino group and carboxyl or phospholipid group on lipid bilayer would be strong. [19, 20] Cholesteryl hemisuccinate (CHMES) has been utilized to make surrounding pH-responsible lipidic nanocarriers because of the involvement of its carbonyl group[21, 22]. From these estimations, I tried investigating the interaction between the lipid bilayer and cpHDL derived from DOPE, DOPE, and CHEMS.

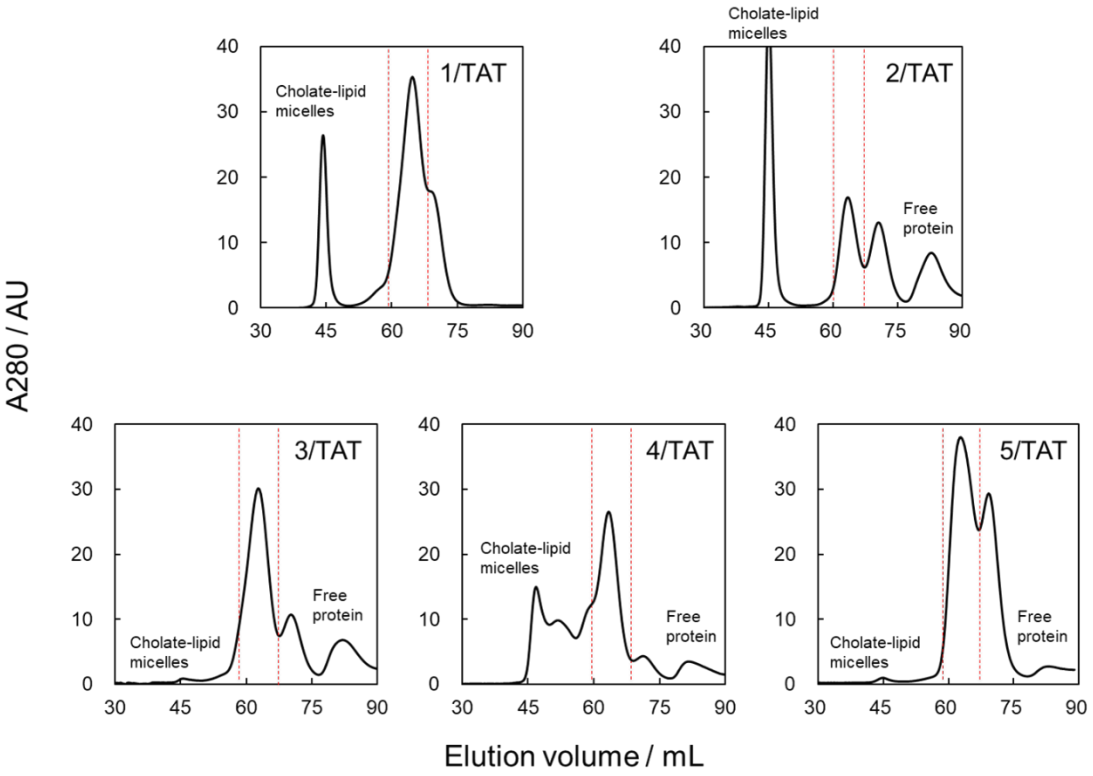

Figure1. Size-exclusion chromatography(SEC) of the prepared HDL derivatives of 1/TAT,2/TAT, 3/TAT, 4/TAT, and 5/TAT. Fractions between the elution volume of 60 and 70 mL (surrounded region by red-dotted line) were collected and concentrated for the subsequent evaluation. Former peaks indicated a large cholate-lipid micelles and later peaks indicated free Apo-A1 proteins as shown in panels.

At first, the suitable molar ratio of DOPE for cpHDL synthesis was declined by preparation in various ratios of DOPE in the cholate dialysis method (Table 1). The cpHDL formation efficiency decreased in response to an increase in DOPE molar ratio and was declined to zero at 80% mola ratio of DOPE (data not shown).

These results are in accordance with those of a previous report, wherein DOPE tend to prevent HDL formation[23]. Therefore, DOPE molar ratio was fixed at 50%. Next, cpHDL synthesized with 50% DOPE (2/TAT) was derivatized with addition of CHEMS (12.5, 25, and 50 mol%) in ingredient lipids. (Fig. 1 and Table 1). At 50% CHEMS (0% DOPC and 50% DOPE) compositions, discoidal HDL nanoparticle was not synthesized (data not shown). This data indicated that main component of HDL lipids should be DOPC, as predicted above. The split main peak would indicate that the ratio of supposable two shape of HDL, saddle shape and discoidal- shape. [24] In this research, I chose to purify main products for each batch. The diameters of the two cpHDL derivatives (ca. 10 nm) were like the

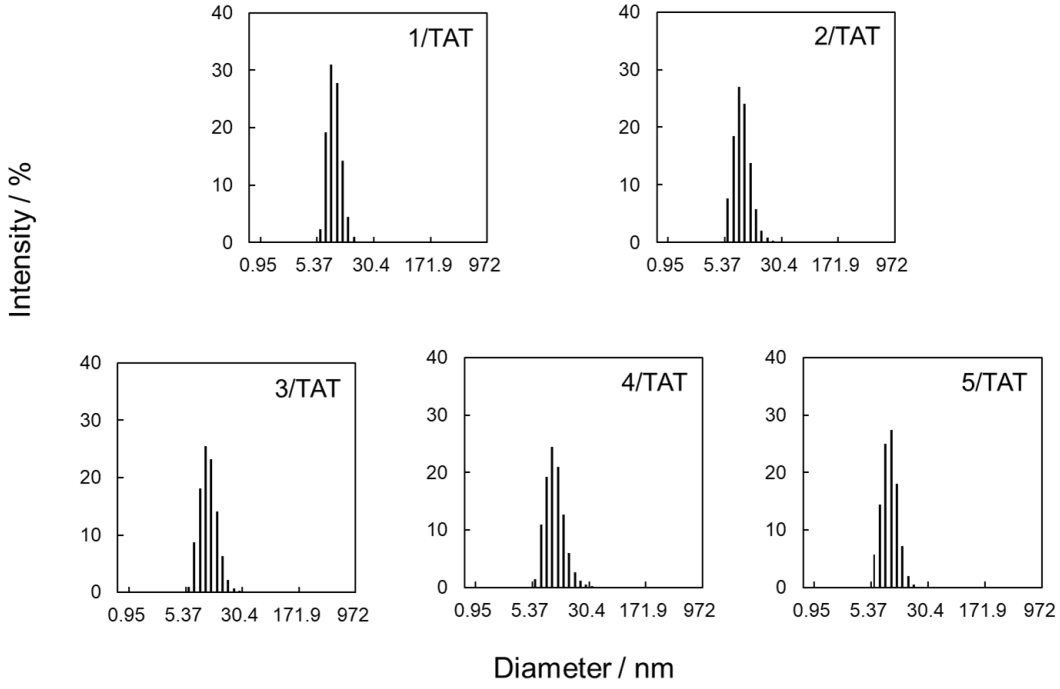

Figure 2. Size distribution of the purified HDL derivatives of 1/TAT, 2/TAT, 3/TAT, 4/TAT, and 5/TAT. All HDLs were diluted with PBS and measured by dynamic light scattering.

diameter of the original cpHDL without CHEMS (Fig. 2 and Table 1). The zeta potential of 2/TAT (–17.1 ± 0.5 mV) at pH 7.4 dramatically declined along with an increase in the CHEMS amount (Table 1). This negative shift was accordance with results of a gel mobility shift assay by using native agarose gel electrophoresis (Fig. 3A). The distance of gel electrophoreses well correlated with

the surface charge of HDL derivatives and there was no decomposition of HDLs. CBB stained protein and florescent labeled lipid band images were collocated well in every samples. The decrease in the solution pH, on the other hand, resulted in the immobile band in the gel shift assay and positive shift value toward almost zero in the zeta potentials of cpHDL derivatives with CHEMS. The band location and surface charge value were comparable to that of 2/TAT with no CHEMS (Table 1, Fig. 3B). These data also clearly indicated that the HDL derivatives contained CHEMS which has carboxyl group. They are deprotonated under neutral pH condition and protonated under mild-acidic condition. These results clearly demonstrate that the two 2/TAT derivatives (3/TAT and 4/TAT) successfully incorporated CHEMS in an adding content dependent manner.

From the above patches of the surface design, I supposed that 4/TAT would be a rich donor/acceptor of hydrogen bonding. To confirm our success of surface design of HDL. I also checked the molar ratio of contents in cpHDL in 4/TAT by LC/MS/MS analysis. To our knowledge, there are no actual observation of consistence between HDL components and the preparation ratio of the mixed lipid material in cholesterol dialyses method.[24] The major characteristic ions for DOPC, DOPE and CHEMS were their molecular ions [M+H] (positive ion mode) or [M-H] (negative ion mode) at m/z of 786.4, 744.3 and 485.3, respectively, and when subjected to collision-induced dissociation, they yield a fragment at m/z 184.0, 603.4 and 99.0, respectably (Fig.4). Fig.4 shows the LC-MS/MS chromatograms of precursor and product ion at 786.4>184.0 for DOPC, 744.3>603.4 for DOPE or 485.3>99.0 for CHEMS of authentic standard (Fig .4D, S, F) and the extract from 4/TAT (Fig. 4.G, H, I). The extract from 4/TAT showed the same retention time as each authentic standard at 51.5, 43.7 and 24.3 min for DOPC, DOPE and CHEMS. The concentration of these three compounds in 1mL of methanol extraction were 6.0±0.8, 11.0±1.3, and 3.1±0.4 μg/mL, respectively, which corresponded to the molar ratio of 1.2:2.3:1. This result clearly shows that the composition of components in 4/TAT was almost same as that of starting material of 4/TAT preparation based on the cholate dialysis method (1:2:1, Table1).

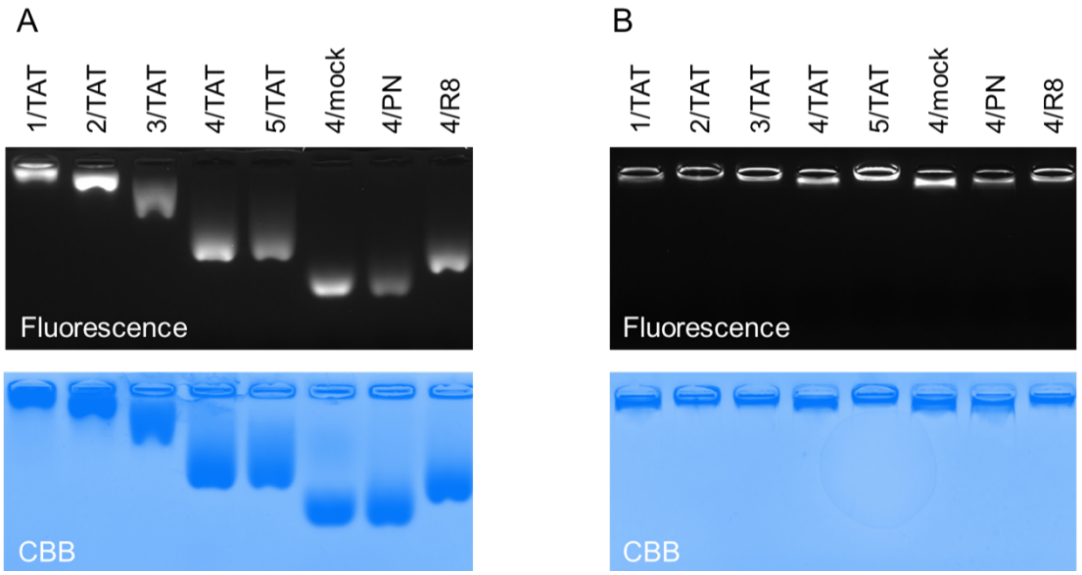

Figure 3. Native agarose gel (0.8% agarose) mobility shift assay for HDL derivatives at pH 7.4 (A) or 5.5 (B). After peforming electrophoresis, Rho-DPPE fluorescence from HDL lipids was detected and the agarose gel was subjected to CBB staining to confirm the co-localization of lipid and protein moiety of HDL derivatives. Rho-DPPE fluorescence was detected under UV (302 nm) excitation by a Gel Doc XR imager (Bio-Rad).

The fusogenicity of these cpHDL derivatives was evaluated by a Förster Resonance Energy Transfer (FRET)-based lipid-mixing assay (Fig.5). [25] In this assay, cpHDL were mixed with 100 nm liposome in the same lipid basis concentration (15 μM of both sample). cpHDL included NBD-PE and Rho-PE at a molar ratio of 1% of the total lipid. Without lipid mixing, NBD-PE and Rho-PE locate in the vicinity area within cpHDL (~100 nm^2) so that FRET quench observed fluorescence intensity from NBD-PE. According to the lipid mixing between cpHDLs and liposomes, NBD-PE and Rho-PE diffused into large liposome lipid bilayer (~30000 nm^2) and green NBD-PE fluorescence turn to emerge.

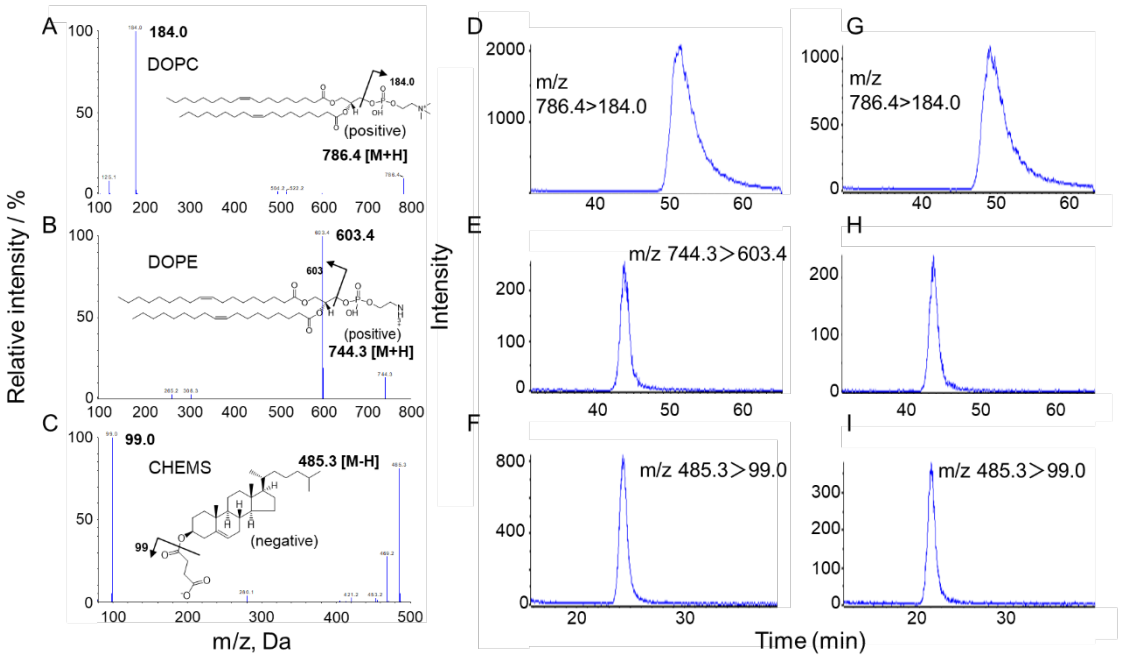

Figure 4. Product ion spectra of pure DOPC (A), DOPE (B), and CHEMS (C) and chromatograms of LC-MS/MS analysis of precursor product ion at 86.4 > 184.0 for DOPC (D, G), 744 > 603.4 for DOPE (E, H), and 485.3 > 99.0 for CHEMS (F, I) of authentic standard (D, E, and F) or the lipid extraction from 4TAT (G, D, and I).

At neutral condition (pH =7.4), no cpHDL derivatives show significant lipid mixing as far as our examination (Fig. 6A-6E, green line). At mildly acidic condition (pH=5.5), however, a strong lipid mixing was induced for 4/TAT (Fig.6A, red line). The fusogenicity of 4/TAT at pH 5.5 was significantly higher than that of well-known two fusogenic liposomes, which are named as Fulip-1 or Fulip-2 in Fig. 6F [21, 26]. These results indicate that HDL containing TAT peptide at the terminals of Apo-A1 mutants, which then been introduced as a DDS carrier, was successfully endowed with acidic environment-dependent fusogenicity by incorporation of CHEMS and DOPE. [26, 27]. This results also suggested the occurrence of lipid supply from HDL to liposome in an environmental-selective manner. It should be noted that the first decrease of Lipid mixing ration shown in Fig. 6A-D are caused by solution condition changes such as temperature adjusting from room

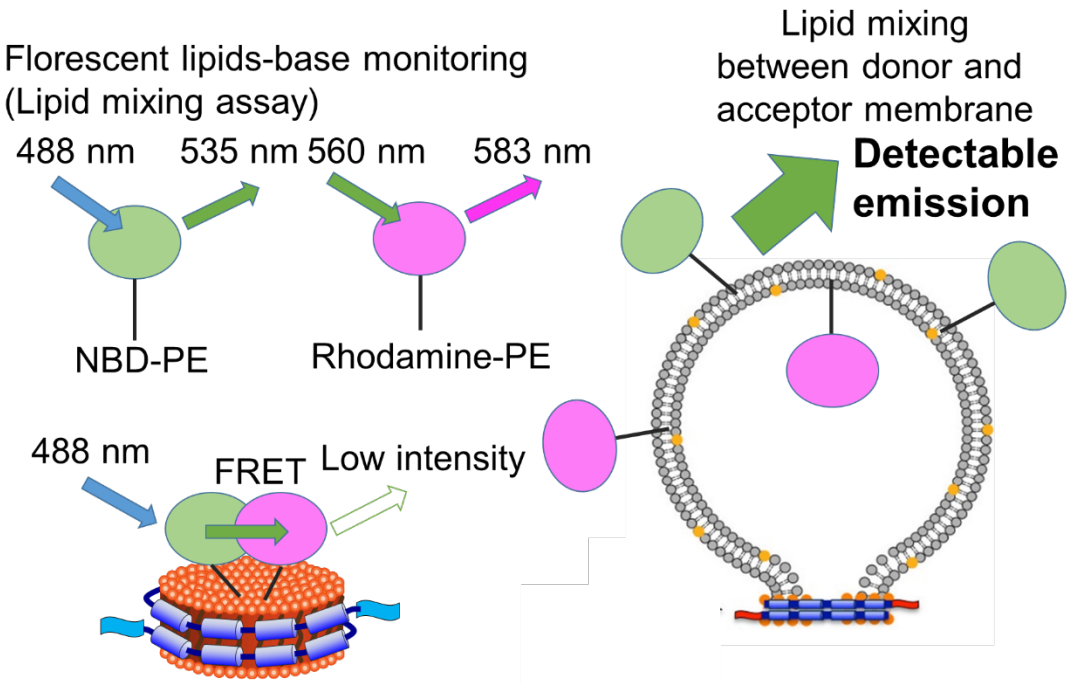

Figure 5. Schematic illustration of the lipid mixing assay based on Fluorescence resonance energy transfer

temperature to 37°C and do not relate with lipid exchange.

The low pH-selective fusogenic ability of 4/TAT declined in response to a decrease in the ratio of CHEMS (Fig. 6A-D), demonstrating that the protonation of the carboxyl group of CHEMS at pH 5.5 was responsible for this effect. [21, 28] The replacement of all DOPE in 4/TAT with DOPC (5/TAT) did not show significant lipid mixing (Fig. 6E). These data indicated that the co-existence of CHEMS and DOPE in the lipid bilayer of cpHDL are fundamental for the remarkable acidic pH-selective lipid-mixing. The role of DOPE is still in an enigma, but I estimate that the protonation of an amino group of DOPE in acidic conditions may increase the

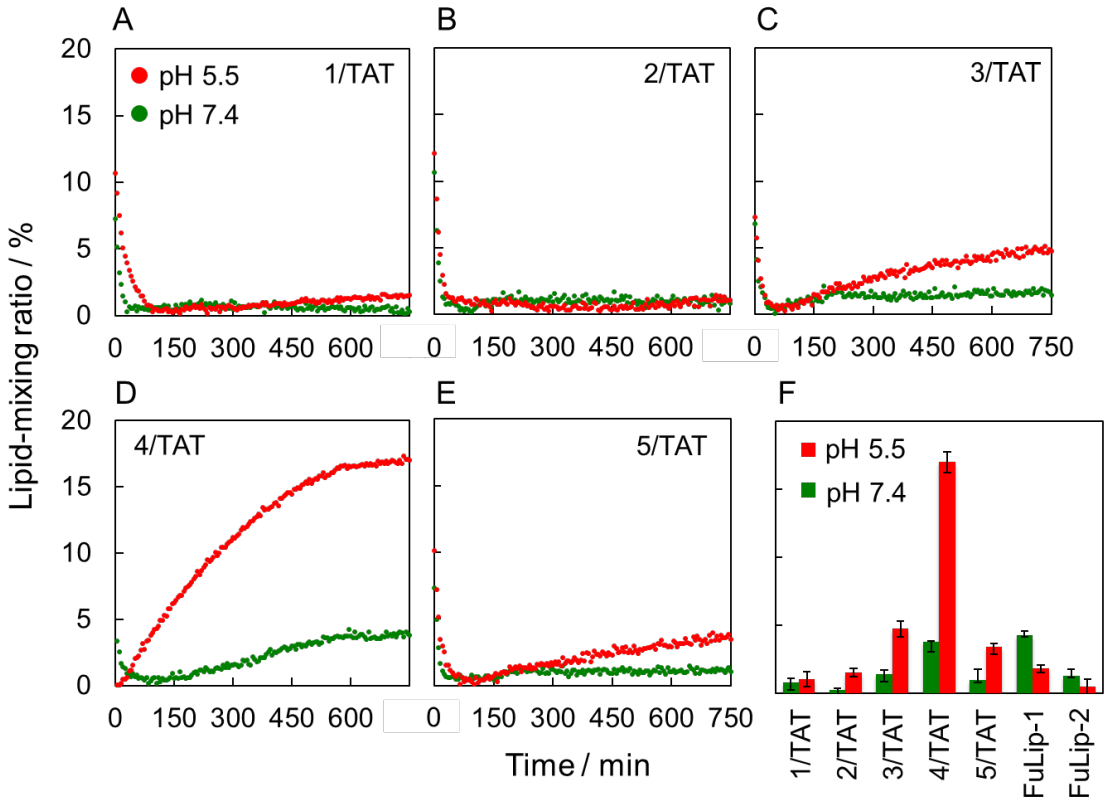

Figure 6. Results of time-dependent lipid-mixing monitoring of 1/TAT (A), 2/TAT (B), 3/TAT (C), 4/TAT (D), and 5/TAT (E) with 100 nm-sized DOPC/DOPS (9/1) liposomes at 37 °C. Lipid-mixing activities of known fusogenic liposomes with SOPC/DOPE (75/25) (FuLip-1) and DOPC/DOPE/CHEMS (25/50/25) (FuLip-2) were evaluated for reference (n = 3). All samples were prepared with 50 mM MES buffer containing 150 mM NaCl (pH 5.5, red) or PBS buffer (pH 7.4, green) to adjust concentration followed by mixing assay. Lipid-mixing values after the assay were summarized as a function of lipid composition (F).

number of hydrogen bonding between 4/TAT and liposomes as I mentioned above. Previous reports suggested that the carboxyl group of CHEMS was a well-known membrane fusion inducer [28]. To collect more information related to the role of the carboxylate group in this lipid-mixing process, CHEMS in 4/TAT was replaced with Chol at different molar ratios (5, 12.5 and 25 mol%) and the molar ratio of DOPE and DOPC were kept as 25 mol% and 50 mol% to obtain 6/TAT, 7/TAT and 8/TAT, respectably (Fig. 7).

Lipid mixing ratio significantly decreased for 6/TAT and 7 TAT at mildly acidic condition and showed almost no lipid mixing ability in 8/TAT. These data clearly

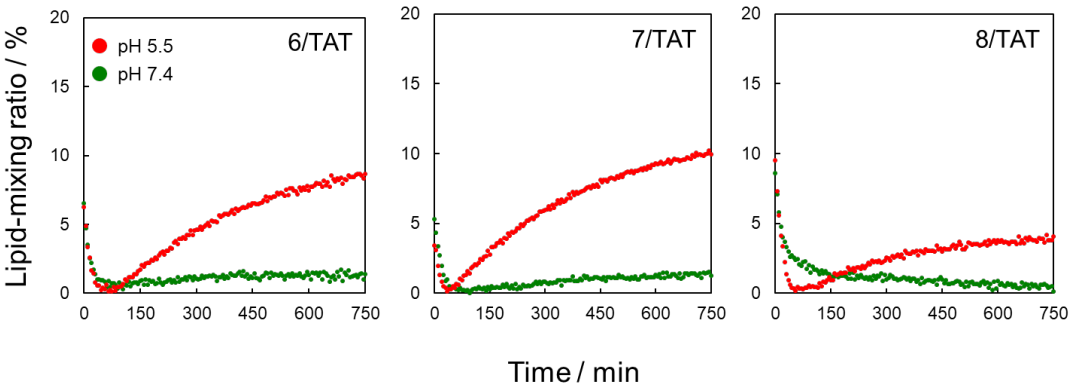

Figure 7. Lipid-mixing ratio of 6/TAT, 7/TAT, and 8/TAT at both pH conditions. All data represent the average of triplicates.

verified that the necessarily of CHEMS in this lipid mixing process. To gain more insight in the role of CHEMS. The physical property of HDLs in both pH conditions were evaluated because the characteristic of Nano-bio interface would be generally affected on the free energy of adhesion. Moreover, the change of physical behavior, such as the tendency of membrane fluidity sometimes leads the membrane fusion and adhesion. I measured the two major physical parameter of the lipid/protein Nanodiscs, hydrophobicity and fluidity. Hydrophobicity means a tendency of invention of water molecules into the lipid bilayer and was evaluated by using Laurdan, a sensitive fluorescent probe to surrounding polarity. Fluidity was evaluated by using DPH (1,6-diphenyl-1,3,5-hexatriene), a fluorescence anisotropy probe for molecular motion (See detail in experimental section 8. and 7.). This pH-selective fusogenicity of 4/TAT at least in part correlated with the protonation-derived hydrophobic membrane of the HDLs at pH=5.5 (Fig. 8A), while the membrane fluidity is likely to have no association with the high fusogenicity of 4/TAT (Fig. 8B). They mentioned that this lipid mixing is not explained explicitly from these two properties of the lipid membranes of HDLs. Other possible mechanism is related to protonation of the histidine tag (His-tag) for Ni-column purifications of our apoA-I mutants at the N terminus (see experimental section 2. Cloning and expression of apoA-I mutants), because the histidine imidazole ring has a pKa of ca. 6. I cannot completely decline the possibility of contribution of its cationization in some way at pH 5.5 to

the low pH-dependent fusogenicity of 4/TAT but given that 2/TAT and 5/TAT showed the much less activity at pH 5.5, respectively, contribution of His-tag, all cpHDL derivatives have, if any, would be small compared with other conditions.
I studied the mechanism of membrane fusion in detail by altering CPP moiety at C-terminal of my Apo-A1 mutant. (Fig. 9A). TAT peptide in 4/TAT was removed (4/mock) or replaced with penetratin (RQIKIWFQNRRMKWKK) (4/PN), Arg8 (4/R8), or Arg11 (4/R11). Unfortunately, 4/R11 was hardly yielded by our HDL preparation method and stop to investigate further. However, other three derivatives were successfully constructed, purified and exhibited similar diameters to one of 4/TAT in DLS analysis and SEC profile (Fig. 9B, C). The former three derivatives and 4/TAT was also characterized by using EM (electron microscopy) analysis and the diameters were almost same in all samples (Fig. 9D). I confirmed that the three CPP derivatives could be utilized as a control to

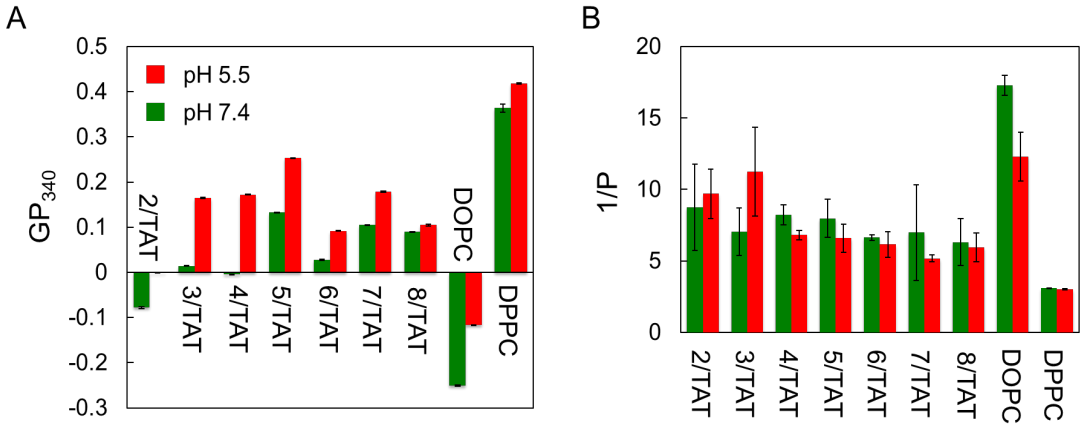

Figure 8. Estimated membrane polarity (A) and fluidity (B) of HDL derivatives. General polarization (GP340) of HDL derivatives and liposomes was measured as an indicator of membrane polarity by using 6-dodecanoyl-2 dimethylaminonaphthalene (Laurdan) at both pH conditions (n = 3).Laurdan dictate membrane fluidity as the water content in the membrane, as indicated by the low value of gel phase DOPC liposomes and high value of sol phase DPPC(1,2-dipalmitoyl-sn-glycero-3-phosphocholine) liposome in the right of (A). Fluorescence polarization (1/P) of HDL derivatives and liposomes was evaluated as an indicator of membrane fluidity at both pH conditions (n = 3). The reciprocal of the steady-state fluorescence polarization value (P) of 1,6-diphenyl-1,3,5-hexatriene (DPH) in lipid bilayers is an indicator of the membrane fluidity.1/P indicates the rotation tendency of the rod-shaped DPH. DOPC- and DPPC-liposomes work as control to verify our system in that they showed relatively high and low values, respectively. All of HDL derivatives showed similar values, irrespective of the solution pH.

investigates the works of CPP peptides on lipid mixing process without at least explicit disturbance. Low pH selective fusogenicity was observed for 4/R8 and 4/PN, but 4/PN have lower fusogenicity than 4/TAT and 4/R8 (Fig. 10A,B)) and 4/mock did not show any fusogenicity (Fig. 10 C). These results indicate that the presence of CPP is essential in the occurrence of membrane fusion and the effect is depended by the number of Arg residues in CPP (Fig. 10D).

To gain more insight about the mechanism of the lipid mixing of 4/TAT, 4/R8, and 4/PN, the lipid mixing acceptors, liposome of liposomes of DOPC/DOPS(1,2-dioleoyl-sn-glycero-3-phospho-l-serine) = 90/10, were derivatized by changing

the lipid compositions. I supposed that at least either of surface charge or acyl chain length would be a factor related to lipid mixing so I choose to DOPC liposome and POPC liposome as liposome derivatives. The surface charge of liposome is lower than DOPC liposome. Lipid mixing by all three HDL variants was inhibited to some extent with liposomes containing DOPC only compared with DOPC: DOPS=90:10 liposome, but was completely suppressed in liposomes containing POPC only (Fig. 10 E-H). Furthermore, DLS analysis after the lipid mixing assay showed the existance of a micrometer-sized distribution in the mixture of 4/TAT and DOPC/DOPS=90/10 liposomes, but not observed in liposomes alone (Fig. 11). It should be noted that aggregation itself sometimes increase the fluorescence intensity but the possibility was excluded by fusogenic-living cell membrane fusion assay as you shall see below.

The data indicates that the CPP peptide of 4/TAT play a significant role of CPP-membrane adhesion and induced the following lipid mixing. Since the previously studied HDL mutant with TAT peptide (and POPC) was bound to the plasma membrane of adherent cells in a face-to-face manner [17], such aggregation induction would be explained by gathering two liposomes by a single 4/TAT via their binding to the both sides of the 4/TAT membrane. These observations indicate that both the electrostatic interaction and membrane fluidity of liposomes are critical factors influencing the lipid mixing in three HDL derivatives.

It should be noted that the aggregation of nanomaterial itself sometimes increase the fluorescence intensity, but I decline the possibility from the living cell assay as you shall see. Accumulation of HDL on membrane itself did not cause the increase of fluorescence but incubation in acidic pH induced the lipid mixing-driven fluorescence change.

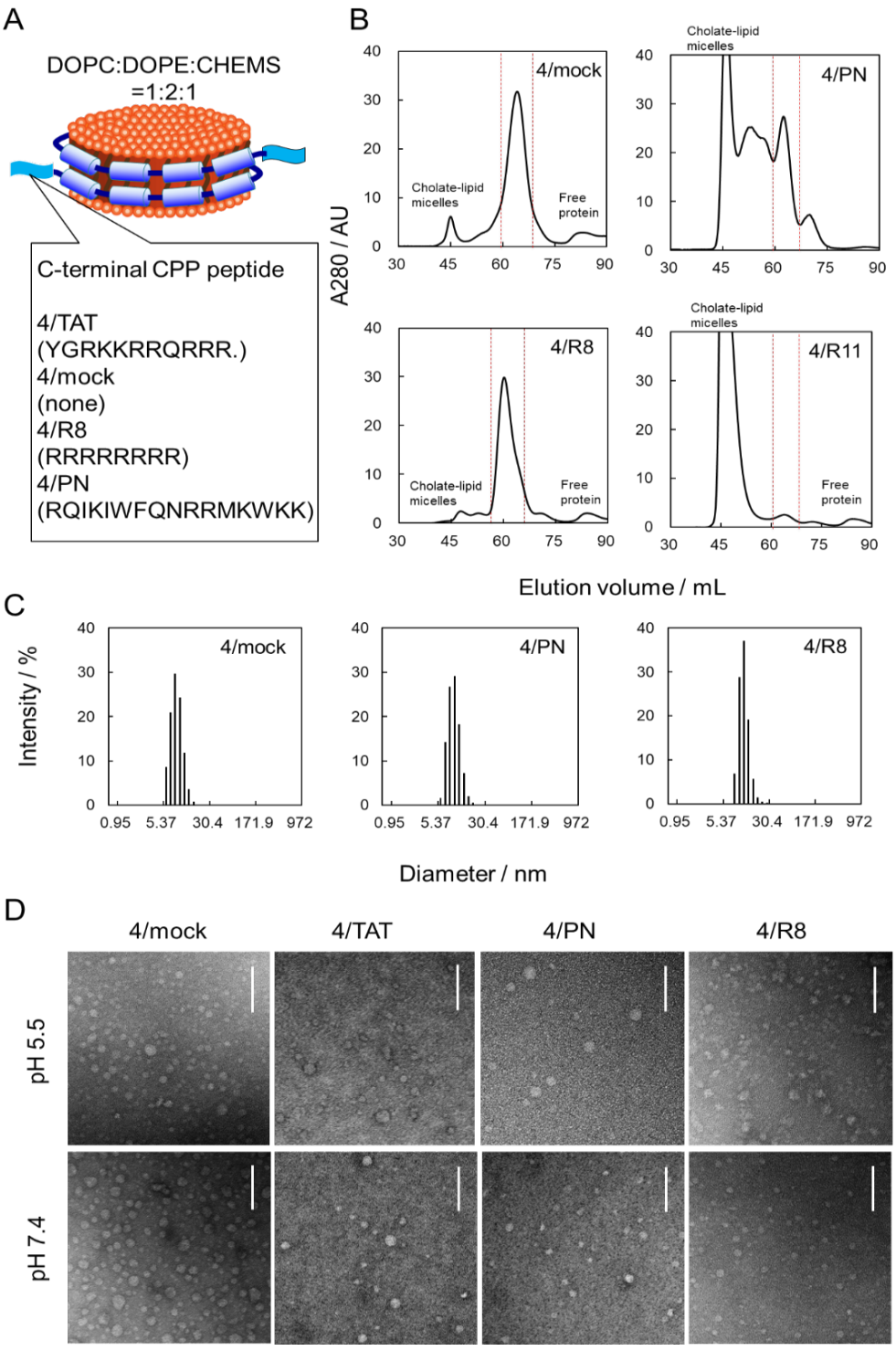

Figure 9. Illustration of modified cp HDLs derivatives, 4/TAT,4/mock,4/R8,4/PN (A) and characteristics of the cp HDL derivatives by using SEC chromatography (B), DLS mesurement (C,) and electron microscopy (D). scale bar, 100 nm.

To measure fusogenicity of HDL mutants and pH dependency of the fusogenicity, octadecyl rhodamine B chloride (RhoB) was utilized in mammalian living cells experiments[29]. RhoB is a fluorescently label for the cpHDL lipid bilayer. 4/TAT was chosen as representative because HDL mutants embracing TAT peptide have been tested in various studies in previous live mammalian cell systems.[15-17, 30-32] And the behavior of 4/TAT in lipid mixing is investigated in detail in this study. 1/TAT (no CHEMS) and 4/mock (no TAT peptide) were used as a control. Both

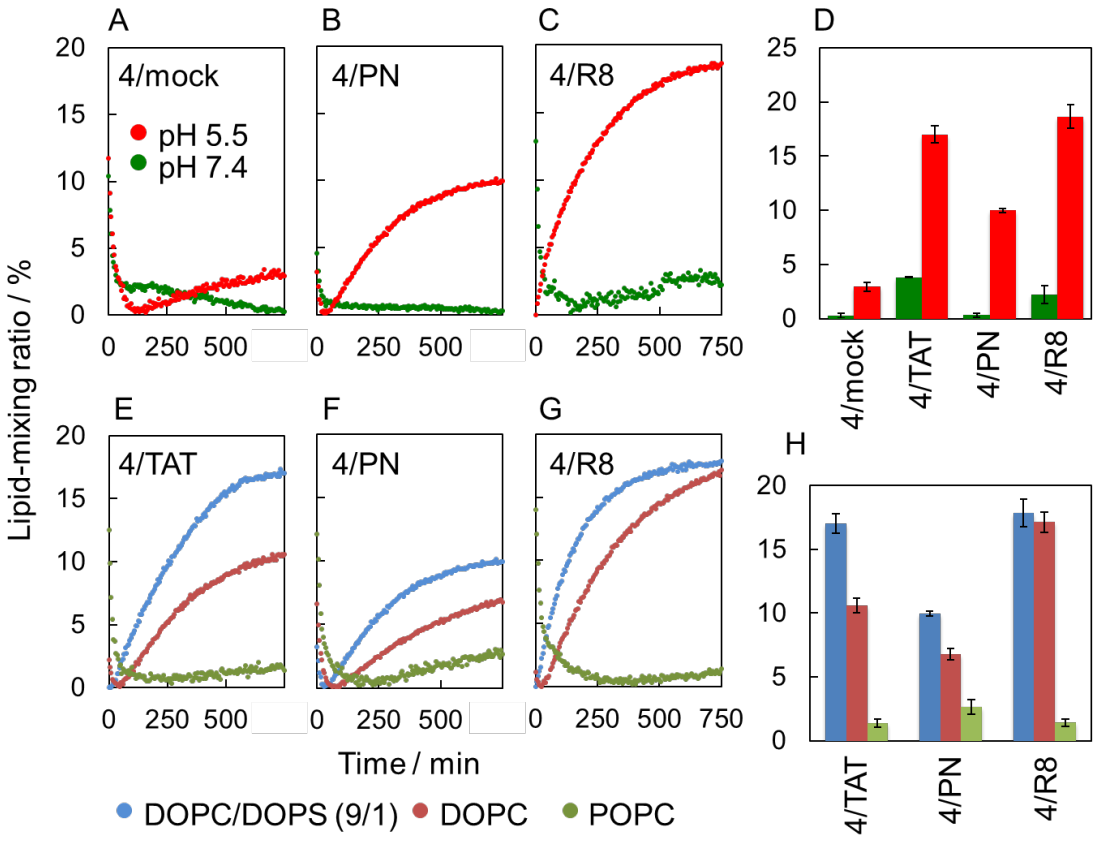

Figure 10. Results of lipid-mixing assay between 4/mock (A), 4/PN (B), and 4/R8 (C) and DOPC/DOPS=9:1 liposome at pH 5.5 (red) and pH 7.4 (green). Lipid-mixing ratios were illustrated as a function of cell-penetrating peptide (D). Lipid-mixing ratio of 4/TAT (E), 4/PN (F), and 4/R8 (G) with different membrane properties of liposomes at pH 5.5. DOPC (red), POPC (green), and DOPC/DOPS (9/1) (blue) liposomes were incubated with indicated HDL derivatives at pH 5.5. Lipid-mixing ratios after the assay were illustrated as a function of lipid composition of liposomes (H).

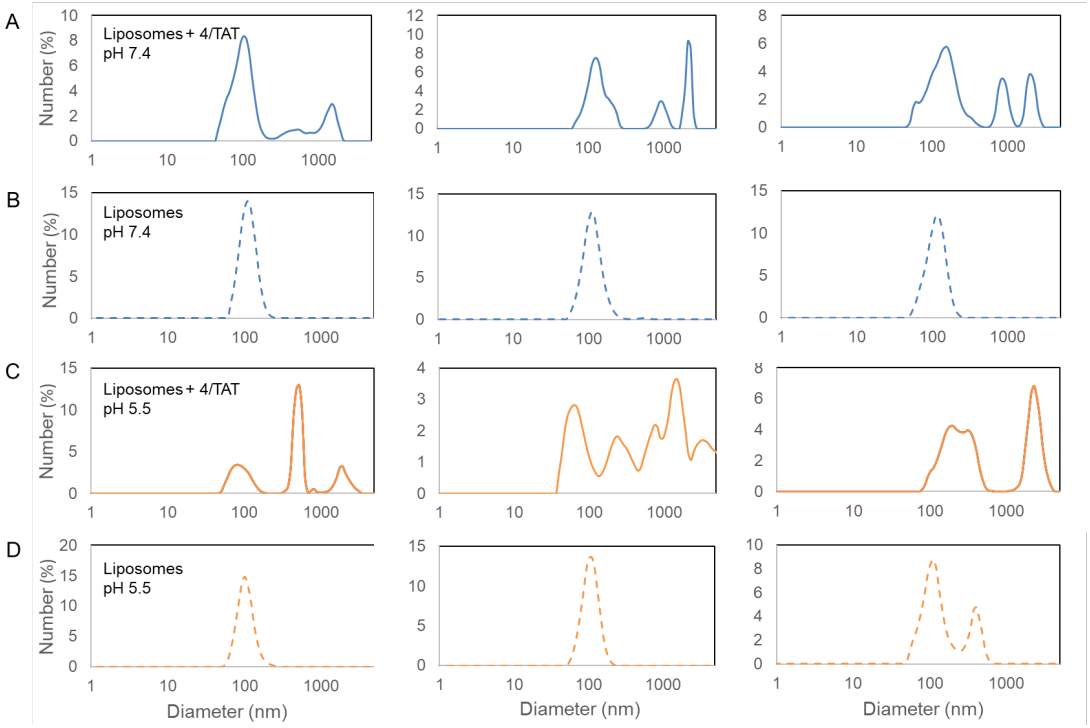

Figure 11. Size distribution after the lipid mixing assay (37ºC, 750 min) of liposomes and 4/TAT at pH 7.4 (A), liposomes alone at pH 7.4 (B), liposomes and 4/TAT at pH 5.5 (C), and liposomes alone at pH 5.5 (D). Results of the three trials are shown in each condition.

1/mock and 4/mock did not exhibit the plasma membrane binding/internalization at either pH conditions, as predicted from lipid mixing assay results (Fig. 12A). On the other hand, 4/TAT bound to the plasma membrane of T24 cells, established cell line of urinary bladder carcinoma, in the presence of FBS (Fetal bovine serum) even at neutralized condition (pH=7.4) (Fig. 4A). The binding ability of 4/TAT was much stronger than the binding ability of 1/TAT, which have a more cationic surface (Table 1), and this tendency was essentially same at pH 6.4 (Fig.12A). Further acidification below pH 6.4 of the serum-containing cell medium led to clouding and aggregation of serum components, inhibiting live cell studies at pH 5.5. Therefore, I decided to use serum-free medium at pH 5.5. instead of usual medium. As shown in Fig.12B, C, the fluorescence signal on cell membrane was more intense at pH 5.5 than at pH 7.4. Because the intrinsic fluorescence intensity of 4/TAT was almost same in both pH conditions (Fig.12E),

this microscopic result indicates that the binding of 4/TAT to the cell membrane was enhanced at pH 5.5. Next, pulse-chase experiments were performed to determine whether lipid mixing between 4/TAT and the cell membrane of T24 cells occurred in pH-selective manner (see Experiment. Confocal analysis). RhoB fluorescence is to some extent self-quenching in a limited compartment of the 4/TAT disc membrane and diffusion of RhoB are result in the stronger fluorescence intensity. The diffusion-induced recovery of fluorescent intensity is thought to be monitored the lipid mixing between the two. As shown in Fig.12D, the signal of RhoB fluorescence from the cell membrane seemed to be stronger at pH 5.5 than at pH 7.4. This result suggests that 4/TAT could undergo mildly acidic pH-dependent membrane fusion with living T24 cell membranes. Flow cytometric analysis of the cells in Fig.12D was also carried out, but the significant difference in fluorescence intensity was not clear. This could be due to inadequate lipid mixing; however, the fluorescence intensity of the microscopic images clearly indicates the occurrence of lipid mixing.

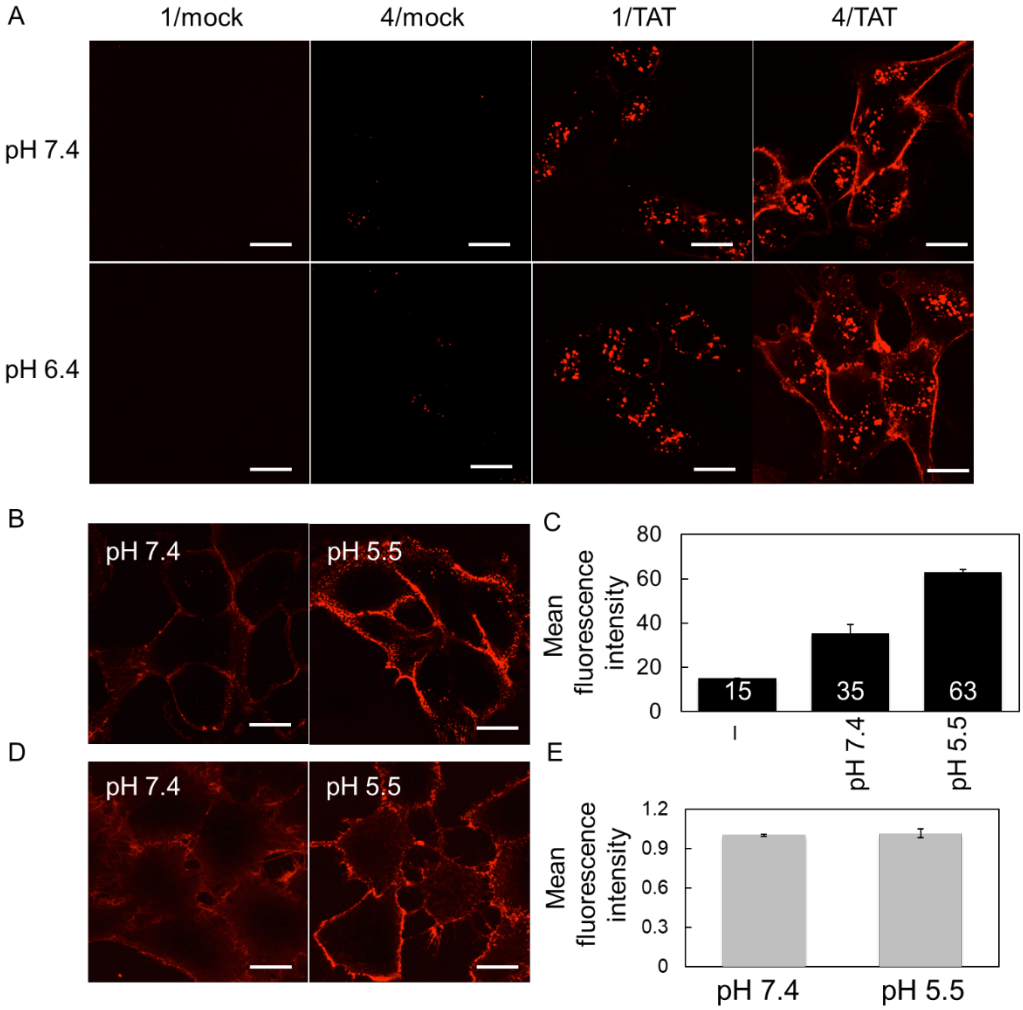

Figure 12. pH-depending affinity of 4/TAT toword the living cell membrane of T24 cells under neutral and mild acidic condition. Confocal microscopic images of live cells incubated with octadecyl rhodamine B (RhoB)-labeled 1/mock, 4/mock, 1/TAT, or 4/TAT (10 μg protein/mL) in the McCoy'5A medium containing FBS at pH 7.4 (upper) or 6.4 (lower) for 1 h at 37 °C (A). In the absence of FBS condition, the plasma membrane affinity of RhoB-labeled 4/TAT at pH 7.4 and 5.5 was also measured by imaging (B) and flow cytometric assay (n = 3) (C). Confocal analysis of T24 cells were treated with RhoB-labeled 4/TAT for 1 h at 4 °C and pH 7.4 and incubated with fresh serum-free media of pH 7.4 (left) and pH 5.5 (right) for 5 min (D). The fluorescence of 4/TAT in both pH condition (E). Scale bar 10 μm.

4-3. Discussion

High-density lipoproteins are natural biomaterials with a protein-lipid bilayer structure that can be functionalized in a variety of ways. The protein-lipid bilayer engineering of HDLs using TAT peptides and cationic lipids has been reported, as drug carriers[33] that can escape from endosomes and plasma membrane adhesive covering material for plasmonic nanoparticle[31]. In this study, a series of HDL mutants with multiple kinds of CPPs and lipid compositions were prepared and evaluated for their lipid supply activity using liposomes and live mammalian cells. I found that one HDL mutant (4/TAT) with TAT peptide and a horizonal surface as a mixture of 25 mol% DOPC, 50 mol% DOPE and 25 mol% CHEMS showed promising germination activity under weakly acidic conditions. The coexistence of TAT peptide, DOPE, and CHEMS with 4/TAT was found to be necessary for efficient the HDL and accepter membrane fusion. (Fig. 6B, D, C, E and 7).

The replacement of CHEMS in 4/TAT with Chol to prepare 6/TAT, 7/TAT, and 8/TAT resulted in the forfeit of fusogenicity at pH 5.5 (Fig. 7), as also observed following replacement with DOPE (Fig. 6B). Thus, CHEMS and Chol worked as an accelerator and a bystander, respectively, for this lipid mixing at pH 5.5. This observation is contradictory at a first glance because both CHEMS and Chol are neutral at pH 5.5 and their ζ- potential was almost same o. However, it should be noted that the strength of hydrogen bonding is strong in the condition at the place of HDL-membrane contact and the change of potential in Table 1 indicates that the existence of strong a lot of hydrogen bound donor, protonated carboxylic groups. Although the reason of stronger impact of CHEMS in fusogenicity is still vague, but its protonated succinate group may be inserted between the molecule arrangement of acceptor lipid bilayer and/or slightly fluidize the lipid membrane, resulting in trigger of the lipid mixing derived from the bulkiness and hydrophobicity of the group, respectively. Kulig et al. reported a computational simulation of Chol- or CHEMS-containing membrane structure and mentioned that the deuterium order parameter (higher the value, more ordered is the bilayer) was significantly lower for CHEMS than for Chol [34] . Although this seems to be

inconsistent with the results in Fig. 7B, it would be interesting to utilize Chol derivatives with longer or bulkier alkyl carboxylic acid groups instead of CHEMS to study their effect on fusogenic activity of HDL derivatives.

cpHDL derivatives bearing penetratin (4/PN) only exhibited the lower lipid mixing activity and no membrane adhesion and fusion was observed for 4/mock lacking CPPs even though mutants with eight arginine (4/R8) showed fusogenecity not at all inferior to 4/TAT (Fig. 10A–D). The number of positively charged residues in these derivatives at pH 5.5 was similar (7 for PN, 8 for TAT and Arg8), suggesting that the number of Arg residues may have a significant impact on carcinogenicity (3 for PN, 6 for TAT and 8 for Arg8) In terms of internalization, Arg-rich peptides have been exhibited a superiority to Lysine-rich peptide sequences[35, 36], and this difference was involved in the adhesive on micrometer-sized liposomes[37]. In a previous study using a 1/TAT derivative containing POPC instead of DOPC, the replacement of two Arg residues of TAT with two Lys residues significantly reduced the membrane affinity of TAT to the same degree as its racking derivatives.[30] This superiority of Arg has been explained as resulting from the bidentate hydrogen bonding and electrostatic interaction with phosphate, carboxylate and sulfate groups with the side chain of Arg. [36, 38] The removal of the lipid with anionic head group (DOPS) from the host membrane caused a drastic decrease in the lipid-mixing ratio for all fusogenic derivatives (Fig. 10E–G). Thus, the membrane binding between the Arg residues of CPPs and DOPS head anionic group based on the hydrogen bonding and electrostatic interaction would play a critical role in the subsequent lipid mixing at pH 5.5.

From above discussions, related to the protonation of DOPE and CHEMS, insertion of the group of CHEMS into the counterpart membrane and the role of CPP peptide, I supposed the model of lipid mixing process as the following description. First, cpp peptide attached on cell membrane via hydrogen bonding with protonated Arg and the surface of membrane. This works like an anchor of cpHDLs on lipid membrane. Next, hydrogen bonding between the surface protonated Amino and carboxylic groups bond the two surface of cp HDL and acceptor membranes. Finally, the hydrogen bonding and insertion of a part of

CHEMS molecules make a hydrophobic condition where the contact areas and induce an exchange of lipid layers and following lipid diffusion from cpHDLs to acceptor membrane.

In live mammalian cell assay, 4/TAT showed a higher affinity for the cell membrane in the presence of serum than 1/TAT lacking DOPE and CHEMS as well as 4/mock lacking the TAT peptide (Fig. 12A). Given that 4/TAT (Fig. 6A) has a higher lipid mixing ratio than 1/TAT (Fig. 6A) and 4/mock (Fig. 10A) this high binding affinity of HDL to the cell membrane is not surprising, since the binding of the two membrane structures is the first step in lipid mixing; the apparent lack of pH dependence, evident from the lack of significant enhancement in binding at pH 6.4, is a result of the lack of Inconsistent with the results shown.10D. Inadequate acidification of the cell medium (pH 6.4) compared to serum-free buffer (pH 5.5) for liposome studies may be the main reason why CHEMS protonation significantly altered the physical properties of the membrane at pH below 5.5.[28] In addition, the formation of plasma protein coronas [39-41] around 4/TAT and/or the binding of Ca^{2+} to CHEMS [28] in 4/TAT may affect its biding to the plasma membrane. These considerations were supported by the results shown in Fig. 12B, C.

At least two major plasma membrane receptors of HDL were existing on plasma membrane of mammalian in vivo. (scavenger receptor class B type 1 and ATP-binding cassette transporter A1). [42] These receptors work as a supporter of lipid transportation between the HDL and plasma membrane, which can be regarded as a type of lipid mixing. In other word, the CPP-plasma membrane interaction could be equivalent to the HDL-receptor binding in terms of the opening of the lipid mixing. Therefore, the presence of these receptors would enhance the fusogenicity DOPE and CHEMS included HDLs, such as 4/TAT and 4/mock, in living cells if expressed. Alternatively, CPPs of 4/TAT may not be required for the lipid mixing with cells expressing the receptors in future therapeutic application of this fusogenic HDLs.

HDL can embrace lipophilic drugs such as all-trans retinoic acid [43] as well as small RNA derivatives in cholesterol-conjugated manner [44]in the lipid bilayer. The

incorporation limitation of former type drugs is generally up to 15% of total number of lipid molecules within the final HDL discs, which was between 12.5% and 25% of CHEMS in 3/TAT and 4/TAT, respectively (Fig. 6). Thus, it is not astounded that incorporated drug or lipidic molecules modulates its fusogenicity, relying on the loading ratio and physicochemical properties of drugs incorporated. In the case of the latter drug, the bulkiness and negative charge of siRNA may influence the interaction of the HDL and acceptor membrane.

An extracellular mildly acidic environment is a main characteristic of tumor tissue. To develop tumor-targeted oriented drug delivery carriers, the difference in the pH between normal and tumor tissues has been regarded a first-choice input parameter to allow carriers to distinguish the two tissues. [45, 46] Fig. 12D exhibited that the surface of HDL derivatives, like virus envelopes, conceivably became fusogenic in response to mild acidified surroundings under serum-free condition. 4/mock with the lipid content like that of 4/TAT did not retain the plasma-membrane affinity and not perform cellular internalization, whereas 1/TAT was mostly internalized into the cell and not kept on the plasma membrane (Fig. 12A). This result indicates that the co-existence of and DOPC/DOPE/CHEMS bilayer and the TAT peptide sequence in 4/TAT is significant for the plasma membrane-oriented binding. The activity of membrane fusion is lower than the expectation from liposome lipid mixing assay. The relatively weak of pH dependency for 4/TAT (Fig. 12A) may indicate that CHEMS in lipid bilayers do not act well as an intrinsic machinery for response to pH 6.4 condition. Due to the pH of tumor tissue was reported to be only 0.4 unit lower then neutral[47], further modification of HDL surface is perhaps requires. Previously report mentions that a membrane-destabilizing poly (propyl methacrylate-co-methacrylic acid) derivative exhibits binding to the cationic mutants of HDL and controlled their cellular interactions in a pH-dependent manner even in the presence of serum[33]. Thus, co-utilization of such polymer and this fusogenic surface would lead a design for a more effective lipid supply and manipulation of membrane lipid composition.

The potential of this fusogenetic HDL will be realize in a phase of application on plant cells. The lipid molecule itself works as a gate of information on plant cells.

Recently, a kind of glycolipid molecules, GIPCA, form a complex and work as a calcium ion gates on cell membrane[48]. Moreover, the lipid composition of plant cell membrane would be changed dynamically to reacted on cell membrane. As an example, the composition of a kind of glycolipids, was changed to react an outer phosphate-lack condition [49]. Suppling of lipid molecules would be a direct manipulation method of plant cell behavior due to these lipids themselves activity on cell membrane. Fortunately, the cell cultures media of a major model plant cell, tobacco BY-2, has a mildly acidic pH around pH=5.6, the best condition for lipid mixing by using this fusogenic HDL derivatives.[50] A systematic research of interaction between CPP peptide and plant cell reported that R8 peptide has a high plant membrane affinity[51]. Our results would be a flagship model of lipid-base nanotechnology of plant cells.[52]

In conclusion, I achieved an invention of environmental-selective lipid supply from guest HDL to host lipid bilayer, model and cell membrane. This technology does not require any sophisticated artificial requirements. Due to the characteristic of HDL as a novel drug delivery carrier, our derivatives also have a potential as a tumor-like tissue selective adhesive carrier. The role of each components, DOPE, CHEMS, CPP peptide, of HDL were investigated in detail and they provide a chart of design the surface of future developed nanodevice toward other lipid supply method. contents of this chapter are a good handbook for lipid component manipulator on mammalian and, in future, plant cells.

4-4 Conclusion

I developed a high-density lipoprotein (HDL) mutants that can selectively fuse with the lipid membrane and provide HDL side lipids under mildly acidic conditions selectively by modifying the lipid composition and protein structure of HDL, which can be adapted to non-raft nanostructures on the membrane such as lipid cluster. Mildly acidic conditions are a characteristic of human cancer tissue and are physiologically significant. To increase the membrane affinity, cell-penetrating peptides (CPPs) were attached to the HDL. DOPC, a highly fluidic phospholipid, DOPE, containing a primary amine, and CHEMS, a Chol derivative, were utilized as lipids. Various kinds of HDL derivatives were prepared systematically and their fusiogenic activities were measured.

A HDL derivatives, containing DOPC:DOPE:CHEMS=1:2:1 in molar ratio and TAT peptide as CPP, showed the highest membrane fusion activity and fused with plasma membrane of living cells. The co-existence of DOPE and CHEMS were essential and the amount of arginine in CPP peptide sequence was required for high-activity of membrane fusion.

I proposed as a reason of the high fusogeninc ability of this HDL. First, arginines of CPP form hydrogen bonds with the lipid membrane to keep HDL aside target membrane, protonated primary amines of DOPE molecules form additional hydrogen bonds between them to promote adhesion, and finally, the succinyl groups of CHEMS molecules, which are protonated under mildly acidic condition selectively and has increased lipophilicity, is inserted into the lipid membrane. I have an assumption the space between the lipid and HDL membranes becomes extremely hydrophobic under above process and the two membranes fuse together as other membrane-fusiogenic carriers or membrane-fusion process of viral infection. I believe that fusogenic HDL can supply any lipids of which additionally incorporated into the lipid bilayer to the target lipid membrane and aid in the formation of non-raft nanostructures on there.

4-5. Experimental section.

Materials and Regents

The lipids DOPS, DOPC, DOPE, DPPC, and POPC were purchased from NOF (Tokyo, Japan), while, Rho-DPPE (N-(lissamine rhodamine B sulfonyl)-1,2-dipalmitoyl-sn-glycero-3-phosphoethanolamine), NBD-DPPE (N-(7-nitro-2-1,3-benzoxadiazol-4-yl)-1,2-dipalmitoyl-sn-glycero-3-phosphoethanolamine), , SOPC (1-stearoyl-2-oleoyl-sn-glycero-3-phosphocholine), CHEMS, and Extruder set were bought from Avanti Polar Lipids (Alabaster, AL, USA). DPH and Chol were obtained from Sigma-Aldrich (St. Louis, MO, USA). Laurdan was supplied from AnaSpec, Inc (Fremont, CA, USA). FBS(Fetal bovine serum) was supplied from Japan Bioserum (Hiroshima, Japan). Dulbecco's phosphate-buffered saline (PBS) and trypsin-ethylenediaminetetraacetic acid buffer (EDTA; 0.05% trypsin, 0.53 mM EDTA-4Na) were purchased from Invitrogen (Carlsbad, CA, USA). Cell Counting Kit-8 and n-dodecyl-beta-D-maltopyranoside and were provided by Dojindo Laboratories (Kumamoto, Japan). glass-bottomed dishes were purchased from Greiner bio-one (Frickenhausen, Germany). Cell culture dishes were purchased from BD Bioscience (San Jose, CA, USA). RhoB was purchased by Thermo Fisher Scientific (Waltham, MA, USA). SDS-PAGE precast gel and McCoy's 5A media were supplied by Wako (Osaka, Japan). DC Protein Assay Kit was supplied from Bio-Rad Laboratories (Hercules, CA, USA). Spectra/Por Dialysis Membranes (molecular weight cut-off [MWCO], 3,500 and 50,000) were suppled from Spectrum Laboratories (Rancho Dominguez, CA, USA). Escherichia coli strain BL21(DE3) was procured from Novagen (Madison, WI, USA). Ni Sepharose resin was obtained from GE Healthcare Life Sciences (Little Chalfont, Buckinghamshire, UK).

Preparation, cloning and expression, of apoA-I mutants

The pCold I vector was utilized for the large-scale preparation of N-terminal 43 residue-deleted apoA-I protein and its mutant containing TAT peptide at the C terminus [15]. It should be notified the N-terminal 44 residue-deleted apoA-I mutant was utilized instead of N-terminal 43 residue-deleted apoA-I sequence for the

preparation of apoA-I mutants protein bearing 4/PN (penetratin), R8(octa-arginine), and R11(undeca-arginine) peptides. Nucleic acid sequences encoding the four cell penetrating peptides were annealed and ligated between the PstI and XbaI sites of pCOLD I vector for their C-terminal fusion. These oligonucleotides were synthesized by using primer extension method. Sequences of annealing forward and reverse primers was shown as follows:

Forward primers

PN, 5′-attctgcagcgccagattaaaatttggtttcagaaccgccgcatg-3′;

R8, 5′-atctgcagcgccgccgccgccgccgccgccgctaatctagaaaactgctggataattggg-3′;

R11, 5′-atctgcagcgccgccgccgccgccgccgccgccgccgctaatctagaaaactgctggataattggg-3′

Reverse primers

PN, 5′-attctagatttttttttccatttcatgcggcggttctgaaaccaaa-3′;

R8 and R11, 5′-cccaattatccagcagttt-3′

The all mutants of apoA-I were expressed in BL21(DE3) E.coli cell line in accordance with the protocol from manufacturer and purified mutant protein was extracted from the E.coli using a Ni Sepharose resin column under denaturation buffer conditions. After dialysis against 0.4 mM hydrochloric acid (HCl) at 4°C with a Spectra/Por Dialysis Membrane (MWCO, 3,500), these were lyophilized to remove all buffers and HCl and stored at –80°C.

Preparation of HDL derivatives

Reconstituted high-density lipoprotein derivatives were prepared by minor improvement method based on previous reports. Briefly, the solutions in chloroform of DOPC, DOPE, CHEMS, and Chol were mixed at described molar ratios in a round-table glass flask. Fluorescently labeled lipids, NBD-DPPE, and Rho-DPPE for model membrane lipid-mixing assay or RhoB for plasma membrane-oriented fusion assay were also added at 1% molar ratio of the total lipid. The organic solvent was evaporated and removed completely by overnight vacuum with a freeze drier. The dried lipid film was dispersed in PBS buffer at pH=7.4 containing 30 mg/mL of sodium cholate at a final cholate: lipids molar

ratio of 4:1. Each of apoA-I mutants was dissolved in PBS containing 4 M urea and was mixed with the lipid-cholate dispersant at a protein/lipid molar ratio of 1/50. The protein/lipid/cholate mixture was kept overnight at room temperature to mature precursor of reconstituted HDLs. The matured mixture was dialyzed against 3 L of PBS three times at room temperature by using a Spectra/Por Dialysis Membrane (MWCO 50,000). The reconstituted HDL derivative dispersant was centrifuged at 4°C and 15,300 ×g and for 30 min to separate any debris as a precipitation. Purification of the HDL derivatives from large cholate micellar and Apo-AI mutants was performed by a size-exclusion chromatography method with a Superdex-200 HiLoad 16/600 column (GE Healthcare) using 2 mM EDTA,150 mM sodium chloride (NaCl), 50 mM Tris/HCl (pH 7.5), and 0.5 mM phenylmethanesulfonyl fluoride (PMSF). The detection wavelength of the chromatography was set as 280 nm, while the elution rate was fixed at 1 mL per 1 min. Fractions of size-exclusion chromatography including HDL derivatives were recollected and concentrated by Amicon Ultra-15 (MWCO 50 kDa) disposal centrifugal filter to ensure enough concentration of HDL derivatives for the following experiments. The concentration of HDL was measured by Lowry method.

Liposome preparation

The parched lipid film (DPPC, DOPC, POPC, SOPC/DOPE = 75/25, or DOPC/DOPS = 90/10) was dispersed in 50 mM MES buffer containing 150 mM NaCl (pH 5.5) or PBS buffer (pH=7.4) at a lipid concentration of 1 mg/mL. The hydrated lipids were extruded using extruder (Avanti) equipped with a 100 nm of pore size polycarbonate membrane filter.

Dynamic light scattering and surface charge analysis

The zeta potential and hydrodynamic diameter of HDL derivatives and liposomes were measured using a Zeta Sizer Nano Z (Malvern, Worcestershire, UK) and Nanotrac UPA-EX250 particle size analyzer (Nikkiso, Tokyo, Japan), respectively.

Lipid-mixing assay

The extent of lipid supply as measured by lipid-mixing assays using model liposomes was performed as reported by Lei et al.[25] I performed lipid mixing assay with each liposomes and HDL derivatives. 15 μM of HDL derivatives 15 μM of liposome was mixed in a 96-well Costar white plate and incubated at 37°C while intermittent plate shaking. The concentration of both nanomaterials were based on lipids. The time dependent change of fluorescence derived from NBD-PE was monitored continuously at an excitation wavelength of 460 nm, emission wavelength of 538 nm, and 530 nm emission cutting-off filter using SpectraMax M2&M2e Microplate Reader (Molecular Devices). After enough time for fusion, 750-min, 20 μL of 10% n-dodecyl-beta-D-maltopyranoside was appended into the fusion system to destroy all lipidic structures, and intensity from NBD-PE was collected for another 40 min to determine the maximum intensity of NBD fluorescence as a value from completely relaxed condition of FRED. The NBD fluorescence data were converted into the time-lapse monitor value of the percentage of intensity of NBD-PE fluorescence under FRED-free condition. Therefore, each fluorescence intensity in the lipid-mixing assay was normalized by subtracting the minimum fluorescence (Fmin) and dividing by the maximum fluorescence (Fmax) measured under the following condition with added 20 μL of 10% n-dodecyl-beta-D-maltopyranoside. Generally, n-dodecyl-beta-D-maltopyranoside is hard to cause the increase or decrease of the emission of coexisting fluorescence molecules. The definition of lipid-mixing ratio was 100 × (F – Fmin)/(Fmax – Fmin).

Determination of lipid content

The molar ratio of CHEMS, DOPE, and DOPC in an HDL derivative with the most prominent lipid mixing ability (4/TAT) was measured by LC/MS/MS analysis. The analyses were performed with a Sciex API3200 Qtrap LC/MS/MS system equipped with an electrospray ionization (ESI) source. Each content was separated at 20°C by using a reverse-phase C18 analytical column (Eclipse Plus C18 column, 3.5 μm, 4.6 mm i.d. ×100 mm; Agilent, CA, USA). The condition of

mobile phase liquid was 95% methanol aqueous solution containing 5 mM ammonium acetate and a flow rate was 0.2 mL/min. CHEMS was analyzed in the negative ion mode and DOPE and DOPC were analyzed in the positive ion mode. The quantitative analyses were performed by using MS/MS-MRM of the precursor/product ion for CHEMS (m/z: 485.3>99.0), DOPE (m/z: 744.3>603.4), and DOPC (m/z: 786.4>184.0). The analytical conditions were described as follows: gas temperature, 350°C ; ion spray voltage, –4,500 V (CHEMS) and 5,500 V (DOPC and DOPE) ; de-clustering potential, –60 V (CHEMS), 66 V (DOPE), and 86 V (DOPC); entrance potential, 8.5 V; collision Energy, –36 V (CHEMS), 51 V (DOPE), and53 V (DOPC); cell exit potential, –34 V (CHEMS), 64 V (DOPE), and 56 V (DOPC). 4/TAT was freeze-dried to destroy its discoidal structure, and a mixture of the lipids was extracted from the lipid/protein mixture with methanol and subjected to the analysis.

Evaluation of the membrane polarity

The hydrophobic fluorescent probe molecule, Laurdan, show different florescent spectra in response to the polarity of surrounding environment. Its emission spectra shift to a red region originated from dielectric relaxation with water.[53] Thus, generalized polarization, defined as GP340 = (I440 – I490)/ (I440 + I490), was determined as an indicator of the membrane polarity by obtaining the fluorescent intensities (I) of Laurdan by excitation with 340 nm wavelength light at 37°C. The final concentrations of lipids and Laurdan in the analytical condition were 100 and 1 μM, respectively.

Evaluation of the membrane fluidity

The membrane fluidity of HDL derivatives was evaluated with a fluorescent probe, DPH.[54] DPH is a rod-shaped probe and the fluorescence polarization reflects how the molecule move. DPH was appended to an HDL dispersant at a DPH / lipid was 1/10 at a molar ratio. The final concentrations of DPH and lipids were 25 and 250 μM, respectively. After incubation for 30 minutes at 37°C, the fluorescence polarization of DPH was obtained using a spectrofluorometer (excitation/emission,

360/430 nm). Samples were excited by vertically polarized light, and the emission intensity was monitored through an detector oriented parallel (I//) and perpendicular (I⊥) to determine the polarization direction of the excitation light. The DPH polarization (P) was defined as P = (I// – GI⊥)/(I// + GI⊥), G = i⊥/i// where i⊥ and i// are emission intensities perpendicular and parallel to the horizontally polarized light, respectively. The membrane fluidity was evaluated on the calculated reciprocal of polarization, 1/P.

Specimen preparation for EM observation

HDL samples for EM observation were prepared according to the optimized negative staining protocol established by Zhang et al [55]. A 15 μL drop of HDL dispersant (0.75-1 μg/mL protein) in 50 mM MES/150 mM NaCl buffer (pH 5.5) or PBS buffer (pH 7.4) was put on a collodion-coated 400-mesh copper grid (Nisshin EM Corp., Tokyo, Japan). After 15 s, the excess dispersant was eliminated by blotting with a filter paper. The grid was washed by briefly floating it on a 30 μL drop of either of the buffer solutions on parafilm and then drying with a filter paper. This washing procedure was performed thrice. Finally, a 30-μL drop of 1% (w/v) uranyl acetate solution (pH 4.5) was put on the grid and kept for 1 min for staining. The excess solution was absorbed by a filter paper gently, and the sample on the grid was air-dried at room temperature.

Cell culture

T24 cell line, derived from human urinary bladder cancer, were supplied from the National Cancer Institute (Frederick, MD, USA). T24 cells were cultured in McCoy'5A media containing 10% FBS, 100 μg/mL streptomycin and 100 U/mL penicillin under a humidified atmosphere of 5% CO2 and 95% air at 37°C. They were passaged every 3-4 days by using trypsin.

Confocal analysis

Cells were generally seeded at a density of 2.0 × 10^5 cells/mL on cell culture dishes and cultured for 1 day before treatment with 10 μg/mL of HDL derivatives

labeled with Rho-DPPE at 37°C for 1h in cell culture media which is adjusted at pH 7.4 or 6.4 condition and contained 10% FBS. After rinse with ice-cold fresh media, cells were monitored with a confocal laser scanning microscope, OLYMPUS FV-10i-LIV (Tokyo, Japan).

For the serum-free experiments with the HDLs, McCoy's 5A media at pH 7.4 or 5.5 were utilized. The pH of media is adjusted by using concentrated HCl solutions. To minimize the internalization of HDLs into cells, the short-time HDL treatment was performed for 10 min at 37°C.

For the pulse-chase experiment, cells were treated with 4/TAT including RhoB for 1 h at 4°C and pH 7.4 and in the absence of FBS to let 4/TAT bind to the plasma membrane while inhibiting its internalization. The cells were then treated with fresh McCoy's 5A media (pH 7.4 or 5.5) for 5 min at 37°C to start lipid mixing between 4/TAT and the plasma membrane.

FACS (Fluorescence-activated cell sorter) measurement

T24 cells were seeded at a density of 2.0×10^5 cells/mL in a 24-well plate and cultured for 1 day. 10 μg/mL HDL derivatives were appended on cell culture media and the samples were kept for 10 min at 37°C without serum. After that, cells were rinsed twice with each pH-adjusted McCoy's 5A medium (pH 7.4 and 5.5) and harvested. The cells were immobilized with 4% paraformaldehyde in PBS buffer and analyzed using a Guava® easyCyte flow cytometry system (Merck Millipore, Darmstadt, Germany). The non-treated cells were utilized as a negative control to estimate the autofluorescence. A total of 3,000 cells were counted for evaluation the ability of the HDL derivatives. Assays were carried out in triplicates.

4-6. References

1. Primakoff, P. & Myles, D.G. Cell-cell membrane fusion during mammalian fertilization. *FEBS Lett.* **581**, 2174-2180 (2007).
2. Oren-Suissa, M. & Podbilewicz, B. Cell fusion during development. *Trends Cell Biol.* **17**, 537-546 (2007).
3. Duelli, D. & Lazebnik, Y. Cell-to-cell fusion as a link between viruses and cancer. *Nat. Rev. Cancer* **7**, 968–976 (2007).
4. Harrison, S.C. Viral membrane fusion. *Nat. Struct. Mol. Biol.* **15**, 690-698 (2008).
5. Rothman, J.E. The principle of membrane fusion in the cell (Nobel lecture). *Angew. Chem. Int. Ed. Engl.* **53**, 12676-12694 (2014).
6. Chernomordik, L.V. & Kozlov, M.M. Mechanics of membrane fusion. *Nat. Struct. Mol. Biol.* **15**, 675-683 (2008).
7. Matz, C.E. & Jonas, A. Micellar complexes of human apolipoprotein A-I with phosphatidylcholines and cholesterol prepared from cholate-lipid dispersions. *J. Biol. Chem.* **257**, 4535-4540 (1982).
8. Denisov, I.G. & Sligar, S.G. Nanodiscs in Membrane Biochemistry and Biophysics. *Chem. Rev.* **117**, 4669-4713 (2017).
9. Mo, Z.C., Ren, K., Liu, X., Tang, Z.L. & Yi, G.H. A high-density lipoprotein-mediated drug delivery system. *Adv Drug Deliv Rev* **106**, 132-147 (2016).
10. Kuai, R., Li, D., Chen, Y.E., Moon, J.J. & Schwendeman, A. High-Density Lipoproteins: Nature's Multifunctional Nanoparticles. *ACS Nano* **10**, 3015-3041 (2016).
11. Ng, K.K., Lovell, J.F. & Zheng, G. Lipoprotein-Inspired Nanoparticles for Cancer Theranostics. *Acc. Chem. Res.* **44**, 1105-1113 (2011).
12. Murakami, T. Phospholipid nanodisc engineering for drug delivery systems. *Biotechnol J* **7**, 762-767 (2012).
13. Bricarello, D.A., Smilowitz, J.T., Zivkovic, A.M., German, J.B. & Parikh, A.N. Reconstituted Lipoprotein: A Versatile Class of Biologically-Inspired Nanostructures. *ACS Nano* **5**, 42-57 (2011).
14. Ryan, R.O. Nanodisks: hydrophobic drug delivery vehicles. *Expert Opinion on Drug Delivery* **5**, 343-351 (2008).
15. Murakami, T., Wijagkanalan, W., Hashida, M. & Tsuchida, K. Intracellular drug delivery by genetically engineered high-density lipoprotein nanoparticles. *Nanomedicine (London, U. K.)* **5**, 867-879 (2010).
16. Mathew, S. *et al.* Exclusive Photothermal Heat Generation by a

Gadolinium Bis(naphthalocyanine) Complex and Inclusion into Modified High-Density Lipoprotein Nanocarriers for Therapeutic Applications. *ACS Nano* **7**, 8908-8916 (2013).

17. Numata, T. *et al.* Utilization of photoinduced charge-separated state of donor-acceptor-linked molecules for regulation of cell membrane potential and ion transport. *J. Am. Chem. Soc.* **134**, 6092-6095 (2012).

18. Ellens, H., Bentz, J. & Szoka, F.C. Fusion of phosphatidylethanolamine-containing liposomes and mechanism of L.alpha.-HII phase transition. *Biochemistry* **25**, 4141-4147 (1986).

19. Maréchal, Y. *The Hydrogen Bond and the Water Molecule* (Elsevier B.V., 2007).

20. Desiraju, G.R. & Steiner, T. *The Weak Hydrogen Bond: In Structural Chemistry and Biology* Vol. 9. (Oxford University Press, USA, 2001).

21. Fattal, E., Couvreur, P. & Dubernet, C. "Smart" delivery of antisense oligonucleotides by anionic pH-sensitive liposomes. *Adv Drug Deliv Rev* **56**, 931-946 (2004).

22. Simoes, S., Moreira, J.N., Fonseca, C., Duzgunes, N. & de Lima, M.C. On the formulation of pH-sensitive liposomes with long circulation times. *Adv Drug Deliv Rev* **56**, 947-965 (2004).

23. Bonomo, E.A. & Swaney, J.B. Effect of phosphatidylethanolamine on the properties of phospholipid-apolipoprotein complexes. *Biochemistry* **29**, 5094-5103 (1989).

24. Miyazaki, M., Tajima, Y., Ishihama, Y., Handa, T. & Nakano, M. Effect of phospholipid composition on discoidal HDL formation. *Biochim. Biophys. Acta* **1828**, 1340-1346 (2013).

25. Shi, L. *et al.* SNARE proteins: One to fuse and three to keep the nascent fusion pore open. *Science* **335**, 1355-1359 (2012).

26. Murcia, M.J., Minner, D.E., Mustata, G.-M., Ritchie, K. & Naumann, C.A. Design of Quantum Dot-Conjugated Lipids for Long-Term, High-Speed Tracking Experiments on Cell Surfaces. *J. Am. Chem. Soc.* **130**, 15054–15062. (2008).

27. Ba, H., Rodriguez-Fernandez, J., Stefani, F.D. & Feldmann, J. Immobilization of gold nanoparticles on living cell membranes upon controlled lipid binding. *Nano Lett.* **10**, 3006-3012 (2010).

28. Lai, M.-Z., Vail, W.J. & Szoka, F.C. Acid- and calcium-induced structural changes in phosphatidylethanolamine membranes stabilized by cholesteryl hemisuccinate. *Biochemistry* **24**, 1654-1661 (1984).

29. Blumenthal, R., Bali-Puri, A., Walter, A., Covel, D. & Eidelman, O. pH-dependent fusion of vesicular stomatitis virus with vero cells. Measurement by dequenching of octadecyl rhodamine fluorescence. *THE JOURNAL OF BIOLOGICAL CHEMISTRY* **262**, 13614-13619 (1987).
30. Murakami, T., Okamoto, H. & Kim, H. Structural and functional changes in high-density lipoprotein induced by chemical modification. *Biomater Sci* **3**, 712-715 (2015).
31. Tatsuya Murakami *et al.* Mesoscopic Metal Nanoparticles Doubly Functionalized with Natural and Engineered Lipidic Dispersants for Therapeutics. *ACS Nano* **8**, 7370-7376 (2014).
32. Nakatsuji, H. *et al.* Thermosensitive Ion Channel Activation in Single Neuronal Cells by Using Surface-Engineered Plasmonic Nanoparticles. *Angew. Chem. Int. Ed.* **54**, 11725-11279 (2015).
33. Kim, H. *et al.* Polymer-coated pH-responsive high-density lipoproteins. *J. Control. Release* **228**, 132-140 (2016).
34. Kulig, W. *et al.* How well does cholesteryl hemisuccinate mimic cholesterol in saturated phospholipid bilayers? *J. Mol. Model.* **20**, 2121 (2014).
35. Futaki, S. Oligoarginine vectors for intracellular delivery: design and cellular-uptake mechanisms. *Biopolymers* **84**, 241-249 (2006).
36. Futaki, S. & Nakase, I. Cell-Surface Interactions on Arginine-Rich Cell-Penetrating Peptides Allow for Multiplex Modes of Internalization. *Acc. Chem. Res.* **50**, 2449-2456 (2017).
37. Amand, H.L., Bostrom, C.L., Lincoln, P., Norden, B. & Esbjorner, E.K. Binding of cell-penetrating penetratin peptides to plasma membrane vesicles correlates directly with cellular uptake. *Biochim. Biophys. Acta* **1808**, 1860-1867 (2011).
38. Lönn, P. & Dowdy, S.F. Cationic PTD/CPP-mediated macromolecular delivery: charging into the cell. *Expert Opinion on Drug Delivery* **12**, 1627-1636 (2015).
39. Salvati, A. *et al.* Transferrin-functionalized nanoparticles lose their targeting capabilities when a biomolecule corona adsorbs on the surface. *Nat Nanotechnol* **8**, 137-143 (2013).
40. Tenzer, S. *et al.* Rapid formation of plasma protein corona critically affects nanoparticle pathophysiology. *Nat Nanotechnol* **8**, 772-781 (2013).
41. Walkey, C.D. *et al.* Protein Corona Fingerprinting Predicts the Cellular Interaction of Gold and Silver Nanoparticles. *ACS Nano* **8**, 2439-2455 (2014).

42. Rader, D.J. Molecular regulation of HDL metabolism and function: implications for novel therapies. *J. Clin. Invest.* **116**, 3090-3100 (2006).
43. Redmond, K.A., Nguyen, T.-S. & O.Ryan, R. All-trans-retinoic acid nanodisks. *Int. J. Pharm.* **339**, 246-250 (2007).
44. Wolfrum, C. *et al.* Mechanisms and optimization of in vivo delivery of lipophilic siRNAs. *Nat. Biotechnol.* **25**, 1149-1157 (2007).
45. Iyer, A.K., Singh, A., Ganta, S. & Amiji, M.M. Role of integrated cancer nanomedicine in overcoming drug resistance. *Adv Drug Deliv Rev* **65**, 1784-1802 (2013).
46. Jhaveri, A., Deshpande, P. & Torchilin, V. Stimuli-sensitive nanopreparations for combination cancer therapy. *J. Control. Release* **190**, 352-370 (2014).
47. Gerweck, L.E. & Seetharaman, K. Cellular pH Gradient in Tumor versus Normal Tissue: Potential Exploitation for the Treatment of Cancer1. *Cancer Res.* **56**, 1194-1198 (1982).
48. Jiang, Z. *et al.* Plant cell-surface GIPC sphingolipids sense salt to trigger ca^{2+} influx. *Nature* **572**, 341-346 (2019).
49. Tjellstrom, H., Hellgren, L.I., Wieslander, A. & Sandelius, A.S. Lipid asymmetry in plant plasma membranes: Phosphate deficiency-induced phospholipid replacement is restricted to the cytosolic leaflet. *FASEB J.* **24**, 1128-1138 (2010).
50. T. Murashige & Skoog, F. A revised medium for rapid growth and bioassays with tobacco tissue cultures. *Physiol. Plant.* **15**, 473-497 (1962).
51. Numata, K. *et al.* Library screening of cell-penetrating peptide for BY-2 cells, leaves of Arabidopsis, tobacco, tomato, poplar, and rice callus. *Sci. Rep.* **8**, 10966 (2018).
52. Pérez-de-Luque, A. Interaction of Nanomaterials with Plants: What Do We Need for Real Applications in Agriculture? *Frontiers in Environmental Science* **5** (2017).
53. Dinic, J., Biverstahl, H., Maler, L. & Parmryd, I. Laurdan and di-4-ANEPPDHQ do not respond to membrane-inserted peptides and are good probes for lipid packing. *Biochim. Biophys. Acta* **1808**, 298-306 (2011).
54. Blitterswijk, W.J.v., Hoeven, R.P.v. & Meer, B.W.v.d. Lipid structural order parameters (reciprocal of fluidity) in biomembranes derived from steady-state fluorescence polarization measurements. *Biochimica et Biophysica Acta - Biomembranes* **644**, 323-332 (1981).

55. Zhang, L. *et al.* Morphology and structure of lipoproteins revealed by an optimized negative-staining protocol of electron microscopy. *J. Lipid Res.* **52**, 175-184 (2011).

Chapter 5. General Conclusion and Perspective

In this thesis, I explained the significance of membrane properties as a factor in the determination of cell behavior, and I introduced methods to design manipulators of membrane properties using bioactive nanomaterials. Cells are surrounded by a lipid bilayer, and they respond to external information using nanostructures that are found on cell membranes. These nanostructures are closely related to a wide range of biological phenomena, such as immune responses, neurotransmission, cell elongation and development, and viral infections. Thus, nanostructure manipulation could control these processes in a unified manner via cell-engineering technologies.

In chapter two, I created a basic method to analyze giant unilamellar vesicle (GUV)-nanomaterial interactions without ion disturbances. I hypothesized that the salting-in effect exists for the dispersion of biocompatible nanomaterials. Thus far, no detailed reports exist regarding the salting-in effect of biomaterials since its discovery in protein dispersion and aggregation. The first example I found reported that sugar exhibits salting-in and salting-out effects for biocompatible metal nanoparticles. The exact influence that nanomaterial-model lipid raft interactions display is difficult to estimate, due to the contradiction that exists between the poor resistance of GUVs against salts and the intrinsic adjustment that biocompatible nanomaterial designs have for physiological conditions. This result indicates that appropriate concentrations of sugar let both GUV and nanomaterials co-exist in a stable manner and accelerates the clarification of lipid raft-nanomaterial interaction. In regards to nanomaterial–cell membrane interactions, this finding could be utilized to confirm material designs, considering the wide application of biocompatible metal nanoparticles in both *in vivo* and *in vitro* cell experiments.

In chapter three, I went on to manipulate the formation-deformation process of a model lipid raft in the presence of sugar. Lipid rafts are a key structure on cell membranes that determine cell behavior. The results showed that plasma-membrane targeted gold nanorods (pm-AuNRs) accumulated during the Lo phase domain spontaneously, and it induced the deformation of the domain

structure. Furthermore, cholesterol-enriched pm-AuNRs (pm-AuNR-chols) supplied cholesterol, and it generated a model lipid raft on non-raft GUV in a near-infrared laser-induced manner. This is the first example of model lipid raft manipulation for multiple domains at the same time. The size of the lipid raft was almost on the same scale as pm-AuNRs, which is stable and demonstrates a high membrane affinity. This makes pm-AuNRs a prominent candidate for the raft manipulation of cell membranes.

In chapter four, I developed high-density lipoprotein (HDL) mutants that can selectively fuse with the lipid membrane and selectively provide HDL side lipids under mildly acidic conditions by modifying the lipid composition and protein structure of HDL. This process can be used to adapt HDL to non-raft nanostructures (e.g., lipid cluster) on the membrane. This process could potentially be beneficial for use in human cancer tissues, for example, since they are found in mildly acidic conditions.

To increase membrane affinity, cell-penetrating peptides (CPPs) were attached to HDL. A highly fluidic phospholipid (DOPC), a highly fluidic phospholipid containing a primary amine (DOPE), and a Chol derivative (CHEMS) were utilized as lipids. Various kinds of HDL derivatives were prepared systematically, and their fusogenic activities were measured. The HDL derivatives containing DOPC: DOPE: CHEMS=1:2:1 in molar ratio and the TAT peptide as CPP showed the highest membrane-fusion activity, and they fused with the plasma membrane of living cells. The co-existence of DOPE and CHEMS were essential to these results, and the amount of arginine in the CPP peptide sequence was required to produce the high amount of membrane-fusion activity.

The high fusogenic ability of this HDL derivative exhibits three main reasons. First, the arginine found in CPP is able to form hydrogen bonds with the lipid membrane, thus bonding HDL with its target membrane. Second, the protonated primary amines of DOPE molecules are able to then form additional hydrogen bonds between HDL and its target membrane, which further promotes adhesion. Third, the succinyl groups of CHEMS molecules, which are selectively protonated under mildly acidic conditions and increased lipophilicity, are inserted into the lipid

membrane. I hypothesize that the space between the lipid and HDL membranes becomes extremely hydrophobic during the above process, causing the two membranes to fuse together similar to other membrane-fusogenic carriers and the membrane-fusion process of viral infections. I believe that fusogenic HDL could be used to supply lipids to be incorporated into the lipid bilayer of target lipid membranes, in order to aid in the formation of non-raft nanostructures.

The nanostructures described above are a part of the sequential chemical reaction field that is related to cell behavior. Recently, cellular biology moved from a central-dogma based understanding of cell behavior to a system-based understanding. In the traditional model, nuclear and organelle genomes encode all information that a cell needs. Thus, cells use the information found in DNA to express proteins and produce the materials that are needed to survive. Scientists from the fields of biology, biophysics, informatics, and chemistry now consider this traditional attitude to not be enough to understand complicated cellular behavior.[2-5] The key part of this critical attitude toward the central dogma is the fact that the model itself does not consider the creation and extinction of dynamic reaction fields.

The compartmentalization of cells allows complicated sequential reactions in the overcrowded cytoplasm to be performed selectively in a manner that saves time and space. Nanostructures, including lipid nanostructures of cell organelles, lipid rafts, and other lipids or lipid/protein nanostructures, are created by cells to further increase the impact of this compartmentalization. As mentioned in the first chapter, nanostructures on plasma membranes provide the fundamental reaction site that is commonly needed for various kinds of cell behavior.

Cell nanostructures can be classified into three representative types: two-dimensional membrane nanostructures distinguished by their physical phases (lipid-based nanostructures) [2], three-dimensional nanostructures that exhibit lipid bilayer boundaries (organelles), and three-dimensional nanostructures that exhibit no membrane boundaries but are distinguished by their physical phases.[4] The third category includes three-dimensional droplets that are caused by the typical phase, which includes specific partners of proteins or proteins and

bioactive macromolecules, such as DNA or RNA. This droplet formation is called the liquid-liquid phase separation of protein.

The compartmentalization of cells forms the basis for why specific reactions occur in a specific sequence, why signals and information are transacted very accurately, and why cells can recruit components to function as the worked as cell intends. The latter two functions of compartmentalization do not explain timing very well, however. Although previous studies described various interlocking protein combinations and revealed many triggers for the latter two functions, no clear answer exists to the question of when and where the reaction field occurs within cells.

Cell membrane properties change dynamically in a physics-based manner. During my thesis research, I began to consider that membrane properties of the lipid bilayer in/on a cell could determine the timing of the formation of these three-dimensional structures. For organellar, the change of curvature caused by domain formation led the endosome generation and other organellar formation/deformation. The behavior of droplet–lipid membranes during cell interactions are determined by their membrane properties, in the same way that the interactions between nanomaterials and the lipid bilayer are determined by the lipid membrane's physical properties. I hypothesized that local changes in the lipid membrane structure may determine the properties and dynamics of the droplet-membrane in its vicinity, as the lipid membrane structure is spread throughout the cell and changes its shape and properties rapidly. Given the density of intracellular material, the likelihood exists that the droplets and lipid membrane structures interact with each other in the cell, and indeed, some interactions were confirmed in 2020.[6] Manipulation of membrane properties could contribute to the understanding of the formation-deformation of three-dimensional structures, and it could help to further our comprehension of cell behavior in the same was that gene expression manipulation contributed to the understanding of the cell system.

As shown by this study, membrane properties are becoming a variable that can be externally manipulated[7-9]. This study opens up a new field biology–synthetic

biology-like concept based on lipid properties–in which the interaction between three-dimensional and two-dimensional membrane-based nanostructures are investigated, and in which the properties of the cell's lipid membrane will be controlled to create a reaction field within the cell to achieve desired properties.

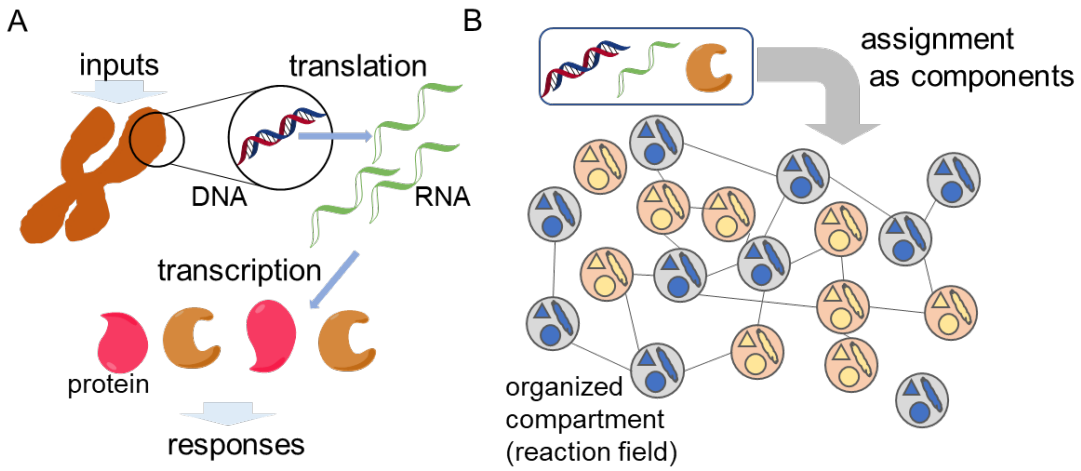

Figure.1 The understanding of cell system from traditional central-dogma based picture (A) and from the emerged new network of reaction field-based picture. In (B), living cell is defined as a characteristic topology of network of reaction field, nanostructures, in advance. The definition requires the characteristic of reaction fields (circles in (B)) which is described by the words of soft matter physics to meet the definition. The requirements also determine the characteristic of components (shown as shapes in circles in (B)) within each reaction fields. In real cells, real materials, such as proteins, lipids, DNA, RNA and others, are assigned as components to form necessary nanostructure. The molecular identity of the network is still not described well, but lipid bilayer on and in a cell is a strong candidate because of the freedom for network formation and nanoscale tunability of physical properties, a candidate of scaffolds of reaction field formation, on plasma membrane and organellar.[1, 2]

Our understanding of cell behavior is shifting from component molecule-based theories to the recognition that cell behavior is a complex of reaction fields and the interaction networks of reaction fields (Fig.1A and B). In this new perspective, proteins and other materials would be assigned on the multi-level construction to meet theoretical requirements from soft matter physics, in the same way that atoms are assigned on electron density map to meet a criterion for structural

elucidation in the structure determination process of x-ray crystallography (Fig.1B). Some unknown components, such as proteins or other molecules, would be predicted as the necessary components to match the requirements from multi-level network.

The manipulation of membrane properties is enthusiastically required to move this field forward. This thesis provided a method of estimating the manipulator-membrane interaction without disturbance and a method to monitor the Lo phase domain formation/deformation. Also, this thesis discussed how typical membrane domains can be targeted in an on-demand and pragmatic manner and how smart lipid suppliers can target plasma membranes. All research was conducted using biocompatible nanomaterials and was relatively easily transported to *in vivo* system.

This thesis contributes design, preparation, and evaluation methods for bioactive nanomaterials aimed at controlling the physical properties of plasma membranes. I hope the results and perspectives provided here can lead to a new cell-engineering technology that is focused on the fundamental parts of cell behavior and confirm the new understanding of cell dynamics based on lipid membrane properties.

References

1. McMahon, H.T. & Boucrot, E. Membrane curvature at a glance. *J. Cell Sci.* **128**, 1065-1070 (2015).
2. Sezgin, E., Levental, I., Mayor, S. & Eggeling, C. The mystery of membrane organization: composition, regulation and roles of lipid rafts. *Nat. Rev. Mol. Cell Biol.* **18**, 361-374 (2017).
3. Shapiro, J.A. Revisiting the central dogma in the 21st century. *Ann. N. Y. Acad. Sci.* **1178**, 6-28 (2009).
4. Hyman, A.A., Weber, C.A. & Julicher, F. Liquid-liquid phase separation in biology. *Annu. Rev. Cell Dev. Biol.* **30**, 39-58 (2014).
5. Holt, C.E. & Schuman, E.M. The central dogma decentralized: new perspectives on RNA function and local translation in neurons. *Neuron* **80**, 648-657 (2013).
6. Lee, J.E., Cathey, P.I., Wu, H., Parker, R. & Voeltz, G.K. Endoplasmic reticulum contact sites regulate the dynamics of membraneless organelles. *Science* **367**, eaay7108 (2020).
7. Rothman, J.E. The principle of membrane fusion in the cell (Nobel lecture). *Angew. Chem. Int. Ed. Engl.* **53**, 12676-12694 (2014).
8. Kim, H. *et al.* Membrane fusogenic high-density lipoprotein nanoparticles. *Biochim Biophys Acta Biomembr* **1861**, 183008 (2019).
9. Nobeyama, T. *et al.* Control of Lipid Bilayer Phases of Cell-Sized Liposomes by Surface-Engineered Plasmonic Nanoparticles. *Langmuir* **36**, 7741-7746 (2020).

Related Publications and Copyright Permissions

This list shows original articles of the following chapters in this thesis and permissions of reuse from each publisher.

Chapter 2.

Title: Colloidal stability of lipid/protein-coated nanomaterials in salt and sucrose solutions

Authors: Tomohiro Nobeyama, Megumi Mori, Kazuki Shigyou, Koji Takata, Ganesh N. Pandian, Hiroshi Sugiyama, and Tatsuya Murakami

ChemistrySelect **2018**, *3* (28), 8325–8331.

License Number: 4910771132762

Chapter 3.

Title: Control of Lipid Bilayer Phases of Cell-Sized Liposomes by Surface-Engineered Plasmonic Nanoparticles

Authors: Tomohiro Nobeyama, Kazuki Shigyou, Hirotaka Nakatsuji, Hiroshi Sugiyama, Naoko Komura, Hiromune Ando, Tsutomu Hamada, and Tatsuya Murakami

Langmuir **2020** *36* (26), 7741-7746.

For copyright license; Reprinted and adapted with permission from (*Langmuir* **2020**, *36*, (26), 7741–7746). Copyright 2020 American Chemical Society.

Chapter 4.

Title: Membrane fusogenic high-density lipoprotein nanoparticles

Authors: Hyungjin Kim, Tomohiro Nobeyama. Shinnosuke Honda, Kaori Yasuda, Nobuhiro, Morone, and Tatsuya Murakami

Biochem. Biophys. Acta - Biomembrane **2019**, *1861* (10), 183008.

For copyright license; please note that, as the author of this Elsevier article, you retain the right to include it in a thesis or dissertation, provided it is not published commercially. Permission is not required, but please ensure that you reference the journal as the original source.